Nuclear Medicine

R · E · V · I · E · W

merged with Problems of Nuclear Medicine

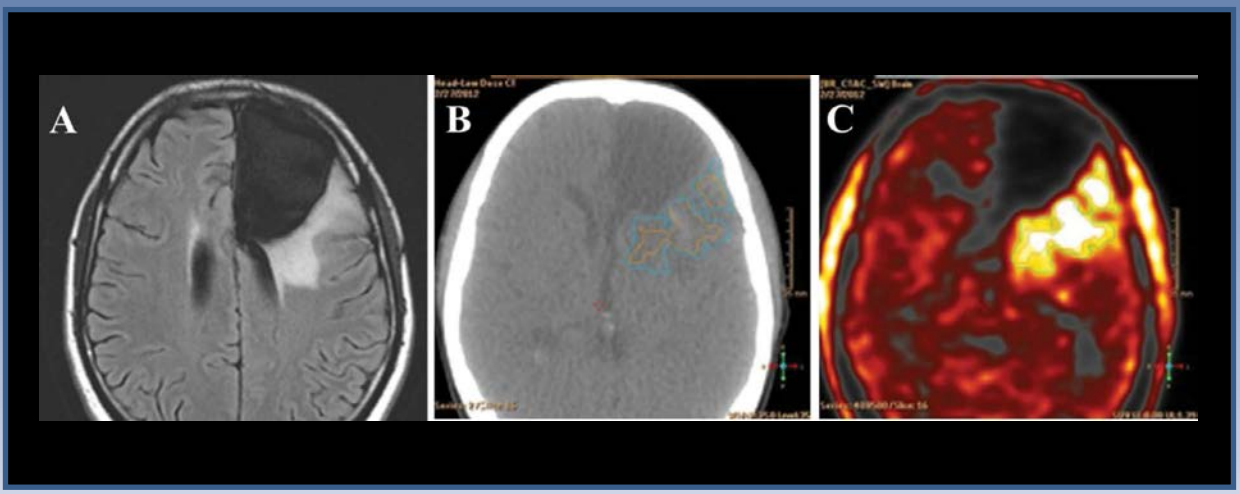

See page 16

ISSN 1506–9680

2019, Volume 22, Number 1

Journal of Polish Society of Nuclear Medicine

Journal of Hungarian Society of Nuclear Medicine

Journal of Serbian Society of Nuclear Medicine

VIA MEDICA

www.journals.viamedica.pl/nuclear_medicine_review

Nuclear Medicine
R · E · V · I · E · W

merged with ***Problems of Nuclear Medicine****

*Following the agreement concluded on 23 February 2011 between the Polish Society of Nuclear Medicine and Via Medica Sp. z o.o. the journal „Nuclear Medicine Review" has merged with „Problemy Medycyny Nuklearnej", a journal published since 1987.

Nuclear Medicine Review (ISSN 1506–9680) is published twice a year by VM Media sp. z o.o., VM Group sp. k., Grupa Via Medica
ul. Świętokrzyska 73, 80–180 Gdańsk, Poland
tel: (+48 58) 320 94 94, fax: (+48 58) 320 94 60; e-mail: redakcja@viamedica.pl, marketing@viamedica.pl
http://www.viamedica.pl

Advertising. For details on media opportunities within this journal please contact the advertising sales department, ul. Świętokrzyska 73, 80–180 Gdańsk, Poland
tel: (+48 58) 320 94 52, e-mail: marketing@viamedica.pl

The Editors accept no responsibility for the advertisement contents.

Single issues/advertising inquires should be addressed to VM Media sp. z o.o., VM Group sp. k., Grupa Via Medica, bank account:
Fortis Bank Polska SA o/Gdańsk 24 1600 1303 0004 1007 1035 9150 — PLN payment;
Fortis Bank Polska SA o/Gdańsk PL 15 1600 1303 0004 1007 1035 9021; SWIFT: PPABPLPK — EUR payment.

Single issues requests should be send to e-mail: prenumerata@viamedica.pl. Electronic orders option available at: www.nmr.viamedica.pl

18-0236.001.001

Indexation: Crossref, DOAJ (Directory of Open Access Journals), EMBASE, ESCI (Emerging Sources Citation Index), Index Copernicus (100.00), MEDLINE, Polish Medical Bibliography, Ministry of Science and Higher Education (12), Scopus, Ulrich's Periodicals Directory.

Editorial policies and author guidelines are published on journal website: www.journals.viamedica.pl/nuclear_medicine_review

Nuclear Medicine
R · E · V · I · E · W

merged with ***Problems of Nuclear Medicine****

2019, Volume 22, Number 1

Editorial V

Original articles

Agnieszka D. Kolasińska-Ćwikła, Sonia J. Konsek, John R. Buscombe, Katarzyna Maciejkiewicz, Andrzej Cichocki, Katarzyna Roszkowska-Purska, Łukasz Sawicki, Michał Tenderenda, Jarosław B. Ćwikła
The Value of Somatostatin Receptor Scintigraphy (SRS) in Patients with NETG1/G2 Pancreatic Neuroendocrine Neoplasms (p-NENs) 1

Andreas Fotopoulos, Konstantinos Papadimitropoulos, Athanasios Papadopoulos, Labros Lakkas, Maria Spiliotopoulou, Tzimis-Dimitrios Kotrotsios, Konstantinos Pappas, Athanasios Notopoulos, Chrissa Sioka
Myocardial ischemia in female patients with rheumatoid arthritis assessed with single photon emission tomography-myocardial perfusion imaging 8

Paulina Cegla, Krystyna Adamska, Ewa Wierzchosławska, Michał Smoleń, Witold Cholewiński
Comparison of ^{18}F-fluoroethylo-L-thyrosine PET/CT and MR in the diagnosis of primary brain tumors referred to radiation therapy 14

Anna Budzyńska, Sebastian Osiecki, Andrzej Mazurek, Stanisław Piszczek, Mirosław Dziuk
Feasibility of myocardial perfusion imaging studies in morbidly obese patients with a cadmium-zinc-telluride cardiac camera 18

Ahmed Elhussein, Mohamed Fawzy, Hany Abdel Rahman, Walid Omar, Elshaymaa Mohamed Hussein
Productivity of 18F-FDG-PET/CT Diagnostic Tool in the Management of Pediatric Lymphoblastic Lymphoma 23

Małgorzata Kobylecka, Łukasz Koperski, Witold Chudziński, Paweł Pihowicz, Joanna Mączewska, Maria Teresa Płazińska, Magdalena Bogdańska, Leszek Królicki
Relationship between parathyroid gland scintigraphy and its histopathology, oxyphil cell content and volume: a retrospective study 29

Clinical vignette

Katarzyna Jóźwik-Plebanek, Artur Dębski, Marek Cacko, Jacek Wnuk, Anna Teresińska
Chronic total occlusion of coronary artery without previous history of myocardial infarction: a role of spect 34

Zehra Pinar Koc, Pelin Özcan Kara, Ahmet Dağ, Ferah Tuncel Daloğlu
In-transit sentinel lymph nodes predicted by F-18 Fluorodeoxyglucose Positron Emission Tomography/Computed Tomography 37

Ramin Sadeghi, Sara Shakeri, Toktam Massoudi, Fatemeh Farahmandfar, Farnaz Nesari Javan
Multiple photopenic vertebrae in the bone scintigraphy of a young man with Gorham disease: CT and MRI correlation 40

Vincenzo Militano, Mark Hughes, Sobhan Vinjamuri, Nagabhushan Seshadri
Incidental detection of os acromiale mimicking a fracture on 18F-Fluoride PET-CT 43

VIA MEDICA

Nuclear Medicine Review 2019, 22, 1: V
DOI: 10.5603/NMR.2019.0010

ISSN 1506–9680

Editorial

Dear Sirs and Madams,

I would like to announce the first issue of "Nuclear Medicine Review" in 2019. The first chapter consists of six original articles. It opens with an article written by Polish colleagues who confirm that somatostatin receptor scintigraphy (SRS) with 99mTc HYNIC-TOC in SPECT or SPECT/CT techniques is an excellent tool for detection of primary neuroendocrine neoplasms G1/G2, assessment of the clinical stage of disease and follow up after treatment. The second article — by Greek researchers — shows that rheumatoid arthritis patients with atypical cardiac complaints are at higher risk of cardiovascular disease. Then, there are two papers from Poland. The first one indicates that PET/CT imaging with ^{18}F-fluoroethyl-L-tyrosine seems to have an additional value in the detection of recurring brain tumors and may be helpful in advanced radiation therapy planning. The second one shows that positive scintigraphy result depends on parathyroid histopathology and gland volume and does not depend on the presence of oxyphil cells.

From Egypt, we received a paper concluding that ^{18}F-FDG-PET/CT is a useful tool for disease extent evaluation of pediatric Lymphoblastic Lymphoma. It could provide a diagnostic hint for BM involvement. ^{18}F-FDG-PET/CT done after induction therapy has a good negative predictive value with higher specificity than CT alone, but is not an indication for treatment intensification due to false positive results. The next article is from Poland again. The authors indicate that the problem with heart mispositioning during imaging on the cadmium-zinc-telluride (CZT) camera affects less than 1% of all performed studies and morbid obesity is not a contraindication to perform myocardial perfusion scintigraphy with the use of such a camera.

The Clinical Vignette section includes four very interesting case presentations sent by our colleagues from the United Kingdom, Turkey, Iran and Poland.

At the end of my letter I would like to wish all of you, dear friends, a Happy New Year!

Yours faithfully,
Grzegorz Kamiński

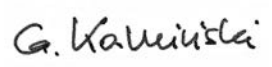

Editor-in-Chief
Nuclear Medicine Review

VIA MEDICA

Nuclear Medicine Review 2019, 22, 1: 1–7
DOI: 10.5603/NMR.a2018.0032

ISSN 1506–9680

Original

The Value of Somatostatin Receptor Scintigraphy (SRS) in Patients with NETG1/G2 Pancreatic Neuroendocrine Neoplasms (p-NENs)

Agnieszka D. Kolasińska-Ćwikła[1], Sonia J. Konsek[2], John R. Buscombe[3], Katarzyna Maciejkiewicz[1], Andrzej Cichocki[1], Katarzyna Roszkowska-Purska[1], Łukasz Sawicki[1], Michał Tenderenda[1], Jarosław B. Ćwikła[2]

[1]MSC Memorial Cancer Centre and Institute Maria Sklodowska-Curie, Warsaw, Poland
[2]School of Medicine, University of Warmia and Mazury, Olsztyn, Poland
[3]Addenbrookes Hospital; Cambridge, UK

Part of this study was presented during EANM 2017 and PNMS 2018

[Received 3 IX 2018; Accepted 12 IX 2018]

Abstract

BACKGROUND: Neuroendocrine neoplasms of the pancreas (p-NEN) are common gastro-entero-pancreatic neuroendocrine neoplasms (GEP-NENs). The aim of this retrospective study was to review the value of Somatostatin Receptor Scintigraphy (SRS) in initial detection of p-NEN, evaluation of tumour extent and as imaging follow-up after radical surgery in patients with confirmed well (NETG1) or moderately (NETG2) differentiated p-NEN based on pathological WHO 2017 classification.

MATERIAL AND METHODS: Overall 281 patients with confirmed p-NEN were enrolled. The SRS was performed to evaluate primary p-NEN, to assess clinical stage of disease, based on current World Health Organization (WHO) classification and during clinical follow-up. A total of 829 examinations were performed over time in these 281 patients using ^{99m}Tc HYNICTOC. Images were acquired between 1–3 h after i.v. injection of radiotracer. Initially whole body WB-SPECT and then WB-SPECT/CT with standard iterative reconstruction were used.

RESULTS: There were 159 patients with NETG1 (57%) and 122 subjects with NETG2 (43%). The female to male ratio was 1.1:1. In 68 patients (22%) with NETG1/G2 eighty-seven SRSs (10%) were performed to confirm initial diagnosis. SRS results were as follow: true positive (TP) = 84 (97%), false negative (FN) = 3 (3%), no true negative (TN) or false positive (FP) results of SRS examination (sensitivity of SRS per patient was 96%). In 198 subjects (66%) SRS was used in evaluation and re-evaluation of the clinical stage. A total of 661 (80%) examinations were carried out in these patients. There were TP = 514 (77%), TN = 136 (21%), FN = 7 (1%) and FP = 4 (1%) results. The sensitivity and specificity per patient were: 96% and 95%. The sensitivity and specificity per study were: 98% and 97%. In 35 patients (12%) SRS was used as imaging follow-up after radical surgery; there were overall 81 examinations (10%) performed. There were 76 (91%) TN results of SRS examinations and in 4 patients we identified recurrence (TP). In total, which consists of initial diagnosis/staging and patient follow-up, the sensitivity of SRS was 96% and specificity 97% per patient and per study sensitivity and specificity was 98%.

CONCLUSIONS: SRS using ^{99m}Tc HYNICTOC acquired in WB-SPECT or WB-SPECT/CT techniques is an excellent imaging modality in detection of primary NETG1/G2 p-NEN. Our study confirms that SRS has high sensitivity and specificity, as a result has tremendous value as an examination method to assess clinical stage of disease and as an imaging follow-up after radical treatment.

KEY words: neuroendocrine neoplasms of the pancreas, p-NENs, gastro-entero-pancreatic neuroendocrine neoplasms, GEP-NENs, Somatostatin Receptor Scintigraphy, SRS

Nucl Med Rev 2019; 22, 1: 1–7

Correspondence to: Agnieszka D. Kolasińska-Ćwikła, Klinika Onkologii, Centrum Onkologii — Instytut im. Marii Skłodowskiej-Curie; ul. Wawelska 15, Warszawa, tel.: 601359657, e-mail: adkolasinska@yahoo.com

Introduction

Neuroendocrine neoplasms (NENs) are a relatively rare, heterogeneous group of various neoplasms which develop from highly specialized neuroendocrine cells located in the entire body. Gastro-entero-pancreatic neuroendocrine neoplasms/tumours (GEP-NENs/NETs) comprise about 70% of all NENs, and about 2% of all neoplasms of the digestive system [1–3].

Neuroendocrine neoplasms of the pancreas (p-NEN) are common gastro-entero-pancreatic neuroendocrine neoplasms (GEP-NENs), which are clinically and functionally heterogeneous [4, 5]. Those tumours derive from the diffuse endocrine system (DES) cells which exist in the gastro-intestinal tract and in the pancreas [3]. According to the latest analysis of the Surveillance, Epidemiology, and End Results (SEER) database an annual incidence of p-NEN is 0.48 per 100,000 population and appears to be increasing in the new millennium, probably as a consequence of using high quality imaging techniques which lead to better and earlier detection of p-NEN [6, 7].

Pancreatic NENs can be functional and non-functional tumours. This classification of p-NENs is based on the presence or absence of clinical symptoms caused by hormonal over-secretion. It has been reported that 60–90% of p-NENs are non-functional (depending on which database is used) and as a result of their clinical silence they are usually diagnosed at more advanced clinical stages (CS) than those which present with a hormonal syndrome. In the case of metastatic disease at the time of initial diagnosis the possibility of a curative resection is limited, but still be considered even advanced disease [4, 5, 8].

The majority of p-NENs occur sporadically, as non-inherited tumours. However, a significant minority are associated with genetic syndromes such as multiple endocrine neoplasia type 1 (MEN1), von Hippel Lindau disease (VHL), von Recklinghausen's syndrome (neurofibromatosis 1), and tuberous sclerosis. Of those tumours which produce detectable hormones multiple insulinomas are less than 5%, gastrinomas from 20% up to 30% are associated with MEN1. In comparison to gastrinomas, glucagonomas and somatostatinomas, well-differentiated insulinomas show benign clinical behaviour and have a notably good prognosis in most of cases. More malignant insulinoma is seen in approximately 10% of cases [4, 5, 9, 10].

The majority of NENs have specific tissue characteristics which include expression of somatostatin receptors (SSTR). Numerous pNENs, including non-functional tumours except insulinomas, have high-level expression of SSTR among which SSTR subtype 2 is mainly expressed by β-cells with a slightly lower expression of SSTR5 mostly by β-cells [4, 7].

This means that p-NENs can be targeted by molecular imaging using somatostatin receptor imagining (SRI) and, as a result, SRS using ^{99m}Tc HYNICTOC has positive uptake for visualizing p-NENs [4, 5, 11–13].

When looking at the prognosis of any p-NEN, the histopathological grade (G) is vital. This grading divides NENs into three groups: tumours of low (G1), moderate (G2), and high (G3) malignancy. The criteria for the assessment of the "G" grading were firstly specified by European Neuroendocrine Tumour Society (ENETS) in 2006 [14] and then were supported by the World Health Organization (WHO). Currently the new pathological classification of NETG1 and NETG2 is used based on UICC/AJCC, which is a new version of previous one based on ENETS/WHO classification from 2010 [15]. The new classification of NENs, including p-NENs is presented in Table 1. Histological malignancy grading was based on two criteria, the first was number of mitotic figures and the second was Ki-67 proliferation index determined by immunohistochemical analysis of expression of MIB1 antibody provided in percentages. If there were differences using both criteria, Ki-67 was used as a preferential one [16]. According to the above classification, two main categories of GEP-NENs were distinguished. The first group includes well-differentiated neoplasms NETG1 and NETG2 with Ki-67 below 20%; the second group consists of poorly-differentiated NET G3 or neuroendocrine carcinomas (NEC) with Ki-67 above 20%.

Various imaging techniques such as computed tomography (CT), magnetic resonance imaging (MRI), ultrasonography (US), endoscopic ultrasonography (EUS), positron emission tomography (PET) and somatostatin receptor scintigraphy (SRS) are performed to localize primary pNENs, assess clinical stage (CS) of disease and also as imaging follow-up.

The following factors including: initial histological grade of p-NEN cells, secretion and presence of local and distant metastases are important in evaluation of clinical stage of disease and help multidisciplinary team (MDT) to plan further treatment of p-NEN [4].

Aim of the study

The aim of this retrospective study was to evaluate whether Somatostatin Receptor Scintigraphy (SRS) using whole body (WB) SPECT or WB-SPECT/CT techniques are effective tools in initial detection of p-NEN, evaluation of tumour extent and alters clinical management during clinical follow-up after radical surgery in

Table 1. Proposed NEN classification according to AJCC/UICC and WHO 2017

NEUROENDOCRINE NEOPLASMS, NEN			
Ki-67 < 20%		Ki-67 > 20%	
NET G1	NET G2	NET G3	NEC
	Well-differentiated tumours		Neuroendocrine cancers
Ki-67 < 3%	Ki-67 from 3% to 20%	Ki-67 > 20%, usually between 21% a 55%	Ki-67 > 21%, usually > 55% — large-cell cancers — small-cell cancers

patients with well (NETG1) or moderate (NETG2) differentiated p-NEN confirmed by pathology.

Material and methods

The protocol for this retrospective study was accepted by the institutional ethics committee. A total of 281 patients with confirmed neuroendocrine neoplasms of the pancreas were included. There were 148 females and 133 males (ratio 1.11:1). In all cases a pathologist specialized in NEN reported and verified the histology results, in each case. The histopathology reports comprised histological grade and the stage of the neuroendocrine neoplasm (TNM) according to AJCC/UICC 2017 classification. Patients and tumour characteristics are presented in Table 2.

In all subjects, diagnosis, treatment and further diagnostic/imaging approaches were discussed within a multidisciplinary team (MDT).

Somatostatin receptor scintigraphy (SRS) was performed to evaluate primary p-NEN, to assess clinical stage of disease, based on current AJCC/UICC classification, and during clinical follow-up. Overall 829 SRS examinations were performed.

In each case 550-740MBq of ^{99m}Tc HYNICTOC (Tektrotyd®; National Centre for Nuclear Research — Polatom, PL) was used. The detailed method of kit labelling with ^{99m}Tc has been described previously [17, 18]. Briefly, the peptide conjugates [HYNIC, Tyr^3] octreotide was synthesized by standard F-moc solid-phase synthesis [19] and used for kits manufacturing under aseptic conditions. The labelling yield exceeded 90% in all cases with the free pertechnetate content in the range of 3.63 ± 1.67% (TLC).

SRS images were acquired between 1 and 3 h after i.v. injection of radiotracer. Initially SRS was performed using a whole-body (WB) SPECT (Single Photon Emission Computed Tomography) method using Symbia-E gamma camera (Siemens Healthcare, IL; USA). Reconstruction algorithms were based on the ordered subset expectation maximization (OSEM), iterative reconstruction software (3D flash) on e-soft workstation. In each case using 30 iteration and 16 subsets, with standard Gaussian filter 9.0, recommended by manufacturer. In each case 128 x 128 matrix with approximately 64 projections (20 seconds per projection) over an 360° rotation were utilized, there was no attenuation correction (non AC).

Then SRS was performed using Discovery 670 Pro SPECT/CT system (GE Healthcare, WI, USA), based on WB-SPECT/CT method of examination. SPECT data was acquired using 128 x 128 matrix with approximately 60 projections (25 seconds per projection) over an 360° rotation. Computed tomography (CT) was performed without i.v. contrast enhancement. Reconstruction algorithms were based on iterative reconstruction algorithm: Evolution — OSEM

Table 2. Patients and tumour characteristics in well (G1) and moderate (G2) differentiated pNENs

	ALL, n = 281	NETG1, n = 159	NETG2, n = 122
Female to male ratio	1.11	1.01	1.26
Mean age (range) in initial diagnosis	54.86 (17-87)	55.23 (17-86)	54.29 (20-87)
Size of the tumour (pathology) mean (SD), mm	33.88 (± 26.22)	27.34 ± 23.62	43.21 ± 28.84
Ki-67 (mean, standard deviation)	4.17 ± 4.60	1.39 ± 1.28	7.89 ± 5.33
pT (initial), n = 281	n = 281	n = 159	n = 122
pT1 (%)	73 (26)	65 (41)	8 (7)
pT2 (%)	71 (25)	48 (30)	23 (19)
pT3 (%)	61 (22)	16 (10)	45 (37)
pT4 (%)	40 (14)	9 (6)	31 (25)
pTx or no data (%)	36 (13)	21 (13)	15 (12)
N base on surgery, n = 281	n = 281	n = 159	n = 122
N0 (%)	126 (45)	95 (60)	31 (25)
N1 (%)	122 (43)	37 (23)	85 (70)
Nx or no data (%)	33 (12)	27 (17)	6 (5)
M base on surgery/follow-up/imaging, n = 281	n = 281	n = 159	n = 122
M0 (%)	139 (49)	97 (61)	42 (34)
M1 (%)	102 (36)	32 (20)	70 (57)
Mx or no data (%)	40 (14)	30 (19)	10 (8)
CS (initial), n = 281	n = 281	n = 159	n = 122
I — IIIa — local (%)	145 (52)	115 (72)	30 (25)
IIIb — regional (%)	33 (12)	13 (8)	20 (16)
IV — distal (%)	103 (37)	31 (19)	72 (59)
Metastases			
Liver (%)	97 (35)	26 (16)	71 (58)
Bones (%)	13 (5)	4 (3)	9 (7)
Lungs (%)	5 (2)	2 (1)	3 (2)

(with resolution recovery) including 4 iterations and 10 subsets with standard Gaussian filter using in each case a Xeleris workstation.

Each SRS was defined as pathological if any focal or diffuse non-physiological accumulation was recognized during examination. Diffuse low-activity intestinal uptake on SRS was defined as non-specific, physiologic bowel uptake. Lesions were assessed due to their intensity of accumulation using the Krenning scale, similar to the standard SRS using Octreoscan™ evaluation. In each case, the Krenning extension of disease was used to classify the extension of the tumour, both methods have been described previously [18–20].

SRS was read by two specialists in nuclear medicine and was interpreted as true positive (TP) when the patient had histologically confirmed p-NEN and there were at least Krenning 2 focal pathologically high uptake of radiotracer. True negative (TN) result was associated with no focal uptake of radiotracer on SRS and no evidence of the presence of disease during at least 12-month follow-up, clinically and on other imaging techniques, including endoscopic ultrasound (EUS), CT and magnetic resonance imaging (MRI) before and after i.v. contrast administration. A false positive (FP) was reported when there was focal high uptake on SRS (at least Krenning 2), but there was no evidence of p-NEN on other imaging techniques, clinically and during clinical and imaging follow-up. A false negative (FN) study was defined when there was confirmable tumour (p-NEN) which was not seen in SRS.

Histological and clinical information including assessment of tumour type based on ACJJ/UICC 2017 classification, including Ki-67 and the initial clinical stage (CS) of disease were available for analysis.

Statistical analysis

The standard statistics using sensitivity, specificity PPV and NPV were used based on pathology reports as gold standard. If no specimen of tumour was available, clinical, biochemical and structural imaging were used to assess final results of examination. In case of negative SRS study and presence of any suspected lesions, patients were evaluated based on clinical follow-up. Differences between groups were assessed using non-parametric Mann-Whitney U test. In each case $P < 0.05$ was defined as significant.

Results

There were 159 subjects with NETG1 (57%) and 122 subjects with NETG2 (43%). In patients with NETG1 the mean age was 55.23 years (range 17–86) and in subjects with NETG2 the mean age was 54.29 (range 20–87). The mean size of the tumour (based on histopathology) were as follows: in NETG1 — 27.34 mm (SD ± 23.62), in NETG2 — 43.21 mm (SD ± 28.84). The mean Ki-67 proliferation index was 1.39 % (SD ± 1.28) in patients with NETG1 and 7.89 % (SD ± 5.33) in those with NETG2. In 54 cases there were no data regarding Ki-67 index and in 103 subjects no information about size of the tumours was available in histopathology reports; in those patients tumour size evaluation was based on structural imaging CT/MRI or EUS.

The image quality of SRS using ^{99m}Tc HYNICTOC was determined by both readers (JRB & JBC) to be excellent or very good; in the cases with small tumours the visualization was difficult but still clear enough to make a diagnosis of p-NET.

The analysis shows that tumours of pT1 and pT2 were usually identified in subjects with NETG1. We detected pT1 tumours in 65 cases with NETG1 (41%) and only 8 with NETG2 (7%) ($P < 0.05$), pT2 in 48 subjects with NETG1 (30%) and in 23 with NETG2 (19%) ($P > 0.05$). In comparison, pT3 and pT4 tumours most frequently occurred in patients with NETG2. We noted pT3 tumours in 45 cases with NETG2 (37%) and in 16 with NETG1 (10%), pT4 in 31 subjects with NETG2 (25%) and in 9 with NETG1 (6%) (Table 2).

The analysis of regional lymph nodes metastasis in patients after surgical treatment revealed no lymph nodes involvement in 126 cases, including 95 with NETG1 (60%) and 31 with NETG2 (25%). There were 122 subjects with metastasis in a single regional lymph (N1), in 37 patients with NETG1 (23%) and in 85 with NETG2 (70%). There were 33 (12%) patients in whom regional lymph nodes could not be assessed (Table 2).

Distant metastasis (M) were noted in 102 patients, in 32 with NETG1 (20%) and in 70 with NETG2 (57%). There were 139 cases with no evidence for metastases. In 40 subjects metastases could not be assessed. There were 97 (35%) patients with metastasis to the liver, including 71 with NETG2 (58%) and 26 with NETG1 (16%). Thirteen subjects (5%) had bone metastases and in 5 (2%) patients we detected lung metastasis (Table 2).

The assessment of clinical stage (CS) revealed that there were 145 patients (52%) with I-IIIa CS, 115 with NETG1 (72%) and 30 with NETG2 (25%). In 33 cases (12%) we noted IIIb CS, in 13 with NETG1 (8%) and in 20 with NETG2 (16%). There were 103 subjects (37%) with IV CS, which included 72 (59%) patients with NETG2 and rest with NETG1 (19%) (Table 2).

In 68 patients (22%) SRS was used to confirm the initial diagnosis and 87 (10%) SRS were carried out. In this group of patients, the results were as follows: true positive (TP) = 84 (97%), false negative (FN) = 3 (3%), no true negative (TN) or false positive (FP) results of SRS examination (sensitivity of SRS per patient was 96%). In 198 subjects (66%) SRS was used in evaluation of the clinical stage and overall 661 (80%) examination were performed. The following results were obtained: TP = 514 (77%), TN = 136 (21%), FN = 7 (1%) and FP = 4 (1%).

The sensitivity and specificity per patient were: 96% and 95%. The sensitivity and specificity per study were 98% and 97%. In 35 patients (12%) SRS was used as imaging follow-up after radical surgery; a total of 81 examinations (10%) were carried out. There were 76 (91%) TN results of SRS and in 4 patients we identified recurrence (TP). In total, which consists of initial diagnosis/staging and follow-up, the sensitivity was 96% and specificity 97% per patient and per study sensitivity and specificity was 98%. Summarized SRS results in all groups of patients are presented in Table 3.

Discussion

As a consequence of recent advances in imaging technology and having better knowledge of p-NENs, the diagnosis and treatment approaches of asymptomatic and symptomatic pNENs have improved. Various structural imaging such as CT, MRI and endoscopic ultrasound (EUS), as well as functional techniques such as somatostatin receptor imaging are currently utilized to localize

Table 3. Results of Somatostatin Receptor Scintigraphy examinations in diagnosis group, staging group and follow-up group

Results of SRS	SRS studies	Diagnosis group, n = 68		Staging group, n = 198		Follow-up group, n = 35	
		NET G1	NET G2	NET G1	NET G2	NET G1	NET G2
TP	602 (73%)	69 (80%)	15 (17%)	216 (33%)	298 (45%)	0	4 (5%)
TN	212 (26%)	0	0	102 (15%)	34 (5%)	51 (63%)	25 (31%)
FN	11 (1%)	2 (2%)	1 (1%)	6 (1%)	1 (< 1%)	0	1 (1%)
FP	4 (< 1%)	0	0	3 (< 1%)	1 (< 1%)	0	0
All	829 (100%)	71 (82%)	16 (18%)	327 (49%)	334 (51%)	51 (63%)	30 (37%)
		87 (10%)		661 (80%)		81 (10%)	

	Diagnosis (n)	Staging (n)	Follow-up (n)	All (%)
NETG1	54	92	13	159 (56.6)
NETG2	15	102	5	122 (43.4)
NETG3	0	0	0	0
SUMA	69	194	18	281

the primary tumour, assess clinical stage (CS) of disease and also as follow-up imaging after radical surgery [2–5].

CT and MRI have a relatively low sensitivity in detecting of low volume disease or multifocality of disease, both of which are common in patients with MEN1 syndrome associated with pNENs. Whilst EUS, which is currently the best method for detection of any focal pancreatic lesions, has a better resolution and sensitivity, it has a limited field of view. It provides very good visualization of the head and body of the pancreas, but the distal part of the pancreatic tail could be problematic in detection of small tumours. Local clinical staging only can be achieved using EUS; therefore, it should be combined with other tests.

In the last 2 decades it has been found that functional imaging of p-NEN plays a key role in evaluation of patients with suspected or confirmed NEN. Numerous studies have demonstrated that the current significance of somatostatin receptor imaging, including SRS, especially using SPECT/CT or PET/CT [4, 17–24]. In our data sets we indicated high accuracy of both the WB-SPECT or WB-SPECT/CT techniques in detection of active disease in patients with p-NEN. To our knowledge, it is the largest series of patients with confirmed NETG1 and NETG2 p-NENs, based on new classification ACJJ/UICC. It has been our standard clinical practice to perform SRS (WB-SPECT/CT) using ^{99m}Tc HYNICTOC as the main imaging technique used for detection of primary p-NENs, staging of disease and in subjects who had previously undergone radical surgery. This approach has been explored by our team for at least previous 14 years [25–27].

Various studies indicated that PET/CT with ^{68}Ga labelled somatostatin analogues is immensely sensitive and has a high specificity for localizing p-NENs [4, 28–29]. Generally, when performing PET/CT using ^{68}Ga SST analogues in greater number of studies for p-NENs, the sensitivity varies from 86% up to 100% and the specificity from 79% up to 100% and is superior to MRI with DWI [30]. But this technique has a limitation which is the detection of insulinomas — the sensitivity decreases to 25% [31]. In addition, access to PET/CT and the ^{68}Ga analogues may be limited.

Most comparative studies used planar ^{111}In pentetreotide and compare to tomographic ^{68}Ga PET/CT, which is methodologically incorrect, because these studies do not compare like with like. Only a few reports compare SRS using ^{99}Tc HYNICTOC vs. ^{68}Ga DOTA-TOC/TATE/NOC. In all these studies SPECT was compared to PET, but SPECT was not performed using current state-of-the-art imaging techniques such as iterative reconstruction and WB-SPECT/CT attenuation correction reconstruction technique, except single recent study which indicated clinical decision change in the one third of cases [32]. However, the authors did not use optimized reconstruction methods with the SPECT/CT.

Compared to previously published studies using ^{68}Ga DOTA-TOC/TATE PET/CT the results of our study, showing a sensitivity and specificity which was always equal or greater than 95% in all group of patients with confirmed p-NETs, shows that, if optimized, the SPECT/CT-based agents compare well with PET. This is particularly true in our study because we have the results of a large number of studies performed in in a large cohort of pNET patients. This clearly indicated the high level of accuracy of SRS using ^{99m}Tc HYNICTOC in this patient group. However, the high prevalence of disease means we can be more certain of the sensitivity than the specificity.

The approach described in our study using ^{99m}Tc HYNICTOC is also cheaper than using PET/CT and can be performed on any working day in most Nuclear Medicine departments. Thus, this technology seems to have a practical advantage compared to quite complicated and expensive PET/CT using ^{68}Ga SST analogues The authors acknowledge that although ^{68}Ga DOTA-TOC/TATE PET/CT is currently is the best functional methods in detection p-NEN, its utility is restricted not just by cost but the need to access a PET/CT scanner and the current shortage of the required gallium/germanium generators.

The results of our study show that SRS with ^{99m}Tc HYNICTOC using the best in SPECT/CT is a highly sensitive and specific imaging technique. According to our results, the high sensitivity of the test per patient was noted in the group of subjects in whom SRS

was performed to assess initial diagnosis. As a consequence, ^{99m}Tc HYNICTOC SRS helped correctly identify those patients without the disease. Therefore, this method can be used to assess the localization and extension of tumour when functional p-NENs are suspected but tumours cannot be detected on cross-sectional images such as CT or MRI. Our data also confirm that ^{99m}Tc HYNICTOC SRS is an appropriate tool in evaluation of clinical stage of disease and in follow-up of pNENs.

A further advantage in using ^{99m}Tc HYNICTOC is the lower radiation exposure compared to standard 111In-pentetreotide (Octreoscam®). The agent is cleared rapidly from the blood; most of the activity is eliminated entirely through the kidneys (64% of the injected dose within 12 h). The effective dose is 0.005 mSv/MBq, which for a patient receiving the recommended maximum administered activity of 740 MBq is only 3.8 mSv [33].

This compares favourably to ^{111}In-pentetreotide which is also cleared rapidly from the blood, with excretion almost entirely through the kidneys giving an effective dose is 0.054 mSv/MBq. For a patient recommended maximum administered activity of 222 MBq is 12 mSv, which is over 3 times higher than with ^{99m}Tc HYNICTOC [34]. The radiation dose in 70 kg patient from ^{68}Ga-DOTATOC/TATE is approximately 2.9–3.2 mSv, which is similar to radiation dose of ^{99m}Tc HYNICTOC [35, 36]. A modern CT used as part of the PET/CT or SPECT/CT will contribute an additional 2mSv to the total effective dose. [34].

Conclusions

The results from this study show the SRS using ^{99m}Tc HYNICTOC acquired in WB-SPECT or WB-SPECT/CT techniques delivers high-accuracy results in the detection of primary well (NETG1) and moderate (NETG2) differentiated p-NEN. It is more widely available than ^{68}Ga-DOTATOC/TATE PET but yields similar results at a lower cost. Furthermore, it is excellent method for the assessment of clinical stage of pNEN and in imaging follow-up in patients after radical surgery.

References

1. Ellis L, Shale MJ, Coleman MP. Carcinoid tumors of the gastrointestinal tract: trends in incidence in England since 1971. Am J Gastroenterol. 2010; 105(12): 2563–2569, doi: 10.1038/ajg.2010.341, indexed in Pubmed: 20823835.
2. Garcia-Carbonero R, Sorbye H, Baudin E, et al. Vienna Consensus Conference participants. ENETS Consensus Guidelines for High-Grade Gastroenteropancreatic Neuroendocrine Tumors and Neuroendocrine Carcinomas. Neuroendocrinology. 2016; 103(2): 186–194, doi: 10.1159/000443172, indexed in Pubmed: 26731334.
3. Kos-Kudła B, Blicharz-Dorniak J, Strzelczyk J, et al. Consensus Conference, Polish Network of Neuroendocrine Tumours. Diagnostic and therapeutic guidelines for gastro-entero-pancreatic neuroendocrine neoplasms (recommended by the Polish Network of Neuroendocrine Tumours). Endokrynol Pol. 2017; 68(2): 79–110, doi: 10.5603/EP.2017.0015, indexed in Pubmed: 28597909.
4. Falconi M, Eriksson B, Kaltsas G, et al. Vienna Consensus Conference participants. ENETS Consensus Guidelines Update for the Management of Patients with Functional Pancreatic Neuroendocrine Tumors and Non-Functional Pancreatic Neuroendocrine Tumors. Neuroendocrinology. 2016; 103(2): 153–171, doi: 10.1159/000443171, indexed in Pubmed: 26742109.
5. Kos-Kudła B, Rosiek V, Borowska M, et al. Pancreatic neuroendocrine neoplasms - management guidelines (recommended by the Polish Network of Neuroendocrine Tumours). Endokrynol Pol. 2017; 68(2): 169–197, doi: 10.5603/EP.2017.2016, indexed in Pubmed: 28540973.
6. Dasari A, Shen C, Halperin D, et al. Trends in the Incidence, Prevalence, and Survival Outcomes in Patients With Neuroendocrine Tumors in the United States. JAMA Oncol. 2017; 3(10): 1335–1342, doi: 10.1001/jamaoncol.2017.0589, indexed in Pubmed: 28448665.
7. Auernhammer CJ, Spitzweg C, Angele MK, et al. Advanced neuroendocrine tumours of the small intestine and pancreas: clinical developments, controversies, and future strategies. Lancet Diabetes Endocrinol. 2018; 6(5): 404–415, doi: 10.1016/S2213-8587(17)30401-1, indexed in Pubmed: 29229497.
8. Halfdanarson TR, Rabe KG, Rubin J, et al. Pancreatic neuroendocrine tumors (PNETs): incidence, prognosis and recent trend toward improved survival. Ann Oncol. 2008; 19(10): 1727–1733, doi: 10.1093/annonc/mdn351, indexed in Pubmed: 18515795.
9. Jensen RT, Berna MJ, Bingham DB, et al. Inherited pancreatic endocrine tumor syndromes: advances in molecular pathogenesis, diagnosis, management, and controversies. Cancer. 2008; 113(7 Suppl): 1807–1843, doi: 10.1002/cncr.23648, indexed in Pubmed: 18798544.
10. Ito T, Igarashi H, Nakamura K, et al. Causes of death and prognostic factors in multiple endocrine neoplasia type 1: a prospective study: comparison of 106 MEN1/Zollinger-Ellison syndrome patients with 1613 literature MEN1 patients with or without pancreatic endocrine tumors. Medicine (Baltimore). 2013; 92(3): 135–181, doi: 10.1097/MD.0b013e3182954af1, indexed in Pubmed: 23645327.
11. Braun M. The Somatostatin Receptor in Human Pancreatic -Cells. Vitam Horm. 2014: 165–193, doi: 10.1016/b978-0-12-800174-5.00007-7.
12. Ballian N, Brunicardi FC, Wang XP. Somatostatin and its receptors in the development of the endocrine pancreas. Pancreas. 2006; 33(1): 1–12, doi: 10.1097/01.mpa.0000226894.16817.e8, indexed in Pubmed: 16804406.
13. Hankus J, Tomaszewska R. Neuroendocrine neoplasms and somatostatin receptor subtypes expression. Nucl Med Rev Cent East Eur. 2016; 19(2): 111–117, doi: 10.5603/NMR.2016.0022, indexed in Pubmed: 27479788.
14. Rindi G, Klöppel G, Alhman H, et al. all other Frascati Consensus Conference participants, European Neuroendocrine Tumor Society (ENETS). TNM staging of foregut (neuro)endocrine tumors: a consensus proposal including a grading system. Virchows Arch. 2006; 449(4): 395–401, doi: 10.1007/s00428-006-0250-1, indexed in Pubmed: 16967267.
15. Brierley JD, Gospodarowicz MK, Wittekind C. TNM Classification of Malignant Tumours. UICC 8th Edition. Wiley Blackwell 2017.
16. Klimstra DS, Modlin IR, Coppola D, et al. The pathologic classification of neuroendocrine tumors: a review of nomenclature, grading, and staging systems. Pancreas. 2010; 39(6): 707–712, doi: 10.1097/MPA.0b013e3181ec124e, indexed in Pubmed: 20664470.
17. Decristoforo C, Melendez-Alafort L, Sosabowski JK, et al. 99mTc-HYNIC-[Tyr3]-octreotide for imaging somatostatin-receptor-positive tumors: preclinical evaluation and comparison with 111In-octreotide. J Nucl Med. 2000; 41(6): 1114–1119, indexed in Pubmed: 10855644.
18. Cwikla JB, Mikolajczak R, Pawlak D, et al. Initial direct comparison of 99mTc-TOC and 99mTc-TATE in identifying sites of disease in patients with proven GEP NETs. J Nucl Med. 2008; 49(7): 1060–1065, doi: 10.2967/jnumed.107.046961, indexed in Pubmed: 18552141.
19. Storch D, Béhé M, Walter MA, et al. Evaluation of [99mTc/EDDA/HYNIC0] octreotide derivatives compared with [111In-DOTA0,Tyr3, Thr8]octreotide and [111In-DTPA0]octreotide: does tumor or pancreas uptake correlate with the rate of internalization? J Nucl Med. 2005; 46(9): 1561–1569, indexed in Pubmed: 16157541.
20. Kwekkeboom DJ, Kam BL, van Essen M, et al. Somatostatin-receptor-based imaging and therapy of gastroenteropancreatic neuroendocrine tumors. Endocr Relat Cancer. 2010; 17(1): R53–R73, doi: 10.1677/ERC-09-0078, indexed in Pubmed: 19995807.

21. Sharma P, Arora S, Dhull VS, et al. Evaluation of (68)Ga-DOTANOC PET/CT imaging in a large exclusive population of pancreatic neuroendocrine tumors. Abdom Imaging. 2015; 40(2): 299–309, doi: 10.1007/s00261-014-0219-5, indexed in Pubmed: 25134801.
22. Sharma P, Arora S, Mukherjee A, et al. Predictive value of 68Ga-DOTANOC PET/CT in patients with suspicion of neuroendocrine tumors: is its routine use justified? Clin Nucl Med. 2014; 39(1): 37–43, doi: 10.1097/RLU.0000000000000257, indexed in Pubmed: 24152621.
23. Treglia G, Castaldi P, Rindi G, et al. Diagnostic performance of Gallium-68 somatostatin receptor PET and PET/CT in patients with thoracic and gastroenteropancreatic neuroendocrine tumours: a meta-analysis. Endocrine. 2012; 42(1): 80–87, doi: 10.1007/s12020-012-9631-1, indexed in Pubmed: 22350660.
24. Rufini V, Baum RP, Castaldi P, et al. Role of PET/CT in the functional imaging of endocrine pancreatic tumors. Abdom Imaging. 2012; 37(6): 1004–1020, doi: 10.1007/s00261-012-9871-9, indexed in Pubmed: 22422069.
25. Cwikla JB, Nasierowska-Guttmejer A, Jeziorski KG, et al. Diagnostic imaging approach to gastro-entero-pancreatic carcinomas of neuroendocrine origin - single NET center experience in Poland. Neuro Endocrinol Lett. 2007; 28(6): 789–800, indexed in Pubmed: 18063942.
26. Michałowska I, Ćwikła JB, Pęczkowska M, et al. Usefulness of Somatostatin Receptor Scintigraphy (Tc-[HYNIC, Tyr3]-Octreotide) and 123I-Metaiodobenzylguanidine Scintigraphy in Patients with SDHx Gene-Related Pheochromocytomas and Paragangliomas Detected by Computed Tomography. Neuroendocrinology. 2015; 101(4): 321–330, doi: 10.1159/000381458, indexed in Pubmed: 25791839.
27. Skowrońska A, Bednarczuk T, Podgórska J, et al. Diagnostic difficulties in neuroendocrine tumours — intrahepatic accessory spleen. Nucl Med Rev Cent East Eur. 2017; 20(2): 103–104, doi: 10.5603/NMR.2017.0017.
28. Ambrosini V, Campana D, Bodei L, et al. 68Ga-DOTANOC PET/CT clinical impact in patients with neuroendocrine tumors. J Nucl Med. 2010; 51(5): 669–673, doi: 10.2967/jnumed.109.071712, indexed in Pubmed: 20395323.
29. Wild D, Bomanji JB, Benkert P, et al. Comparison of 68Ga-DOTANOC and 68Ga-DOTATATE PET/CT within patients with gastroenteropancreatic neuroendocrine tumors. J Nucl Med. 2013; 54(3): 364–372, doi: 10.2967/jnumed.112.111724, indexed in Pubmed: 23297077.
30. Schmid-Tannwald C, Schmid-Tannwald CM, Morelli JN, et al. Comparison of abdominal MRI with diffusion-weighted imaging to 68Ga-DOTATATE PET/CT in detection of neuroendocrine tumors of the pancreas. Eur J Nucl Med Mol Imaging. 2013; 40(6): 897–907, doi: 10.1007/s00259-013-2371-5, indexed in Pubmed: 23460395.
31. Sharma P, Arora S, Karunanithi S, et al. Somatostatin receptor based PET/CT imaging with 68Ga-DOTA-Nal3-octreotide for localization of clinically and biochemically suspected insulinoma. Q J Nucl Med Mol Imaging. 2016; 60(1): 69–76, indexed in Pubmed: 24740163.
32. Kunikowska J, Lewington V, Krolicki L. Optimizing Somatostatin Receptor Imaging in Patients With Neuroendocrine Tumors: The Impact of 99mTc-HYNICTOC SPECT/SPECT/CT Versus 68Ga-DOTATATE PET/CT Upon Clinical Management. Clin Nucl Med. 2017; 42(12): 905–911, doi: 10.1097/RLU.0000000000001877, indexed in Pubmed: 29076910.
33. Grimes J, Celler A, Birkenfeld B, et al. Patient-specific radiation dosimetry of 99mTc-HYNIC-Tyr3-octreotide in neuroendocrine tumors. J Nucl Med. 2011; 52(9): 1474–1481, doi: 10.2967/jnumed.111.088203, indexed in Pubmed: 21795364.
34. Sundin A, Arnold R, Baudin E, et al. Antibes Consensus Conference participants. ENETS Consensus Guidelines for the Standards of Care in Neuroendocrine Tumors: Radiological, Nuclear Medicine & Hybrid Imaging. Neuroendocrinology. 2017; 105(3): 212–244, doi: 10.1159/000471879, indexed in Pubmed: 28355596.
35. Velikyan I, Sundin A, Sörensen J, et al. Quantitative and qualitative intrapatient comparison of 68Ga-DOTATOC and 68Ga-DOTATATE: net uptake rate for accurate quantification. J Nucl Med. 2014; 55(2): 204–210, doi: 10.2967/jnumed.113.126177, indexed in Pubmed: 24379222.
36. Pettinato C, Sarnelli A, Di Donna M, et al. 68Ga-DOTANOC: biodistribution and dosimetry in patients affected by neuroendocrine tumors. Eur J Nucl Med Mol Imaging. 2008; 35(1): 72–79, doi: 10.1007/s00259-007-0587-y, indexed in Pubmed: 17874094.

Original
Nuclear Medicine Review 2019, 22, 1: 8–13
DOI: 10.5603/NMR.2019.0001

ISSN 1506–9680

VIA MEDICA

Myocardial ischemia in female patients with rheumatoid arthritis assessed with single photon emission tomography--myocardial perfusion imaging

Andreas Fotopoulos[1] MD, PhD, Konstantinos Papadimitropoulos[1] MD, Athanasios Papadopoulos[2] MSc, PhD, Labros Lakkas[3] MD, Maria Spiliotopoulou[1] MD, Tzimis-Dimitrios Kotrotsios[1] MD, Konstantinos Pappas[3] MD, PhD, Athanasios Notopoulos[1] MD, PhD, Chrissa Sioka[1] MD, PhD

[1]Department of Nuclear Medicine, University Hospital of Ioannina, Greece
[2]Department of Medical Physics, University Hospital of Ioannina, Greece
[3]Department of Cardiology, University Hospital of Ioannina, Greece

[Received 23 IX 2018; Accepted 18 I 2019]

Abstract

BACKGROUND: Non-specific cardiac symptoms in female patients with rheumatoid arthritis (RA) could indicate early cardiovascular disease.

MATERIALS AND METHODS: Myocardial perfusion imaging (MPI), with 99mTc tetrofosmin stress–rest single photon emission computer tomography (SPECT), in 13 RA female patients with atypical cardiac symptoms, was compared to 44 weight- and age-matched females with similar cardiac complaints (control group). Smoking, hypertension, diabetes mellitus, dyslipidemia, obesity and cardiac heredity were recorded and compared between the study and control group. MPI was assessed using 17 segment polar map and with a scale of 0 to 5 scoring.

RESULTS: Patients with RA demonstrated higher cardiovascular risk (46%) compared to control individuals (17%). In addition, patients with RA had more irreversible myocardial ischemic abnormalities in their MPI than the control group. Dyslipidemia and obesity was found more frequent in RA patients with MPI SSS $\geq$ 4.

CONCLUSION: RA patients with atypical cardiac complaints are at higher risk for cardiovascular disease; early detection and monitoring of this patient group could potentially reverse or successfully manage the consequences of the upcoming cardiovascular disease.

KEY words: myocardial perfusion imaging, myocardial ischemia, tetrofosmin, risk factors, females, rheumatoid arthritis

Nucl Med Rev 2019; 22, 1: 8–13

Introduction

Rheumatoid arthritis (RA) is an inflammatory disease involving multiple systems that predominantly cause joint destruction but also affect extra-articular organs resulting in significant functional disabilities and reduced quality of life [1–4]. Patients with either RA or other chronic inflammatory rheumatoid diseases may develop progressive cardiovascular disease [5]. These cardiovascular complications consist of increased rate of coronary artery disease and systemic atherosclerosis [6].

Correspondence to: Andreas Fotopoulos, MD, PhD, Professor, Department of Nuclear Medicine, University Hospital of Ioannina, 1 Stavrou Niarchou Street, Ioannina 45110, Greece, Phone: +30-26510-99377, Email: professor.fotopoulos@yahoo.com

Several cardiovascular imaging modalities exist, such as nuclear imaging, cardiac computed tomography and carotid ultrasonography, to evaluate patients with increased cardiovascular risk [7]. Myocardial perfusion imaging (MPI), employing single photon emission tomography (SPECT), is a highly reliable imaging method to assess myocardial ischemia. Its sensitivity has been reported to reach 85%, specificity of 83%, positive predictive value of 66%, negative predictive value of 94% and accuracy of 84% [8]. Myocardial perfusion imaging with pharmacologic stress may represent the imaging test of choice in female patients with reduced exercise capability such as the RA patients, reaching sensitivity of 80–85% and specificity of 84–93% [9].

Several risk factors have been linked to coronary-artery disease in RA patients. Metabolic syndrome seems to exist in a higher rate in patients with RA, consisted of 31% in patients with early RA and 42% in patients with long-standing RA, compared to only 11% in

Table 1. Characteristics of the patients (median, min-max), information concerning cardiac risk factors and myocardial perfusion imaging

Characteristics	Patients (#13)	Control group (#44)	P
Age (median, ± SD)	67.8 ± 8.34	67.5 ± 7.53	NS
Weight	71.85 (53–90)	70.98 (54–93)	NS
Smoking	3 (23.1%)	4 (9.1%)	0.038
Hypertension	10 (76.9%)	34 (77.3%)	NS
Diabetes Mellitus	2 (15.4%)	10 (22.7%)	NS
Dyslipidemia	9 (69.2%)	29 (65.9%)	NS
Obesity	3 (23.1%)	11 (25.0%)	NS
Cardiac Heredity	5 (38.5%)	16 (36.4%)	NS
MPI SSS < 4	7 (53.8%)	37 (84.1%)	0.022*
MPI SSS ≥ 4	6 (46.2%)	7 (15.9%)	0.004*

MPI: myocardial perfusion imaging; b. SSS: summed stress score; c. NS: non-significant; d. SD: standard deviation; e. * $p \leq 0.05$ was considered to be statistically significant

matched control individuals [10]. Thus, early detection of metabolic syndrome and control of risk factors such as smoking, dyslipidemia, hypertension, and obesity is warranted in RA patients [6]. Traditional risk factors for cardiovascular disease seem to confer the same risk for either RA or non-RA patients [11, 12].

In this retrospective study, we evaluated the rate of myocardial ischemia and the role of cardiac risk factors, after using –99mTc-TF-SPECT MPI in female patients with rheumatoid arthritis and compared them to an age and weight matched control group.

Patients and methods

Study Participants

An extensive request in the medical records of the Nuclear Medicine Department of our University Hospital between 2011 and 2016 has been achieved summing up patients with RA who were subjected to myocardial perfusion imaging with 99m Tc tetrofosmin in stress–rest single photon emission computer tomography (MPI – 99mTc-TF-SPECT). For retrieving specific data, inclusion criteria were applied such as no other disease existed than RA, atypical cardiac complaints such as chest wall pain, palpitations, without known cardiac disease, and negative electrocardiograph (ECG). We found 16 patients with RA who underwent the test, 13 females and 3 males. All patients followed one day protocol. The stress protocol was either pharmacological or Bruce treadmill exercise test. Patients when subjected to 99mTc-TF-SPECT MPI were routinely recorded with ECG at the beginning and continuously monitored during stress time. Any changes in ECG were noted in the medical charts. The imaging protocol used for 99mTc-TF-SPECT MPI has been described in our previous studies [13, 14] and performed according to published guidelines [15]. According to our search, only three male patients were found and finally excluded from the study due to their minimal contribution to the whole dataset, and thus, only the 13 females were evaluated. For the selection of the healthy individuals, 120 female patients that underwent the same test without positive RA diagnosis were initially selected to form the control group. These females had the test for atypical cardiac complaints such as nonspecific chest pain or palpitations with no medical disease, negative history for cardiac disease, negative clinical evaluation and negative ECG prior to MPI. Among these females, 44 were age- and weight-matched with the RA patients and finally selected to form the control group. In both groups, major cardiovascular risk factors were recorded, including smoking when either active or ceased within the last 3 months prior to the test, hypertension and/or diabetes mellitus and/or dyslipidemia, obesity and family history of cardiovascular disease.

This retrospective study was performed after approval by the Hospital's Clinical Research Committee. As a retrospective analysis of MPI data, prior written patients consent was not obtained since it was not required by our Hospital's Clinical Research Committee. All subjects were blinded during statistical analysis.

MPI evaluation

For MPI evaluation, two nuclear medicine physicians independently evaluated the images, and a third nuclear medicine physician participated when a difference in MPI scoring among the two nuclear medicine physicians existed. Scoring was evaluated with a 17-segment polar map, [16] with a scale of 0 to 5, according to the severity of the myocardial perfusion deficit. Thus, when there was normal isotope uptake by the total area of myocardium. the score was 0. When there was a mild decreased activity, the score recorded as 1. Mild to moderate decreased activity had a score of 2. Moderately decreased myocardial activity was rated as 3. Score 4 denoted a severely compromised myocardial isotope uptake, and score 5 characterized the lack of myocardial tracer activity. All segments were scored according to the grade of the defect seen and these individual scores were then summed to offer a measurement of abnormality of the entire myocardium. Thus, stress and rest MPI was evaluated as the summed stress score (SSS) and the summed rest scores (SRS) of the 17-segment polar map. Myocardial perfusion imaging scan was evaluated as abnormal when SSS was ≥ 4, with mild ischemia when SSS was graded from 4 to 8, moderate from 9 to 13, and severe when summed score was > 13. [17] The difference between the summed stress and summed rest scores (SSS-SRS) were reflective of the burden and non-reversible nature of the existing ischemia [18].

Statistical Analysis

For statistical analysis and MPI evaluation, we used SPSS version 20 for windows (SPSS, Chicago, IL), and Microsoft Excel version 2013 (© Microsoft). Rheumatoid arthritis patients and control group were separately analyzed after splitting into two subgroups (one with SSS < 4 and another with SSS ≥ 4). Risk factors were evaluated in each group and each subgroup. Baseline characteristics were described using median and frequencies for categorical variables (using a 2 test for comparisons of discrete variables). $P < 0.05$ was considered significant. Furthermore, due to the small number of RA patients, we evaluated the summed segments (basal, mid and apical segments) of anterior, anteroseptal, inferoseptal, inferior, inferolateral, anterolateral and apical cardiac wall.

Results

The characteristics and MPI of the 13 RA patients and 44 control females are shown in Table 1. Comparison of patients with RA and control females demonstrated a statistically significantly higher number of patients in the RA group with a MPI value of SSS ≥ 4, (6/13, 46%) compared to control females 7/44 (16%) ($P = 0.004$), (Tab. 1). Among the RA patients, one had mild ischemia (1/6, 16%), four had moderate ischemia (4/6, 68%) and one had severe ischemia (1/6, 16%). All patients with abnormal MPI test in the control group had only mild ischemia.

Among all patients with RA, a total of 221 segments (17 x 13) were evaluated in MPI SSS and 221 segments in SRS. Of them, 23 segments in SSS and 18 segments in SRS had at least a mildly decreased activity scored with 1. Total score in those segments were 69 in SSS and 34 in SRS. The difference SSS-SRS was 5 segments with total score of 35. Control females had 748 segments (17 x 44) evaluated with 46 segments exhibiting decreased activity in SSS and 15 in SRS. Total score in those segments were74 in SSS and 26 in SRS. The difference SSS-SRS was 31 segments with total score of 48. Assessment of MPI in all 102 segments of the 6 RA patients with SSS ≥ 4 revealed 16 segments that exhibited score1 in SSS and 14 segments with score 1 in SRS. Total score was 57 and 29 respectively. The difference SSS-SRS was 2 segments with total score of 28. Among the 119 segments of the 7 control females with SSS ≥ 4, 14 segments scored 1 in SSS and 5 segments similarly scored 1 in SRS. Total score was 35 in SSS and 8 in SRS. The difference SSS-SRS was 9 segments with total score of 27 (Table 2).

Thus, among the RA patients, there were 5/23 (22%) myocardial segments having 51% reversible abnormalities assessed by the SSS-SRS MPI. In the contrary, the control females had milder abnormalities consisting of 31/46 segments with 67% reversible abnormalities in their SSS-SRS MPI. Among those RA patients with a SSS ≥ 4, only 2/16 (13%) segments demonstrated changes in SSS-SRS MPI consisting with 49% reversibility. In the contrary, control females had 9/14 (64%) myocardial segments with 77% reversible lesions. These results suggest that patients with RA had more irreversible myocardial ischemic abnormalities in their MPI than the control group.

An additional analysis has been performed based on the different cardiac segments. As shown in Table 3, although the anterolateral segment may be the most affected part of the myocardium in patients with RA, the results could be noted with skepticism due to the small number of RA patients. In the rest of myocardium, the number of segments with ischemia showed only a minor increase in the RA compared with the control group. However, this minor increase could be due to statistically insignificant variations secondary to small size of patients' dataset. The cardiovascular risk factors in RA and control patients are shown in Table 4. It appears that more RA patients with SSS ≥ 4 compared to those with SSS < 4 had hypertension, dyslipidemia and obesity. In addition, more RA patients than control females with SSS ≥ 4 had dyslipidemia and obesity.

Table 2. Number of segments and total score evaluated in MPI (summed stress score, summed rest score and their difference) in RA patients and control females

Individuals		Segments/MPI	Summed scores
Control all	Total	748/44	
	SSS	46/44	74
	SRS	15/44	26
	Difference SSS-RSS	31/44	48
RA all	Total	221/13	
	SSS	23/13	69
	SRS	18/13	34
	Difference SSS-RSS	5/13	35
Control SSS ≥ 4	Total	119/7	
	SSS	14/7	35
	SRS	5/7	8
	Difference SSS-RSS	9/7	27
RA SSS ≥ 4	Total	102/6	
	SSS	16/6	57
	SRS	14/6	9
	Difference SSS-RSS	2/6	28

a. RA: patients with rheumatoid arthritis; b. MPI: myocardial perfusion imaging; c. SSS: Summed stress score; d. SRS: Summed rest score

Table 3: Evaluation of the segments in MPI in patients and controls with SSS ≥ 4

	Segments SSS ≥ 4/Segments SRS	
MPI	RA	Controls
anterior	8/4	8/2
anteroseptal	2/1	0/0
inferoseptal	8/3	3/1
inferior	11/8	4/1
inferolateral	0/0	3/0
anterolateral	20/8	10/5
Apex	8/5	0/0

a. MPI: myocardial perfusion imaging; b. SSS: summed stress score; c. SRS: summed rest score; d. RA: patients with rheumatoid arthritis

Limitations of the study

The limitations of the study included its retrospective nature and the small number of RA patients. In addition, limited data was available concerning disease activity and the anti-inflammatory

Table 4. Risk factors in patients with rheumatoid arthritis and control individuals according to MPI summed stress score

	Patients with Rheumatoid arthritis		Control Group
Risk factors	SSS < 4	SSS ≥ 4	SSS ≥ 4
Total risk factors	12	16	18
Smoking	3/7 (43%)	0/6 (0%)	0/7 (0%)
Hypertension	4/7 (57%)	5/6 (83%)	6/7 (86%)
Diabetes Mellitus	1/7 (14%)	1/6 (17%)	3/7 (43%)
Dyslipidemia	4/7 (57%)	5/6 (83%)	3/7 (43%)
Obesity	0/7 (0%)	3/6 (50%)	2/7 (29%)
Cardiac Heredity	2/7 (28%)	2/6 (33%)	4/7 (57%)
With 1 risk factor	2/7(28%)	0/6 (0%)	2/7 (28%)
With 2 risk factors	3/7 (44%)	3/6 (50%)	1/7 (16%)
With 3 risk factors	2/7 (28%)	0/6 (0%)	2/7 (28%)
With 4 risk factors	0/7 (0%)	3/6 (50%)	2/7 (28%)

a. MPI: myocardial perfusion imaging; b. SSS: summed stress score

drugs used for management. Furthermore, no body mass index could be calculated since only weight but not height was recorded in the medical charts of the patients.

Discussion

In the present study, higher cardiovascular risk was found in RA patients with nonspecific cardiac symptoms compared to controls with similar symptoms. Specifically, in our study, 58% of RA patients had myocardial abnormalities in MPI, indicating ischemia. In accordance with our results, another study in 18 RA patients without a known cardiac disease reported a rate of myocardial abnormalities of 45% [19]. However, in that study, only 78% were females, and the imaging method performed was MRI. Asymptomatic RA patients may display myocardial ischemia at similar levels to DM patients [20]. In a study of 106 females with RA the incidence of coronary heart disease has been reported as 7 per 1000 patients-years [20]. Right and left ventricular diastolic dysfunction is diagnosed more frequently in patients with early stage RA, with left ventricular diastolic dysfunction linked to coronary heart disease [22].

This high rate of cardiac abnormalities in RA patients even without any clinical symptoms or ECG changes may be due to microvasculitic abnormalities [23]. When a systemic inflammation is present in RA patients, the cardiac disease may be manifested with more clinical findings and atherosclerosis might lead to increased cardiovascular morbidity [24]. Thus, apart from traditional risk factors, atherosclerosis in RA patients may be aggravated by disease activity, such as polymorphonuclear cell counts, radiographic evidence of cumulative inflammation, serum uric acid increased levels, hypothyroidism [25], and increased erythrocyte sedimentation rate [26]. However, another study reported no correlation of coronary artery disease in RA patients with the titers of rheumatoid factor, body mass index and hypercholesterolemia [27]. In our study due to lack of detailed information about the disease activity of RA patients and mode of treatment we were not able to assess these parameters in relation to cardiovascular risk.

Overall in our study, the traditional cardiovascular risk factors were not significantly different between patients and control females even though RA that exhibited an abnormal MPI had a higher rate of dyslipidemia and obesity compared to control individuals. However, diabetes mellitus and cardiac heredity were attributes seen at higher rates in controls than in RA patients in our study. In accordance with our study, previously published results indicate that the traditional cardiovascular risk factors in RA patients cannot entirely explain their increased incidence of coronary heart disease [28]. Although the traditional cardiovascular risk factors were similar in a group of 68 RA patients compared to 64 controls, RA patients had the propensity to develop coronary artery disease twice as frequently as the control individuals [11]. In addition, another study indicated that RA patients develop cardiovascular disease almost ten years earlier than their age- and sex-matched individuals and tend to suffer twice as frequently myocardial infarction compared to their counterparts [29]. Apart from myocardial infarction, heart failure due to left ventricular diastolic dysfunction is linked to increased cardiovascular mortality in patients with RA. Thus, diagnosis of heart failure in early asymptomatic stages is more likely to be treatable in RA patients [30, 31]. A study in 144 RA women, exhibiting low risk of cardiovascular disease as assessed by the Systematic COronary Risk Evaluation (SCORE), showed that one-third of them, experience high-risk atherosclerosis when age older than 49.5 years and/or cholesterol levels over 5.4 mmol/l suggest that they should be managed appropriately [32]. Similar conclusions of increased subclinical atherosclerosis were made in another prospective study in 71 RA patients ≤ 60 years old compared to 40 age- and sex-matched controls [33].

In conclusion, our results corroborate other studies that show increased incidence of cardiovascular risk in RA female patients compared to control individuals. The presence of increased risk even in patients with minimal or atypical cardiac symptoms indicates that early detection of the increased risk in RA patients is warranted in order to monitor or pharmaceutically reverse the indolent cardiovascular disease.

Acknowledgment

None

Conflict of interest

None

Disclosures of funding

N/A

References

1. Backman CL. Employment and work disability in rheumatoid arthritis. Curr Opin Rheumatol. 2004; 16(2): 148–152, indexed in Pubmed: 14770102.
2. Sokka T. Work disability in early rheumatoid arthritis. Clin Exp Rheumatol. 2003; 21(5 Suppl 31): S71–S74, indexed in Pubmed: 14969054.
3. Kojima M, Kojima T, Ishiguro N, et al. Psychosocial factors, disease status, and quality of life in patients with rheumatoid arthritis. J Psychosom Res. 2009; 67(5): 425–431, doi: 10.1016/j.jpsychores.2009.01.001, indexed in Pubmed: 19837205.
4. Cutolo M, Kitas GD, van Riel PL. Burden of disease in treated rheumatoid arthritis patients: going beyond the joint. Semin Arthritis Rheum. 2014; 43(4): 479–488, doi: 10.1016/j.semarthrit.2013.08.004, indexed in Pubmed: 24080116.
5. Faccini A, Kaski JC, Camici PG. Coronary microvascular dysfunction in chronic inflammatory rheumatoid diseases. Eur Heart J. 2016; 37: 1799–1806, doi: 10.1016/j.semarthrit.2013.08.004, indexed in Pubmed: 24080116.
6. Mellana WM, Aronow WS, Palaniswamy C, et al. Rheumatoid arthritis: cardiovascular manifestations, pathogenesis, and therapy. Curr Pharm Des. 2012; 18(11): 1450–1456, indexed in Pubmed: 22364129.
7. Furer V, Fayad ZA, Mani V, et al. Noninvasive cardiovascular imaging in rheumatoid arthritis: current modalities and the emerging role of magnetic resonance and positron emission tomography imaging. Semin Arthritis Rheum. 2012; 41(5): 676–688, doi: 10.1016/j.semarthrit.2011.08.007, indexed in Pubmed: 22000818.
8. Ogino Y, Horiguchi Y, Ueda T, et al. A myocardial perfusion imaging system using a multifocal collimator for detecting coronary artery disease: validation with invasive coronary angiography. Ann Nucl Med. 2015; 29(4): 366–370, doi: 10.1007/s12149-015-0955-9, indexed in Pubmed: 25663393.
9. Zhang WC, Tian YQ, Yang MF, et al. [Stress myocardial perfusion single photon emission computed tomography imaging in the detection of coronary artery disease in woman]. Zhonghua Yi Xue Za Zhi. 2007; 87(37): 2623–2626, indexed in Pubmed: 18162150.
10. Chung CP, Oeser A, Solus JF, et al. Prevalence of the metabolic syndrome is increased in rheumatoid arthritis and is associated with coronary atherosclerosis. Atherosclerosis. 2008; 196(2): 756–763, doi: 10.1016/j.atherosclerosis.2007.01.004, indexed in Pubmed: 17266963.
11. Luck Y, Baron M, Bardakjian S, et al. The role of rheumatologists vis-à-vis assessment of traditional cardiovascular risk factors in rheumatoid arthritis. Clin Rheumatol. 2014; 33(6): 769–774, doi: 10.1007/s10067-014-2522-5, indexed in Pubmed: 24526251.
12. Liao KP, Liu J, Lu B, et al. Association between lipid levels and major adverse cardiovascular events in rheumatoid arthritis compared to non-rheumatoid arthritis patients. Arthritis Rheumatol. 2015; 67(8): 2004–2010, doi: 10.1002/art.39165, indexed in Pubmed: 25917955.
13. Sioka C, Exarchopoulos T, Tasiou I, et al. Myocardial perfusion imaging with (99 m)Tc-tetrofosmin SPECT in breast cancer patients that received postoperative radiotherapy: a case-control study. Radiat Oncol. 2011; 6: 151, doi: 10.1186/1748-717X-6-151, indexed in Pubmed: 22067743.
14. Giannopoulos S, Markoula S, Sioka C, et al. Detecting Myocardial Ischemia With Technetium-Tetrofosmin Myocardial Perfusion Imaging in Ischemic Stroke. Neurohospitalist. 2017; 7(4): 164–168, doi: 10.1177/1941874417704752, indexed in Pubmed: 28974994.
15. Arumugam P, Harbinson M, Reyes E, et al. Procedure guidelines for radionuclide myocardial perfusion imaging with single-photon emission computed tomography. Nucl Med Commun. 2013; 34(8): 813–826, doi: 10.1097/MNM.0b013e32836171eb, indexed in Pubmed: 23719150.
16. Cerqueira M. Standardized myocardial segmentation and nomenclature for tomographic imaging of the heart: A statement for healthcare professionals from the Cardiac Imaging Committee of the Council on Clinical Cardiology of the American Heart Association. Journal of Nuclear Cardiology. 2002; 9(2): 240–245, doi: 10.1067/mnc.2002.123122.
17. Belardinelli R, Cianci G, Gigli M, et al. Effects of trimetazidine on myocardial perfusion and left ventricular systolic function in type 2 diabetic patients with ischemic cardiomyopathy. J Cardiovasc Pharmacol. 2008; 51(6): 611–615, doi: 10.1097/FJC.0b013e31817bdd66, indexed in Pubmed: 18574390.
18. Imaging guidelines for nuclear cardiology procedures, part 2. American Society of Nuclear Cardiology. J Nucl Cardiol. 1999; 6(2): G47–G84, indexed in Pubmed: 10327112.
19. Kobayashi Y, Giles JT, Hirano M, et al. Assessment of myocardial abnormalities in rheumatoid arthritis using a comprehensive cardiac magnetic resonance approach: a pilot study. Arthritis Res Ther. 2010; 12(5): R171, doi: 10.1186/ar3131, indexed in Pubmed: 20836862.
20. Toutouzas K, Sfikakis PP, Karanasos A, et al. Myocardial ischaemia without obstructive coronary artery disease in rheumatoid arthritis: hypothesis-generating insights from a cross-sectional study. Rheumatology (Oxford). 2013; 52(1): 76–80, doi: 10.1093/rheumatology/kes349, indexed in Pubmed: 23185038.
21. Castro AM, Carmona-Fernandes D, Rodrigues AM, et al. Incidence and predictors of cardiovascular events in a cohort of patients with rheumatoid arthritis. Acta Reumatol Port. 2016; 41(3): 213–219, indexed in Pubmed: 27682808.
22. Kirillova IG, Novikova DS, Popkova TV, et al. [Left and right ventricular diastolic dysfunction in patients with early rheumatoid arthritis before prescribing disease-modifying antirheumatic therapy]. Ter Arkh. 2015; 87(5): 16–23, doi: 10.17116/terarkh201587516-23, indexed in Pubmed: 26155615.
23. Momose S. [Detection of myocardial lesions by dipyridamole thallium-201 scintigraphy in patients with rheumatoid arthritis]. Ryumachi. 1995; 35(3): 559–565, indexed in Pubmed: 7570210.
24. Shul'gin DN, Olisaeva DR, Fomicheva OA, et al. [Single-photon emission computed tomography in the diagnosis of myocardial perfusion abnormalities in patients with rheumatoid arthritis: preliminary data]. Ter Arkh. 2012; 84(8): 78–80, indexed in Pubmed: 22994096.
25. Dessein PH, Joffe BI, Veller MG, et al. Traditional and nontraditional cardiovascular risk factors are associated with atherosclerosis in rheumatoid arthritis. J Rheumatol. 2005; 32(3): 435–442, indexed in Pubmed: 15742434.
26. Chung CP, Oeser A, Raggi P, et al. Increased coronary-artery atherosclerosis in rheumatoid arthritis: relationship to disease duration and cardiovascular risk factors. Arthritis Rheum. 2005; 52(10): 3045–3053, doi: 10.1002/art.21288, indexed in Pubmed: 16200609.
27. Li C, Wang Xr, Tang Yd, et al. [A multicenter study of coronary artery disease and its risk factors in rheumatoid arthritis in China]. Beijing Da Xue Xue Bao Yi Xue Ban. 2012; 44(2): 176–181, indexed in Pubmed: 22516983.
28. Maradit-Kremers H, Crowson CS, Nicola PJ, et al. Increased unrecognized coronary heart disease and sudden deaths in rheumatoid arthritis: a population-based cohort study. Arthritis Rheum. 2005; 52(2): 402–411, doi: 10.1002/art.20853, indexed in Pubmed: 15693010.
29. Mavrogeni S, Dimitroulas T, Bucciarelli-Ducci C, et al. Rheumatoid arthritis: an autoimmune disease with female preponderance and cardiovascular risk equivalent to diabetes mellitus: role of cardiovascular magnetic resonance. Inflamm Allergy Drug Targets. 2014; 13(2): 81–93, indexed in Pubmed: 24479835.
30. Mavrogeni S, Dimitroulas T, Gabriel S, et al. Why currently used diagnostic techniques for heart failure in rheumatoid arthritis are not enough: the challenge of cardiovascular magnetic resonance imaging. Rev Cardiovasc Med. 2014; 15(4): 320–331, indexed in Pubmed: 25662926.

31. Santos MJ, Vinagre F, Silva JJ, et al. Cardiovascular risk profile in systemic lupus erythematosus and rheumatoid arthritis: a comparative study of female patients. Acta Reumatol Port. 2010; 35(3): 325–332, indexed in Pubmed: 20975635.
32. Corrales A, Dessein PH, Tsang L, et al. Carotid artery plaque in women with rheumatoid arthritis and low estimated cardiovascular disease risk: a cross-sectional study. Arthritis Res Ther. 2015; 17: 55, doi: 10.1186/s13075-015-0576-7, indexed in Pubmed: 25888724.
33. Södergren A, Karp K, Bengtsson C, et al. The Extent of Subclinical Atherosclerosis Is Partially Predicted by the Inflammatory Load: A Prospective Study over 5 Years in Patients with Rheumatoid Arthritis and Matched Controls. J Rheumatol. 2015; 42(6): 935–942, doi: 10.3899/jrheum.140694, indexed in Pubmed: 25877503.

Original
Nuclear Medicine Review 2019, 22, 1: 14–17
DOI: 10.5603/NMR.2019.0002

ISSN 1506–9680

VIA MEDICA

Comparison of ^{18}F-fluoroethylo-L-thyrosine PET/CT and MR in the diagnosis of primary brain tumors referred to radiation therapy

Paulina Cegła[1], Krystyna Adamska[2, 3], Ewa Wierzchosławska[2, 4], Michał Smoleń[1], Witold Cholewiński[1, 2]
[1]Department of Nuclear Medicine, Greater Poland Cancer Centre, Poznań, Poland
[2]Chair and Department of Electroradiology, Poznan University of Medical Science
[3]3rd Radiotherapy Department, Greater Poland Cancer Centre, Poznań, Poland
[4]Radiology Department Greater Poland Cancer Centre, Poznań, Poland

[Received 5 X 2018; Accepted 18 I 2019]

Abstract

BACKGROUND: The diagnostic efficacy of ^{18}F-FDG-PET imaging in brain tumors is markedly reduced due to high glucose metabolism in normal brain tissue. This requires further research for more sensitive and specific tracers. ^{18}F-fluoroethylo-L-thyrosine (^{18}F-FET) is an interesting PET radiotracer, which shows promising results in patients with brain tumors. The aim of this study was to compare ^{18}F-fluoroethylo-L-thyrosine PET/CT and MRI in the diagnosis of primary brain tumors referred to radiation therapy.
MATERIAL AND METHODS: Thirteen patients (5M, 8F) with mean age of 56y ± 13 and histologically confirmed primary brain tumors were investigated. The MRI scans were performed on MRI 1.5T scanner with FSE, DWI method, T1, T2 and FLAIR sequence. The examination was performed using brain protocol for 35 minutes and prior to PET imaging. The PET scans were performed 20–40 min after intravenous injection of 160 MBq of ^{18}F-FET. Scans were acquired on Gemini TF PET/CT scanner using 3D brain imaging protocol for 10 minutes acquisition time. The reconstructed PET images were evaluated on a dedicated EBW workstation with Time-of-Flight reconstruction algorithms. On reconstructed images, the tumor borders were drawn using dedicated software, based on various threshold values and tumor borders and volumes were calculated on each nuclear image and compared with the volume calculated on the diagnostic MRI. For statistical analysis the t-test was used.
RESULTS: ^{18}F-FET-PET imaging in total showed more abnormal lesions that MRI; however, the difference was not significant ($p > 0.05$). There were two patients with lesions detected only on the MRI study and 4 patients with abnormal tracer uptake within the brain in ^{18}F-FET study with no correlation in the MRI study. ^{18}F-FET-PET method showed 30 lesions in 11 patients with mean SUV_{max} value of 2.33 (range from 1.6 to 3.5). Based on 70% threshold cutoff value, the mean volume of brain focus was calculated on at 31.15 ± 26.89 mm^3 and was in concordance with mean lesion volume measured on the MRI scan 31.51 ± 34.97 mm^3. For radiation planning purposes other-threshold values, as well as gradient based methods were evaluated on ^{18}F-FET-PET imaging.
CONCLUSION: PET/CT imaging with ^{18}F-fluoroethylo-L-thyrosine is complementary to MRI in the diagnosis of primary brain tumors referred to radiation therapy.

KEY words: radiotherapy, brain tumor, positron emission tomography, ^{18}F-fluoroethylo-L-thyrosine, magnetic resonance

Nucl Med Rev 2018; 21, 1: 14–17

Introduction

The most commonly used non-invasive methods of brain imaging include computed tomography (CT) and magnetic resonance (MR) which allow assessment of anatomical structures and are characterized by high sensitivity. The limitation in the application of these imaging methods are changes caused by the applied treatment (e.g. surgery, radiation-induced necrosis). In such cases, the nuclear medicine techniques, in particular positron emission tomography in combination with computed tomography (PET/CT) are helpful. The radiotracer most commonly used in the imaging of tumor metabolism is 2-deoxy-2-[18F]

Correspondence to: Paulina Cegla, Department of Nuclear Medicine, Greater Poland Cancer Centre, Poznań, Poland; e-mail: paulina.cegla@gmail.com

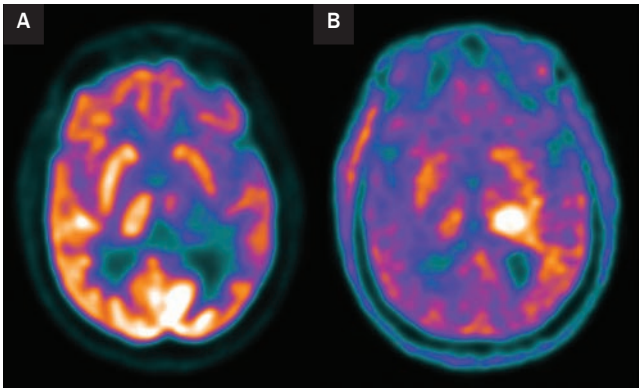

Figure 1. Differences in uptake of ^{18}F-FDG and ^{18}F-FET in primary brain tumor

fluoro-D-glucose (^{18}F-FDG). It has been demonstrated that there is a relationship between histopathological diagnosis and ^{18}F-FDG uptake: high-grade tumors show hypermetabolism, while low-grade tumors — hypometabolism compared to gray matter. Low-grade astrocytomas had low ^{18}F-FDG uptake, while astrocytomas and glioblastoma multiforme are characterized by increased uptake [1–3]. Due to high glucose uptake in healthy brain tissue, more sensitive and specific radiotracers are used in brain tumors imaging.

^{18}F-fluoroethylo-L-thyrosine (^{18}F-FET) is an artificial amino acid showing increased uptake within malignant lesions and also allowing good differentiation in both high and low-differentiated tumors [4]. Differences in uptake of ^{18}F-FDG and ^{18}F-FET in primary brain tumor are shown in Figure 1.

The aim of this study was to compare 18F-fluoroethylo-L-thyrosine PET/CT and MRI in the diagnosis of primary brain tumors referred to radiation therapy.

Material and methods

Retrospective analysis was performed on a group of 13 patients (5M, 8F), with mean age of 56 ± 13y (range 35–77yrs) and histologically confirmed primary brain tumors. Eleven of these patients had craniotomies prior to the study, 2 were without any surgical intervention. The study has been approved by the Institutional Bioethical Committee and all subjects signed an informed consent form. All patients were qualified for radiotherapy treatment and tumors were located in frontal, parietal, temporal and occipital lobes.

The MRI scans were performed on MRI 1.5T scanner using the brain protocol for 35 minutes, with the FSE method in transverse, sagittal and frontal planes, T1- and T2 dependent time, FLAIR sequences and DWI, with intravenous administration of the contrast agent. The PET scans were performed 20–40 min after intravenous injection of 160 MBq of ^{18}F-fluoroethylo-L-thyrosine on Gemini TF PET/CT scanner (Philips) using 3D brain imaging protocol for 10 minutes acquisition time. The reconstructed PET images were evaluated on a dedicated EBW workstation with time-of-flight (TOF) reconstruction algorithms. On reconstructed images, using semi-automatic dedicated software based on various threshold values, tumor borders and volume were calculated on each nuclear image and compared with the volume calculated on the diagnostic MRI. A 70% cutoff method was used to compare PET and MR images. All standardized uptake values (SUVs) used at work are maximum values (SUV_{max}). For statistical analysis the T-test was used.

Results

The ^{18}F-FET-PET study showed more lesions in the brain area than the MRI study; however, the difference was not statistically significant ($p > 0.05$). There were two patients whose lesions were detected only in MRI, and 4 patients in whom PET imaging with tyrosine showed increased radiotracer uptake without reference to MRI (Tab. 1).

Table 1. Sensitivity of MRI and ^{18}F-FET-PET imaging

No.	Diagnosis	MRI		18F-FET-PET		
		N	Scan results (positive/negative)	N	Scan results (positive/negative)	SUVmax.
1	Glioblastoma multiforme	1	+	0	-	-
2	Glioblastoma multiforme	1	+	1	+	1.7
3	Glioblastoma multiforme	4	+	4	+	1.9
4	Oligoastrocytoma Grade II	4	+	1	+	2.8
5	Astrocytoma Grade II	1	+	2	+	2.5
6	Oligoastrocytoma Grade II	0	-	1	+	1.6
7	Glioma Grade II	0	-	5	+	1.9
8	Astrocytoma Grade II	5	+	0	-	-
9	Astrocytoma Grade III	1	+	1	+	1.9
10	Glioblastoma multiforme	4	+	4	+	3.5
11	Oligoastrocytoma Grade II	0	-	3	+	2.7
12	Astrocytoma Grade III	4	+	4	+	2.8
13	Astrocytoma Grade III	0	-	4	+	2.3

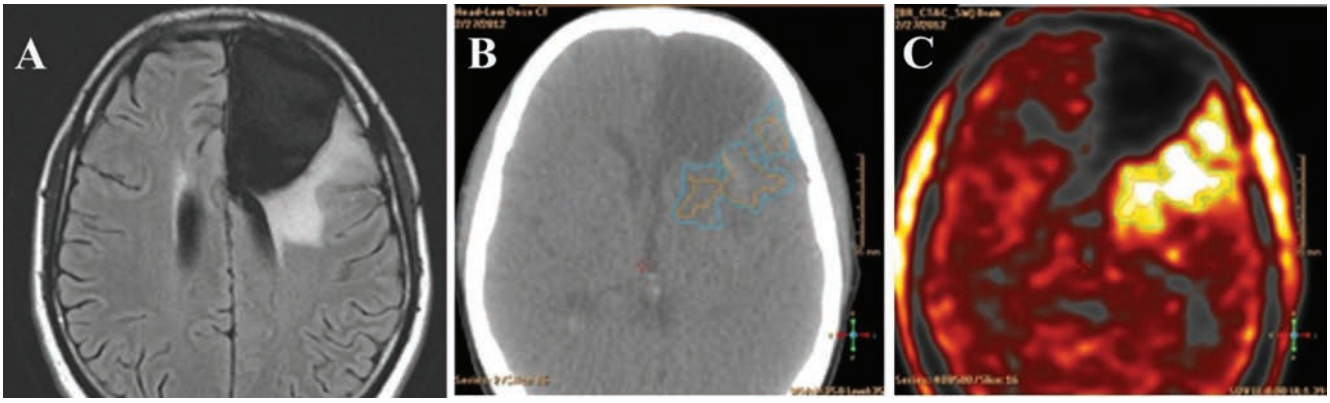

Figure 2. Patient after left-sided craniotomy. (A) MRI images, (B) CT images, (C) ^{18}F-FET-PET images

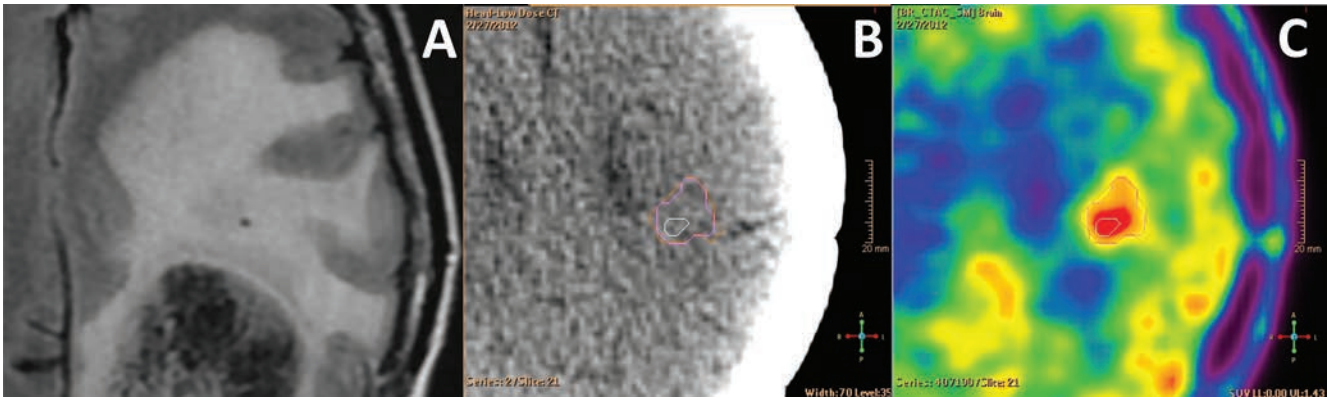

Figure 3. Patient after left-sided occipital craniotomy. (A) MRI images, (B) CT images, (C) ^{18}F-FET-PET images

^{18}F-FET-PET showed 30 lesions in 11 patients with an average SUV_{max} of 2.33 (range 1.6–3.5), while the MRI examination showed 25 lesions in 9 patients.

Based on 70% cutoff, the mean volume in the ^{18}F-FET-PET study was 31.15 ± 26.89 mm^3 and was comparable to the volume of changes measured in the MRI 31.51 ± 34.97 mm^3.

An example of a patient who underwent left-sided frontal craniotomy is showed in Figure 2. In MRI images, after intravenous administration of contrast medium on the back contour of the post-surgical cavity, 4 fine-grained regions of up to 10 mm^3 were found, which corresponded to the resumption of the malignant process. In the ^{18}F-FET-PET study, the area of non-uniformly increased ^{18}F-FET accumulation along the side and rear walls of the post-surgical cavity. The most active focal points are visible at the rear wall and at the side wall. The image suggests an active proliferative process in the left frontal lobe. As another example, a patient after left-sided occipital craniotomy with increased 18F-FET uptake in the lateral part of the post-surgical cavity. In MRI hyperintensive area in T2-weighted images caused by previous treatment which make some difficulties in interpretation of the study (Fig. 3).

An important aspect is the size of the observed lesions in this two studies. In both methods, the formula for the volume of the ellipse was used to assess the volume ($V = 4/3*\varpi*a*b*c$). In the case of 7 lesions, the volumes in MRI were higher than in ^{18}F-FET-PET, while in 9 lesions volumes were higher in ^{18}F-FET-PET than MRI. The mean of all lesions detected in the MRI (25) was 44.70 mm^3 while in the ^{18}F-FET-PET (30) study it was 25.28 mm^3. However, the differences were not statistically significant ($p > 0.05$).

Discussion

Many authors point to the difficulty in differentiating the recurrence of the tumor from postoperative edema, occurring in the area of the post-surgical cavity. Using the PET imaging with^{18}F-fluoroethylo-L-thyrosine does not cause such a problem, because this radiotracer accumulates only in the areas of active proliferative process. This makes it easier to distinguish a tumor from healthy brain tissue, changes occurs postoperatively or under the influence of radiotherapy. Studies have shown that the ^{18}F-fluoroethylo-L-thyrosine PET defines biological tumor volume (BTV) and reflects brain tumor tissue more accurately than MRI [5,6]. Other studies on a small group of patients, suggest that the postoperative ^{18}F-FET-PET is a prognostic factor before radiotherapy [7–10]. This study on PET imaging with ^{18}F-fluoroethylo-L-thyrosine showed more lesions than MRI. The difference in the number of foci between ^{18}F-FET-PET and MRI may result from the difficulty in differentiating MRI lesions caused by the recurrence of the tumor, from edema occurring after the surgical treatment. Similar

studies were conducted by Grosu et al. where they compared ^{18}F-fluoroethylo-L-thyrosine-based biological tumor volume for radiotherapy planning in high-grade glioma with conventional MRI–based gross tumor volume. They found that biological tumor volume and gross tumor volume were different in size and localization in two thirds of the patients [11].

Because of specificity of ^{18}F-fluoroethylo-L-thyrosine which does not accumulate in inflammatory and reactive tissues, imaging with this agent is more accurate in detection of tumor recurrence and gives a better definition of target volumes prior to radiotherapy [12–13]. Kläsner et al. performed a study on a group of 25 patients where they investigated the value of early post-operative ^{18}F-FET-PET to assess the resection status in comparison to intra-operative findings, as well as MRI. They reported complete resection in 12 out of 25 (48%), in 6 out of 25 cases (24%) incomplete resection and in 7 patients ^{18}F-FET-PET showed discordant findings [14]. In our limited study, in 85% PET showed positive scans results, while MRI only in 70%.

The major limitation of this study is a small group of patients and because of that the statistical analysis for sensitivity and specificity was not performed. However even in spite of this, the study showed a comparable value of ^{18}F-FET-PET/CT and MRI in the assessment of primary brain tumors. As a consequence of these observations ^{18}F-FET-PET/MR should be considered as a method which provides better disease status evaluation of primary brain tumor. Another important limitation of this study is that not all lesions detected in both methods were verified by histopathological examination, so false positive findings could not be excluded.

Conclusions

^{18}F-FET-PET/CT and MRI play complementary roles in the diagnosis of primary brain tumors referred to radiation therapy.

References

1. Smits A, Baumert BG. The Clinical Value of PET with Amino Acid Tracers for Gliomas WHO Grade II. Int J Mol Imaging. 2011; 2011, doi: 10.1155/2011/372509, indexed in Pubmed: 21603237.
2. Herholz K, Pietrzyk U, Voges J, et al. Correlation of glucose consumption and tumor cell density in astrocytomas. A stereotactic PET study. J Neurosurg. 1993; 79(6): 853–858, doi: 10.3171/jns.1993.79.6.0853, indexed in Pubmed: 8246053.
3. Goldman S, Levivier M, Pirotte B, et al. Regional glucose metabolism and histopathology of gliomas. A study based on positron emission tomography-guided stereotactic biopsy. Cancer. 1996; 78(5): 1098–1106, doi: 10.1002/(SICI)1097-0142(19960901)78:5<1098::AID-CNCR21>3.0.CO;2-X, indexed in Pubmed: 8780549.
4. Dunet V, Rossier C, Buck A, et al. Performance of 18F-fluoro-ethyl-tyrosine (18F-FET) PET for the differential diagnosis of primary brain tumor: a systematic review and Metaanalysis. J Nucl Med. 2012; 53(2): 207–214, doi: 10.2967/jnumed.111.096859, indexed in Pubmed: 22302961.
5. Kracht LW, Miletic H, Busch S, et al. Delineation of brain tumor extent with [11C]L-methionine positron emission tomography: local comparison with stereotactic histopathology. Clin Cancer Res. 2004; 10(21): 7163–7170, doi: 10.1158/1078-0432.CCR-04-0262, indexed in Pubmed: 15534088.
6. Rachinger W, Goetz C, Pöpperl G, et al. Positron Emission Tomography with O-(2-[18F]fluoroethyl)-l-tyrosine versus Magnetic Resonance Imaging in the Diagnosis of Recurrent Gliomas. Neurosurgery. 2005; 57(3): 505–511, doi: 10.1227/01.neu.0000171642.49553.b0.
7. Suchorska B, Jansen NL, Linn J, et al. German Glioma Network. Biological tumor volume in 18FET-PET before radiochemotherapy correlates with survival in GBM. Neurology. 2015; 84(7): 710–719, doi: 10.1212/WNL.0000000000001262, indexed in Pubmed: 25609769.
8. Jansen NL, Suchorska B, Wenter V, et al. Prognostic significance of dynamic 18F-FET PET in newly diagnosed astrocytic high-grade glioma. J Nucl Med. 2015; 56(1): 9–15, doi: 10.2967/jnumed.114.144675, indexed in Pubmed: 25537990.
9. Pirotte BJM, Levivier M, Goldman S, et al. Positron emission tomography-guided volumetric resection of supratentorial high-grade gliomas: a survival analysis in 66 consecutive patients. Neurosurgery. 2009; 64(3): 471–81; discussion 481, doi: 10.1227/01.NEU.0000338949.94496.85, indexed in Pubmed: 19240609.
10. Piroth MD, Holy R, Pinkawa M, et al. Prognostic impact of postoperative, pre-irradiation (18)F-fluoroethyl-l-tyrosine uptake in glioblastoma patients treated with radiochemotherapy. Radiother Oncol. 2011; 99(2): 218–224, doi: 10.1016/j.radonc.2011.03.006, indexed in Pubmed: 21497925.
11. Grosu AL, Weber WA, Franz M, et al. Reirradiation of recurrent high-grade gliomas using amino acid PET (SPECT)/CT/MRI image fusion to determine gross tumor volume for stereotactic fractionated radiotherapy. Int J Radiat Oncol Biol Phys. 2005; 63(2): 511–519, doi: 10.1016/j.ijrobp.2005.01.056, indexed in Pubmed: 16168843.
12. Grosu AL, Weber WA, Astner ST, et al. 11C-methionine PET improves the target volume delineation of meningiomas treated with stereotactic fractionated radiotherapy. Int J Radiat Oncol Biol Phys. 2006; 66(2): 339–344, doi: 10.1016/j.ijrobp.2006.02.047, indexed in Pubmed: 16765533.
13. Miwa K, Shinoda J, Yano H, et al. Discrepancy between lesion distributions on methionine PET and MR images in patients with glioblastoma multiforme: insight from a PET and MR fusion image study. J Neurol Neurosurg Psychiatry. 2004; 75(10): 1457–1462, doi: 10.1136/jnnp.2003.028480, indexed in Pubmed: 15377696.
14. Nuutinen J, Sonninen P, Lehikoinen P, et al. Radiotherapy treatment planning and long-term follow-up with [(11)C]methionine PET in patients with low-grade astrocytoma. Int J Radiat Oncol Biol Phys. 2000; 48(1): 43–52, indexed in Pubmed: 10924970.
15. Kläsner B, Buchmann N, Gempt J, et al. Early [18F]FET-PET in Gliomas after Surgical Resection: Comparison with MRI and Histopathology. PLoS One. 2015; 10(10): e0141153, doi: 10.1371/journal.pone.0141153, indexed in Pubmed: 26502297.

Original
Nuclear Medicine Review 2019, 22, 1: 18–22
DOI: 10.5603/NMR.2019.0003

ISSN 1506–9680

VIA MEDICA

Feasibility of myocardial perfusion imaging studies in morbidly obese patients with a cadmium-zinc-telluride cardiac camera

Anna Budzyńska, Sebastian Osiecki, Andrzej Mazurek, Stanisław Piszczek, Mirosław Dziuk
Military Institute of Medicine, Warsaw

[Received 21 XII 2018; Accepted 7 I 2019]

Abstarct

BACKGROUND: A novel cardiac SPECT camera with cadmium-zinc-telluride (CZT) based technology has a fixed array of semiconductor detectors paired with pinhole collimators focused on the heart. Image acquisition in obese patients can be challenging because of much smaller detector field of view compared to conventional gamma cameras. The aim of this study was to evaluate the impact on high body mass on the feasibility of CZT myocardial perfusion imaging (MPI). The additional aim was to investigate the mechanism of the banana-shaped/obesity artifact, as referred to in literature, and to attempt at simulating it on a phantom study.

MATERIAL AND METHODS: Study group consisted of 43 patients with morbid obesity (BMI ≥ 40 kg/m^2). All these patients underwent myocardial perfusion imaging on both CZT cardiac camera and general purpose SPECT/CT gamma camera. Control group consisted of all patients who underwent myocardial perfusion imaging on CZT camera throughout one calendar year and whose BMI was lower than 40 kg/m^2. In this group, all repeated studies were re-analyzed for estimating the frequency of heart mispositioning in the camera field of view. The number of studies performed was 1180. A static cardiac phantom was used to simulate a banana-shaped artifact. A series of phantom acquisitions during which the phantom position was altered in the camera field of view was performed.

RESULTS: In control group, 3.7% of all cardiac scintigrams required repetition, 18.9% of which were repeated due to wrong heart positioning; median BMI in this group of patients was 36.0. A banana-shaped artifact was observed in one female patient with BMI 36.0. In morbid obesity group, 32.6% of the studies were non-diagnostic with "truncation effect" on Scan Quality Control (QC). Median BMI in patients with diagnostic scans was 42.0, while in patients with not acceptable quality control test it was 45.0 ($p < 0.05$). Banana-shaped artifacts were observed in 5 non-diagnostic studies. In a phantom study an artifact of banana shape was obtained when gantry was distant from the phantom and target was on the edge of the camera field of view and was slightly truncated.

CONCLUSIONS: Problem with heart mispositioning during imaging on the CZT camera affects less than 1% of all performed studies. Morbid obesity is not a contraindication to perform myocardial perfusion scintigraphy with the use of a CZT camera because over 2/3 of the studies of very obese patients is diagnostic.

KEY words: obesity, BMI, myocardial perfusion imaging, CZT, cardiac camera, image artifacts

Nucl Med Rev 2019; 22, 1: 18–22

Introduction

Myocardial perfusion imaging (MPI) has an established position in ischemic heart disease diagnostics. New generation of semiconductor gamma-cameras dedicated for cardiac imaging became a milestone in the way nuclear cardiac imaging is performed. Novel cardiac camera designs have in common that all available detectors are focused to imaging myocardium. The GE Discovery NM 530c uses Alcyone technology, consisting of a fixed array of solid-state cadmium-zinc-telluride (CZT) detectors paired with pinhole collimators simultaneously imaging the heart. With this camera SPECT acquisition is performed without detector's motion [1]. Main advantages of these systems (compared to

Correspondence to: Anna Budzyńska, Military Institute of Medicine, Szaserów 128 Street, 04–141 Warsaw, Poland; e-mail: abudzynska@wim.mil.pl

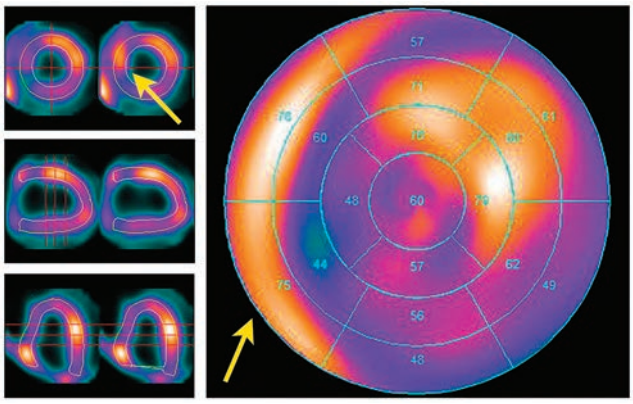

Figure 1. Male patient with BMI = 38. Banana-shaped artifact presented on polar map and short axis scans

conventional scanners) are physical parameters: higher sensitivity, higher energy resolution and better spatial resolution. The CZT technology has enabled reducing both administered activity and acquisition time with preserved high image quality [2], providing clinical information equivalent to conventional SPECT myocardial perfusion imaging [3].

Obtaining good quality, diagnostic myocardial perfusion SPECT images with use of semi-conductor systems and pinhole collimators focused on heart requires heart positioning in the center of the field of view. The volume in which the heart needs to be positioned to be imaged correctly is named the quality field of view (QFOV). This is the volume that represents the intersection of all the 19 views from each pinhole [4]. Accurate reconstruction is performed only within this volume of interest. Due to significantly smaller field of view of Discovery NM 530c compared to conventional cameras appropriate heart positioning could be challenging, especially in obese patients. Literature data indicates that image quality degradation from obesity in patients with BMI of 40 kg/m2 and above is so significant that those patients should be scheduled for MPI scanning on a conventional SPECT camera [5]. However, literature on the topic of MPI in morbidly obese patients is limited. Our seven years of experience with GE Discovery NM 530c indicate, that while correct heart positioning in patients with BMI ≥ 40 is indeed difficult, in most of cases results are diagnostically useful and imaging with conventional SPECT gamma-camera is not necessary.

The aim of this study was to present our experience and evidence that MPI in morbidly obese patients (BMI ≥ 40 kg/m^2) performed with CZT scanner in most cases allows accurate diagnostics. The second aim was to determine the frequency of heart positioning outside the quality field of view and compare it in groups of patients with BMI ≥ 40 kg/m^2 and BMI < 40 kg/m^2.

The additional aim was to investigate the mechanism of the banana-shaped/obesity artifact (Fig. 1), as referred to in literature [5], and to attempt at simulating it in a phantom study.

Materials and methods

Study population

Study group consisted of 43 patients with morbid obesity (BMI ≥ 40 kg/m^2), stage 3 according to WHO classification (Tab. 1). Studies have been performed in three consecutive calendar years.

Table 1. WHO classification of obesity [6]

BMI [kg/m^2]	WHO classification
< 18.5	underweight
18.5–24.9	normal weight
25.0–29.9	overweight
30.0–34.9	class I obesity
35.0–39.9	class II obesity
≥ 40.0	class III (morbid) obesity

Figure 2. Cardiac phantom positioned on the CZT scanner table

All patients underwent MPI on both Discovery NM 530c and general purpose SPECT-CT GE Infinia 3/8''HWK.

Control group consisted of all patients who underwent MPI on Discovery NM 530c throughout one calendar year and whose BMI was lower than 40 kg/m^2. In this group all repeated studies were re-analyzed for estimating the frequency of heart positioning outside the quality field of view. The number of studies performed was 1180. The correctness of heart positioning was assessed with the Scan Quality Control (QC) tool and qualitatively with the use of Myovation application.

Phantom study

A series of acquisitions of static cardiac phantom was performed (Fig. 2). Phantom equipped with reservoir filled with isotope enables left ventricle imaging simulation. It was attached to the frame and placed in the cylindrical vessel filled with water. No external activity was simulated. To attain a banana-shaped artifact the phantom positioning in the field of view was altered between consecutive acquisitions. Synchronous reallocation in x and y axis was accomplished with „camera out" function — automatically moving the gantry away from the phantom. The detector radius values were set as follows: 183, 185, 187, 191, 194, 214 and 221 mm.

Image acquisition and reconstruction

All patients underwent MPI scanning on GE Discovery NM 530c scanner in supine position with hands above the head. 76.7% of patients with morbid obesity and approximately 95% of patients belonging to the control group had additional imaging in prone position. In case of non-diagnostic scans in cardiac-dedicated camera

we analyzed whether patient repositioning enabled obtaining diagnostic images. Injected radiopharmaceutical (99mTc-MIBI) activity in control group was determined empirically and ranged from 8 to 20 mCi depending on body mass. Patients with BMI ≥ 40 kg/m^2 were scheduled for conventional gamma-camera imaging as well, therefore injected activity in this group was 25 mCi. For CZT camera time between injection and imaging was approximately 60 min. Two day Stress/Rest or, if feasible, Stress-only protocol were employed. Rest MPI was omitted in patients without perfusion abnormalities on stress supine and prone myocardial perfusion scintigraphy [7]. Acquisition time for both Stress and Rest study was 5 min. The images were reconstructed on a dedicated GE Xeleris 3 workstation applying a MLEM iterative reconstruction algorithm. The software GE Myovation for Alcyone was used for image reconstruction and a Butterworth filter (cut-off 0.37 cm-1, power value 7) for post-processing of the reconstructed axial slices was applied. All MPI scans were reconstructed in standard axes and polar maps of perfusion were generated using the software package [4, 5].

Phantom acquisitions were performed with standard myocardial perfusion protocol. Digital reconstruction and image analysis was performed – like in patient studies – with dedicated software: GE Myovation for Alcyone.

Scan Quality Control and Image Analysis

In every study raw data projections from 19 detectors with the Scan QC tool supplied by the vendor of the CZT camera were analyzed. Scan QC enables to asses correctness of heart placement in the field of view. Patient's heart (left ventricle) has to be positioned in the center of the QFOV without truncation. Scan QC image analysis is necessary element of cardiac imaging procedure and is performed by physician before patient is dismissed home to assure repositioning and re-imaging option if necessary.

Quality control with Scan QC tool was performed in all of morbid obesity patients. Scan QC in control group was reassessed only if re-imaging was necessary — in that case both original study and repeated study were analyzed. Performing multiple acquisitions in the same patient was caused by extra-cardiac activity denying appropriate perfusion assessment or heart positioning outside the quality field of view. Scan QC analysis allowed the frequency of heart mispositioning to be determined and compared in both groups of patients. All studies with Scan QC assessment performed — regardless of the outcome — were post-processed using Myovation for Alcyone software. Images in short and long axis as well as polar maps were analyzed for visual assessment of banana-shaped artifact presence and truncation in VLA and HLA axis, which correspond to this phenomenon [5].

In phantom study, both raw projections in Scan QC and reconstructed images presented in slices and polar maps were analyzed for verification of phantom reallocation in the field of view and truncation simulation.

Statistical analysis

Descriptive statistics (median, interquartile range [IQR]) as well as statistical tests were performed using Statistica software version 12 (StatSoft). The Mann-Whitney U test was used to check for significant differences in median BMI value between two patient groups (morbid obesity group and control group). A P-value of less than 0.05 was considered statistically significant.

Table 2. The numbers of diagnostic and non-diagnostic stress and rest studies on Discovery NM 530c

	Stress study	Rest study
Diagnostic MPI (positive Scan QC)	23 (10M)	6 (3M)
Non-diagnostic MPI (negative Scan QC)	9 (6M)	5 (3M)

Results

Control group

In one calendar year (2017) total of 1180 MPI studies have been performed. Analysis revealed that 44 cases (17 stress MPI and 27 rest MPI) required repetition; that is 3.7% of all cardiac scintigrams in analyzed year. Thirty-seven studies (14 stress MPI and 23 rest MPI) were repeated due to extra-cardiac activity. In remaining seven (3 stress MPI and 4 rest MPI) the reason of repetition was heart positioning outside the quality field of view or truncation. This represented 18.9% of repeated studies and 0.6% of all studies.

Among scans repeated due to heart mispositioning 3 single and 4 double repetitions have been noted. All single repetitions resulted in acquiring diagnostic scans on Discovery NM 530c after repositioning. When multiple repetitions were required, in one case diagnostic scans on CZT camera were not achieved, due to difficulties in correct positioning in the field of view. It was stress study in patient with BMI 34.4. Diagnostic study (although non-gated) in this patient was achieved in prone position.

Median BMI value in group of patients in whom repetition was due to heart mispositioning in the field of view was 36.0 (IQR = 9.1). In 3 patients BMI indicated 1st degree obesity, in 4 patients 2nd degree obesity.

In studies with negative Scan QC result banana-shaped artifact was observed in one patient (stress MPI) — a female with BMI of 36.0. In additional scans of this patient (2 repetitions) the artifact was not present.

Morbid obesity group

The majority of 43 studies of patients with 3rd degree obesity were stress MPIs (74.4%). There were 29 (13M) technically correct scans with positive Scan QC in first attempt, which represented 67.4% of all studies in this group. Fourteen (9M) studies (32.6%) were non-diagnostic with "truncation effect" on Scan QC (Tab. 2).

Median BMI value in 3rd degree obesity group was 43.0 (IQR 4.9). Median BMI in patients with diagnostic scans was significantly lower than BMI of patients, whose study failed quality control test (42.0, IQR = 3.0 vs. 45.0, IQR = 7.0, $p < 0.05$).

Analysis of repeated studies in this group revealed that only four patients had additional scanning after repositioning on CZT camera. In the majority of cases (71.4%) patients were referred directly to conventional dual-head SPECT gamma-camera. Of four repeated studies on CZT scanner, in 1 case diagnostic images were acquired after repositioning.

Banana-shaped artifacts were observed in 5 non-diagnostic studies (4 stress MPI, 1 rest MPI): 4 original (first attempt) scans and one repeated scan (in original scan in this patient artifact was not present).

Median BMI of patients whose study was non-diagnostic due to mispositioning, with banana-shaped artifacts on polar maps was 49.0 (IQR = 4.1).

Phantom study

In a phantom study an artifact of banana shape was obtained when gantry was distant from the phantom (camera out) and target was on the edge of the camera field of view and was slightly truncated.

Discussion

Fiechter et al. in their work showed that in patients with BMI ≥ 40 kg/m^2, 81% of the CZT scans were non-diagnostic, mainly because the cardiac position was out of focus, causing truncation artifacts of the left ventricle [5]. Our results are different – we demonstrate that over 2/3 of MPI scans of 3rd degree obese patients (BMI ≥ 40 kg/m^2) performed with Discovery NM 530c gamma-camera is diagnostic, provided correct positioning within the field of view. BMI value and chest circumference are only approximate predictors of method feasibility in obese patient. Heart size and its location in chest are of significance as well, which is indicated by the fact, that difficulties in heart positioning in quality field of view occur also in patients with 1st and 2nd degree obesity (control group results). We also believe that technicians' experience is of great importance, which to some degree may explain discrepancies between different centers.

Limitation of our work is that out of 14 studies with negative Scan QC only, in 4 cases repositioning on CZT scanner was attempted. In one case repositioning allowed obtaining diagnostic scans. Remaining 10 patients were referred directly to conventional SPECT system for cardiac imaging.

Interestingly, Gimelli et al. in their work "Evaluation of ischemia in obese patients: Feasibility and accuracy of a low-dose protocol with a cadmium-zinc telluride camera" highlight the aspect of high quality images obtained with GE Discovery NM 530c camera in obese patients [8]. Gimelli et al. point out that although the gantry size may represent a physical limit for obese patients who cannot fit inside the device, their patients did not experience such a problem and all the patients with BMI of > 35 kg/m^2 were able to fit inside the gantry [8]. These results are concordant with our observations.

Fiechter et al. stated that after application of AC, this rate of non-diagnostic studies (81%) significantly decreased to 55% [5]. We state that CT-based attenuation correction use in a study that didn't pass quality control is in principle incorrect because it doesn't deal with source of the truncation artifact which is the incorrect heart position in the camera field of view. In our work we didn't analyze AC images, because attenuation correction has no influence on the study being diagnostic or not (of technical causes). Attenuation correction may only improve diagnostic value of already diagnostic MPI study, provided positive Scan QC result.

The banana-shaped artifact, sometimes visible on polar maps, is often associated in the literature with high BMI. Hence its other name is obesity artifact [5]. We believe that the artifact, although mostly seen in morbidly obese patients, is only indirectly connected to BMI itself. Our department's experience show that it can be observed also in patients with BMI below 40 kg/m^2, and it can be simulated with a cardiac phantom. Furthermore patient repositioning may eliminate the artifact (Fig. 3A and 3B).

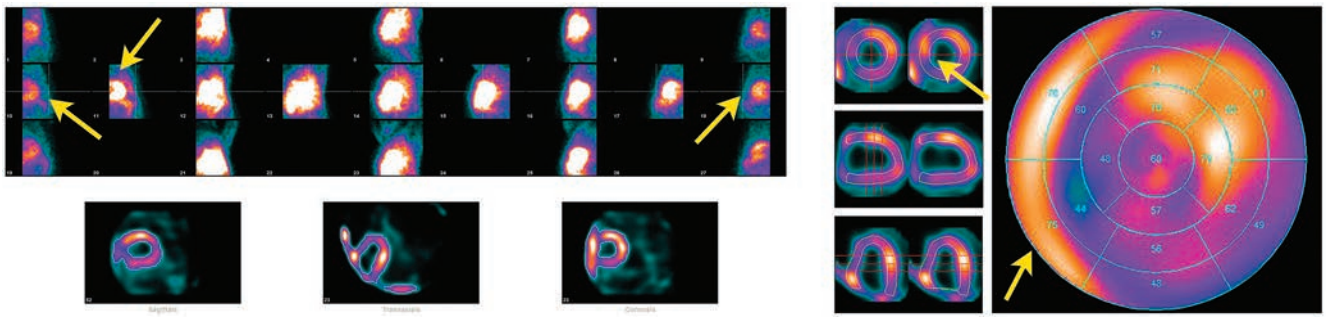

Figure 3A. Unacceptable Scan QC of patient whose polar map with banana-shaped artifact and short-axis slices were shown on Figure 1

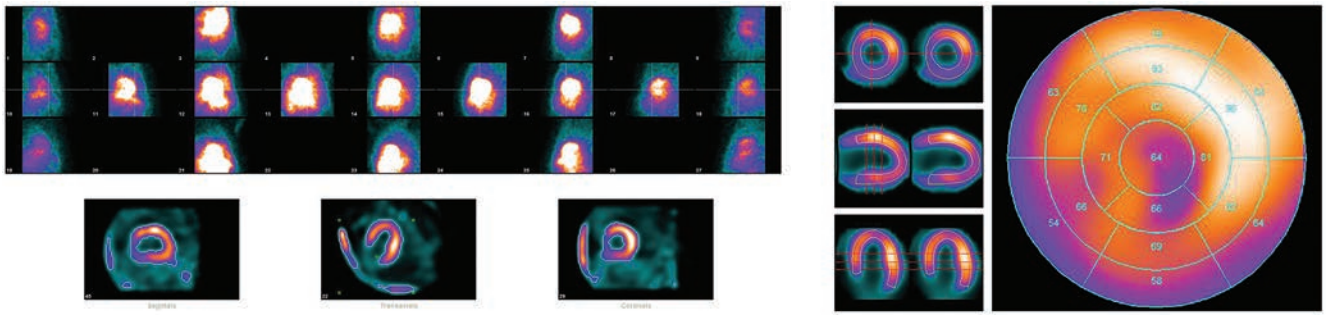

Figure 3B. Correct Scan QC of the same patient after repositioning

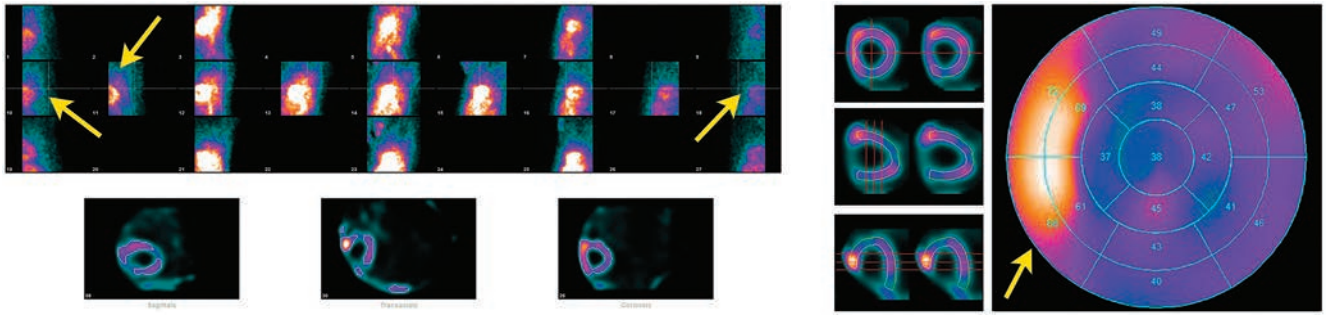

Figure 4. Unacceptable Scan QC (male patient, BMI = 44 kg/m², rest MPI); arrows indicate truncated projections (left) and banana-shaped artifact (right)

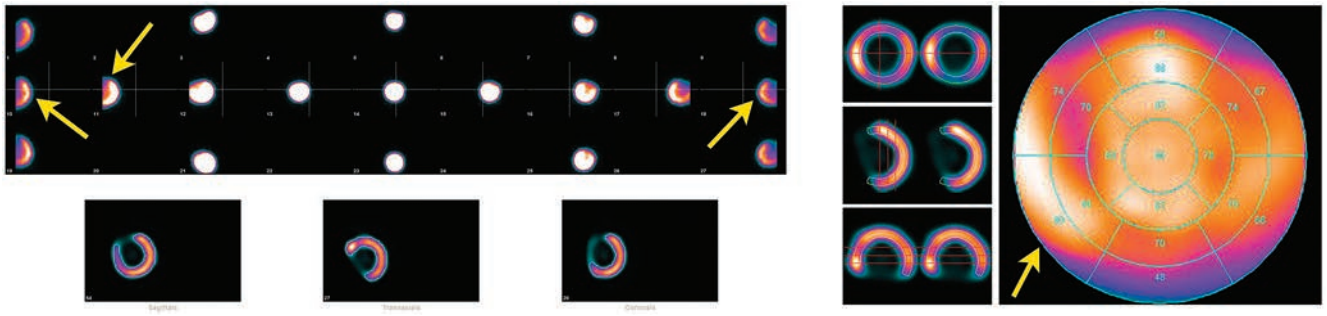

Figure 5. Scan QC of cardiac phantom, truncation on extreme projections visible (left) and banana-shaped artifact on planar map (right)

We believe that incorrect heart positioning in the field of view is essential for banana-shaped artifact presence. In all studies in which we observed this kind of artifact, there was a left ventricle truncation visible on some raw projections displayed with the Scan QC tool (Fig. 3A and Fig. 4). On the other hand, heart truncation present on raw projections does not always generate the banana-shaped artifact.

Phantom studies allowed simulation of an artifact of shape comparable to banana (Fig. 5).

Our study indicates that banana-shaped artifacts are always correlated with negative result of quality control, which highlights importance of such control in a routine practice.

Conclusions

The problem with heart mispositioning during imaging on a semiconductor gamma-camera affects less than 1% of all performed studies. High BMI is associated with difficulties in imaging. Due to the fact that over 2/3 of MPI studies of patients with morbid obesity is diagnostic, imaging on the dedicated cardiac camera with CZT detectors should be attempted in this group, rather than sending these patients directly to a general purpose gamma-camera for MPI scanning.

Acknowledgements

The authors thank Agata Kubik from our Department for valuable input and remarks.

The authors also wish to express their gratitude to Jakub Siennicki from GE Healthcare for consultations regarding application software and hardware.

References

1. Garcia EV, Faber TL, Esteves FP. Cardiac dedicated ultrafast SPECT cameras: new designs and clinical implications. J Nucl Med. 2011; 52(2): 210–217, doi: 10.2967/jnumed.110.081323, indexed in Pubmed: 21233190.
2. Oddstig J, Hedeer F, Jögi J, et al. Reduced administered activity, reduced acquisition time, and preserved image quality for the new CZT camera. J Nucl Cardiol. 2013; 20(1): 38–44, doi: 10.1007/s12350-012-9634-6, indexed in Pubmed: 23143809.
3. Buechel RR, Herzog BA, Husmann L, et al. Ultrafast nuclear myocardial perfusion imaging on a new gamma camera with semiconductor detector technique: first clinical validation. Eur J Nucl Med Mol Imaging. 2010; 37(4): 773–778, doi: 10.1007/s00259-009-1375-7, indexed in Pubmed: 20107783.
4. Hindorf C, Oddstig J, Hedeer F, et al. Importance of correct patient positioning in myocardial perfusion SPECT when using a CZT camera. J Nucl Cardiol. 2014; 21(4): 695–702, doi: 10.1007/s12350-014-9897-1, indexed in Pubmed: 24807623.
5. Fiechter M, Gebhard C, Fuchs TA, et al. Cadmium-zinc-telluride myocardial perfusion imaging in obese patients. J Nucl Med. 2012; 53(9): 1401–1406, doi: 10.2967/jnumed.111.102434, indexed in Pubmed: 22870823.
6. Wąsowski M, Walicka M, Marcinowska-Suchowierka E. Otyłość – definicja, epidemiologia, patogeneza. Postępy Nauk Medycznych. 2013; XXVI(4): 301–306.
7. Piszczek S, Osiecki S, Witkowska-Patena E, et al. The diagnostic efficacy and safety of stress-only supine and prone myocardial perfusion imaging with a dedicated cardiac gamma camera in patients with suspected or known coronary artery disease. Nucl Med Rev Cent East Eur. 2018; 21(2): 104–108, doi: 10.5603/NMR.2018.0028, indexed in Pubmed: 30070351.
8. Gimelli A, Bottai M, Giorgetti A, et al. Evaluation of ischaemia in obese patients: feasibility and accuracy of a low-dose protocol with a cadmium-zinc telluride camera. Eur J Nucl Med Mol Imaging. 2012; 39(8): 1254–1261, doi: 10.1007/s00259-012-2161-5, indexed in Pubmed: 22699527.

VIA MEDICA

Nuclear Medicine Review 2019, 22, 1: 23–28
DOI: 10.5603/NMR.2019.0004

ISSN 1506–9680

Original

Productivity of ^{18}F-FDG-PET/CT Diagnostic Tool in the Management of Pediatric Lymphoblastic Lymphoma

Ahmed Elhussein[1], Mohamed Fawzy[2], Hany Abdel Rahman[2], Walid Omar[3], Elshaymaa Mohamed Hussein[4]

[1] Children's Cancer Hospital Egypt (CCHE [57357]), Cairo, Egypt
[2] National Cancer Institute (NCI), Cairo University, Cairo, Egypt; Children's Cancer Hospital Egypt (CCHE/[57357]), Cairo, Egypt
[3] National Cancer Institute (NCI), Cairo University, Cairo, Egypt
[4] Department of Nuclear Medicine and Radiation Oncology, Faculty of Medicine, Cairo University, Cairo, Egypt

[Received 18 XI 2018; Accepted 27 XII 2018]

Abstract

BACKGROUND: Lymphoblastic lymphoma (LL) comprises approximately 20% of childhood non-Hodgkin lymphoma (NHL); however, few studies had investigated the role of ^{18}F-FDG-PET/CT in pediatric LL patients. We aim in this study to assess the role of ^{18}F-FDG-PET/CT in the initial staging of newly diagnosed pediatric patients with LL as well as in the assessment of response after induction chemotherapy.

PATIENTS AND METHODS: A prospective study enrolled biopsy proven newly diagnosed pediatric LL patients presenting in the Children Cancer Hospital Egypt (CCHE) during the period from October 2014 to October 2016. ^{18}F-FDG-PET/CT was done initially before therapy and after induction chemotherapy in all patients. The patients were followed until the end of April 2018 (mean 23.5 months).

RESULTS: All lymphoma involvement lesions (n = 43) were FDG avid and the intensity of nodal FDG uptake was variable. Two patients (11%) had bone marrow (BM) involvement by < 25% blast cells with corresponding positive BM focal uptake in ^{18}F-FDG-PET/CT (SUVmax = 4 and 4.5). Evaluation post induction phase; CT detected 8 residual lesions in 8 patients (44.4%), while ^{18}F-FDG-PET/CT detected only 3 Deauville-positive residual lesions in 3 patients (16.6%). No intensification of therapy was done in all post-induction positive patients. Repeated ^{18}F-FDG-PET/CT at week 18 for post-induction patients revealed cleared all Deauville-positive residual lesions. On the other hand, repeated CT at week 18 detected regression but still residual in 4/8 (50%) post-induction CT lesions with clearance of the rest (50%).

CONCLUSION: In initial staging, ^{18}F-FDG-PET/CT is a useful tool for disease extent evaluation of pediatric LL. Moreover, it could provide a diagnostic hint for BM involvement. ^{18}F-FDG-PET/CT done after induction therapy has a good negative predictive value with higher specificity than CT alone, but is not an indication for treatment intensification due to false positive results. However, larger sample size is required for better conclusion.

KEY words: pediatric lymphoblastic lymphoma, ^{18}F-FDG-PET/CT, CCHE

Nucl Med Rev 2019; 22, 1: 23–28

Background

Lymphoblastic lymphoma (LL) comprises approximately 20% of childhood non-Hodgkin lymphoma (NHL) [1]. Precursor T-lymphoblastic (T-LL) subtype constitutes 75% of LL cases, with the remainder being precursor B-cell LL (B-LL) [2].

Clinical presentation of LL varies according to immune-phenotype. T-cell lymphoblastic lymphomas most commonly involve the supra-diaphragmatic lymph nodes, especially the anterior mediastinum [3]. On the other hand, B-LL are usually localized in peripheral lymph nodes and extra-nodal sites such as soft tissues, skin and bone [4].

^{18}F-FDG-positron emission tomography/computed tomography (^{18}F-FDG-PET/CT) is emerging as a potential non-invasive diagnostic modality for initial staging as well as assessment of response to therapy and follow-up in pediatric oncology [5]. However, few studies had investigated its role in LL separately, especially in children [6].

The aim of this study was to explore the potential role of ^{18}F-FDG-PET/CT in the initial staging of newly diagnosed pediatric patients with lymphoblastic lymphoma (LL) as well as in the assessment of response to therapy after induction chemotherapy.

Correspondence to: Elshaymaa Mohamed Hussein, Consultant of nuclear medicine, Department of Nuclear Medicine Andradiation Oncology, Faculty of Medicine, Cairo University, Cairo, Egypt;
e-mail: elshaymaahussein@cu.edu.eg

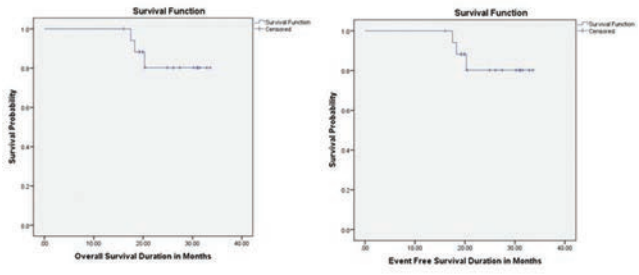

Figure 1. Correlation between results of post-induction ^{18}F-FDG-PET compared to CT and the outcome at last time of follow up

Patients and methods

This prospective study included 18 pediatric patients (14 males and 4 females; median age, 13 years) who were diagnosed and treated for histopathologically confirmed LL at the CCHE during the period from October 2014 to October 2016 and followed until April 2018.

All Patients were treated according to St. Jude Children Research Hospital ALL Total Therapy XV protocol, standard risk arm [7]. Staging was done following Murphy's classification [8] highlighting natural history, management, and end results, emphasizing dissimilarities from lymphomas occurring in adult years. Childhood will arbitrarily be defined as the period from infancy to adulthood, encompassing adolescence, rougly up until the fifteenth to eighteenth years of life. The lymphomas typical of childhood naturally do not vanish at an arbitrary upper threshold in maturity but rather decline in frequency. A separate emphasis on childhood NHL is warranted for numerous reasons, not the least being that a better insight into ontogeny may be gained. Children experience a different spectrum of malignant disease than adults do, the common sites of origin typically being embryonal tissues of the hematopoietic system, central and sympathetic nervous system (including the eye and the adrenal.

As part of the baseline staging work-up, all patients underwent whole-body ^{18}F-FDG-PET/CT scanning; contrast-enhanced CT of the chest, abdomen, and pelvis; and bone marrow aspiration (BMA) and biopsy (BMB), cerebrospinal fluid examination (CSF) and serum lactate dehydrogenase (LDH) level measurement. Evaluation post-induction therapy was done by ^{18}F-FDG-PET/CT, (+/- BMA and BMB which were repeated for initially positive patients only). ^{18}F-FDG-PET/CT was also repeated at week 18 maintenance for positive post-induction patients.

Evaluation of treatment response post induction was done according to CT and BMB, ^{18}F-FDG-PET/CT according to the International Pediatric NHL Response Criteria (IRC) [9].

^{18}F-FDG-PET/CT procedure

Whole body ^{18}F-FDG-PET/CT studies were conducted according to the European Association of Nuclear Medicine (EANM)

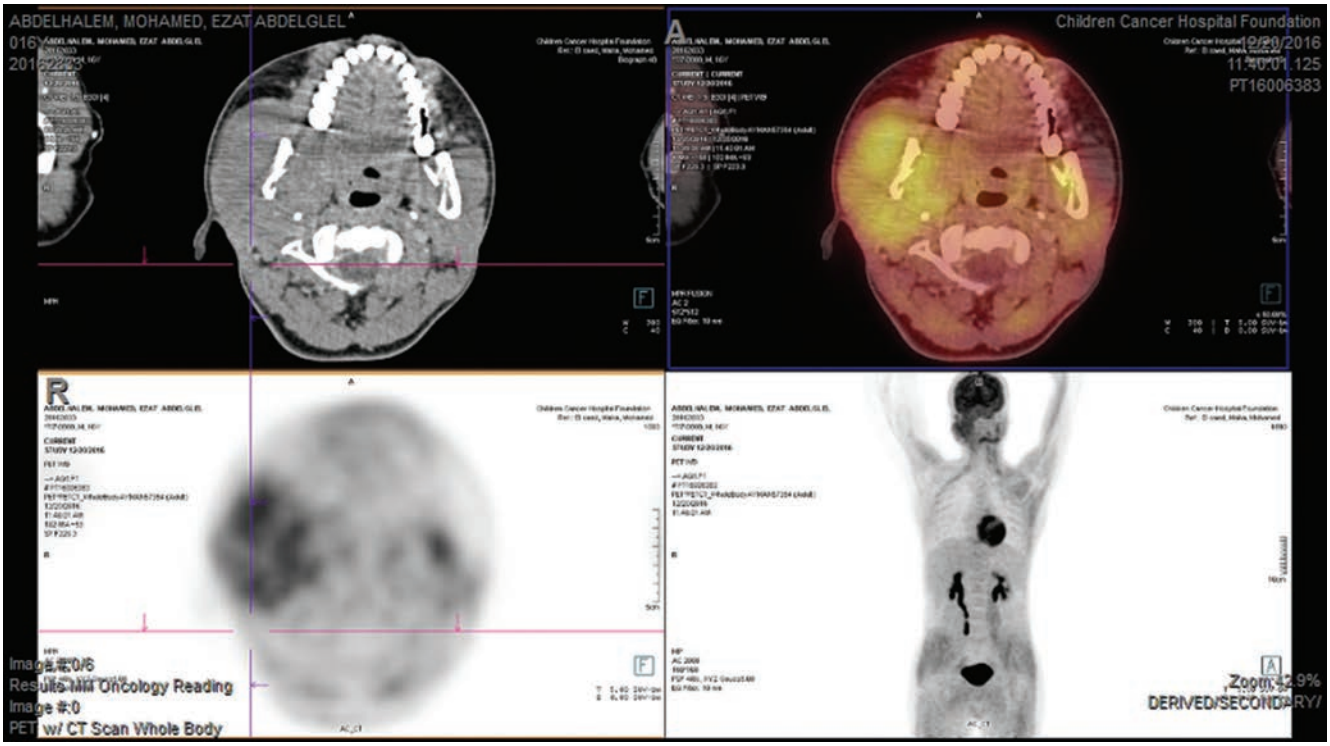

Figure 2. Axial and MIP images of PET/CT and fused18F-FDG-PET/CT images of patient number 2 at initial staging showing: right mandibular mass lesion with SUVmax 4 associated with enlarged right cervical LNs with low grade FDG uptake

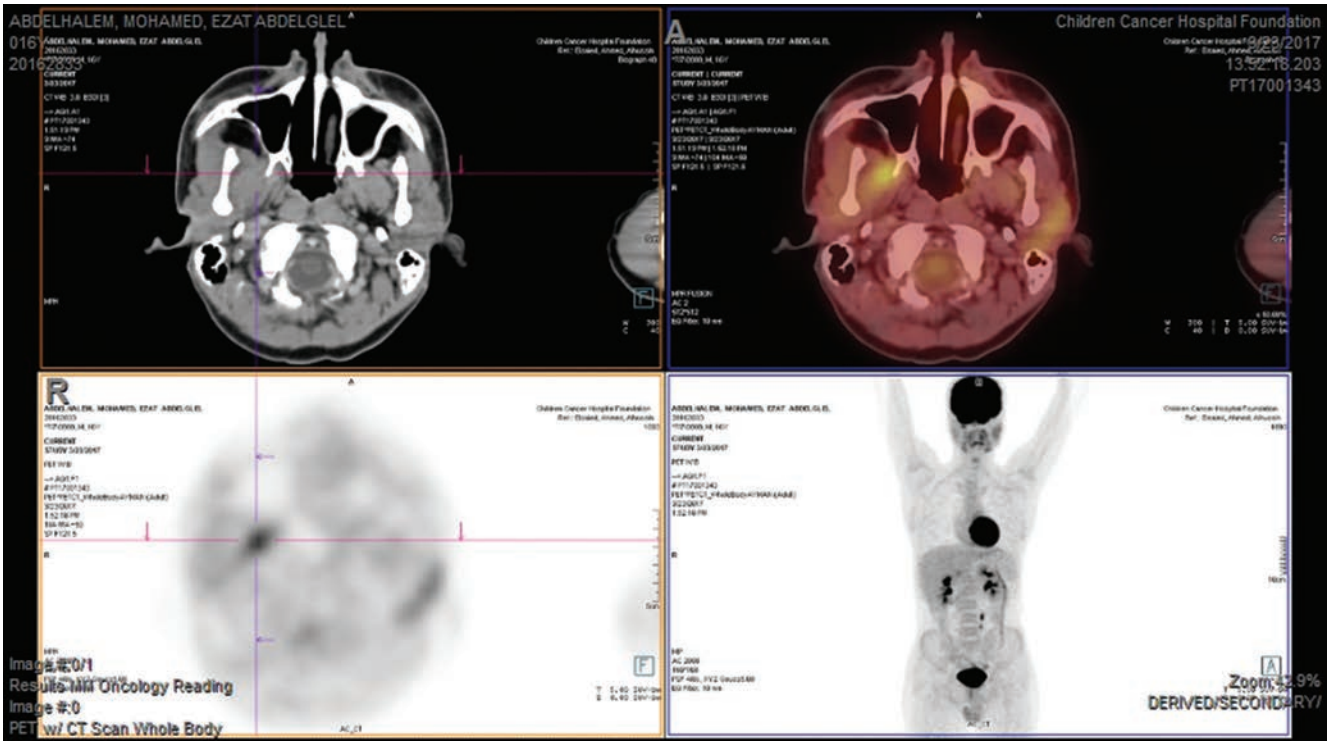

Figure 3. Axial and MIP images of PET/CT and fused18F-FDG-PET/CT images of the same patient's post induction phase showing partial response of the mandibular lesion SUVmax 4 , the patient was scored according to 5-ps as score 4

procedure guidelines for FDG-PET/CT tumor imaging: version 2.0 [10].

Children fasted no less than 4 hours before ^{18}FDG injection dose and blood glucose level was controlled prior to the injection

The study was acquired on a Discovery LS PET/CT imaging system (GE Medical Systems) after intravenous administration of 5–7 MBq/kg of ^{18}FDG or on a mCT Biograph imaging system (Siemens) following intravenous injection of 3 MBq/kg of ^{18}FDG. The images were acquired from the skull to the mid-thigh approximately 60–80 min after ^{18}FDG administration employing 3-D acquisition technique. Subsequent diagnostic CT images were used for attenuation correlation and production of fusion images. The images were reconstructed by ordered-subset expectation maximization (OSEM) iterative reconstruction algorithm with and without attenuation correction.

^{18}F-FDG-PET/CT analysis

All ^{18}F-FDG-PET/CT studies were reviewed by two nuclear medicine physicians using qualitative (visual) analysis and quantitative analysis using the maximum standardized uptakes (SUVmax) values. The SUV was calculated using the equation: SUV = mean activity [region of interest (ROI)] (MBq/ml) / injected dose (MBq) / total body weight (g). Among these SUVs from the targeted ROI, the SUVmax were considered as the highest SUVs of pixels in the ROI. Residual lesions in the 2nd ^{18}F-FDG-PET/CT performed for assessment of response to therapy; are analyzed according to the 5 point scale as recommended by the Lugano criteria [11]staging, and response assessment of patients with Hodgkin lymphoma (HL.

The 5 point scale (5-p-s) is scored as follows: 1 = no uptake; 2 = uptake < mediastinum; 3 = uptake > mediastinum and < liver; 4 = uptake moderately higher than liver at any site; 5 = markedly increased uptake at any involved site. Scores of 4 and 5 are considered positive, while scores of 1–3 are considered negative [12].

Statistical methods

Categorical data were described as counts and percentages while numerical data as SUVmax were reported as mean and standard deviation. Pearson's Correlation was performed to examine the relationship between SUVmax and both tumor size and LDH level. Survival analysis was conducted by Kaplan-Meier method. The Overall Survival is defined as the duration from date of diagnosis to date of last contact or death date, while Event Free Survival is the duration from date of diagnosis to date of last contact or date of first event. Events are: developing 2ry malignancy, death, progression, or relapse. P values less than 0.05 in any test were considered to be statistically significant.

Results

Eighteen patients were included (14 males and 4 females; median age, 13 years), 11 had T-cell (61.1%) while 7 had B-cell lymphoblastic lymphoma (38.9%). Most common presentation site was mediastinal mass (55.5%) followed by head and neck (27.8%), bone marrow infiltration by < 25% blasts (11.1%) and enlarged inguinal LNs (5.6%).

Evaluation of ^{18}F-FDG-PET/CT in initial staging

All lymphoma involvement lesions (n = 43) were FDG-avid and the intensity of nodal FDG uptake was variable. Patients'

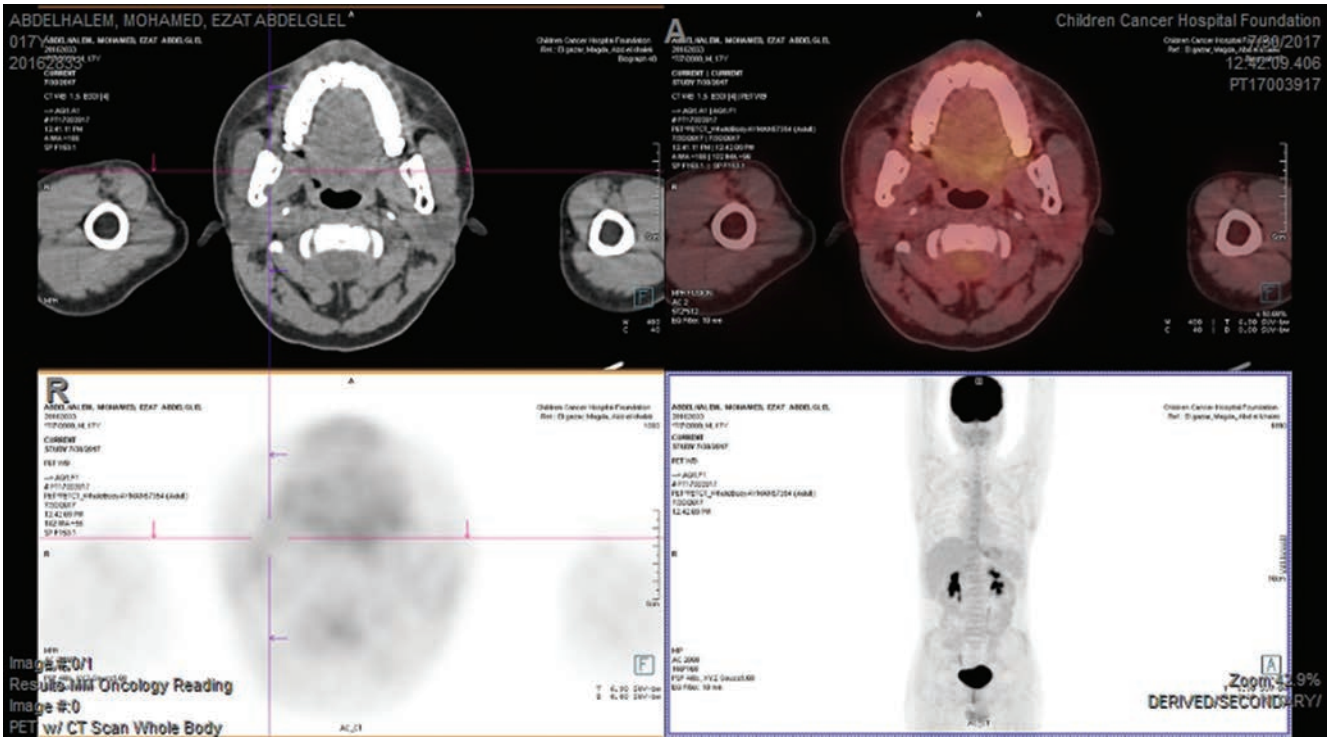

Figure 4. Axial and MIP images of PET/CT and fused ^{18}F-FDG-PET/CT images of the mentioned patient at W18 showing complete metabolic remission of the involved mandibular lesion

characteristics with involved areas and the highest SUVmax are shown in Table 1.

The mean SUVmax of the involved lesions was 5.5. The higher SUVmax at diagnosis was most commonly observed in involved mediastinal lymph nodes, with a mean SUVmax of 5.7.

Two patients (11%) had BM involvement by < 25% blast cells with corresponding positive BM focal uptake in FDG-PET/CT (SUVmax = 4 and 4.5).

There was non-significant correlation between SUVmax of involved lesions and both tumor size (r = 0.356, p = 0.161) and LDH level (r = 0.347, p = 0.172).

Evaluation of ^{18}F-FDG-PET/CT during assessment of response after induction of chemotherapy

Comparison of ^{18}F-FDG-PET/CT results and both CT and BMB was done post induction phase. CT detected 8 residual lesions in 8 patients (44.5%), while FDG-PET/CT detected that only 3 of them (16.7%) considered Deauville-positive.

Ten patients were in CR by CT and BMB (55.5%, n = 10) and all had negative ^{18}F-FDG-PET/CT. On the other hand, 8 patients (44.5%) were in PR; 5 of them (27.8%) had negative ^{18}F-FDG-PET/CT, while 3 were positive (16.7%). No intensification of therapy was done in all post-induction positive patients.

Repeated ^{18}F-FDG-PET/CT at week 18 for post-induction patients revealed cleared all Deauville-positive residual lesions. On the other hand, CT at week 18 detected regression but still residual in 4/8 (50%) post-induction CT lesions with clearance of the rest (50%).

At the time of last follow-up (mean 23.5 months), 15/18 patients (83.3%) were alive. No patient experienced relapse or progression. Two patients died out of progressive infection and sepsis during maintenance course of chemotherapy ALL Total Therapy XV protocol after week 22 and 55. One patient developed acute myeloid leukemia (AML) after 10 weeks of maintenance course of chemotherapy with poor response to therapy and died after 4 courses of AML chemotherapy protocol; none of these patients had positive Deauville score post induction.

We also calculated the sensitivity, specificity, positive and negative predictive values of ^{18}F-FDG-PET/CT in prediction of outcome using last clinical and radiological follow-up as control criteria. We found the specificity of post-induction ^{18}F-FDG-PET/CT was 81% while the negative predictive value was 87% compared to 50% and 80% for post-induction CT respectively (Fig. 1).

Survival Analysis

The 2 years OS was 80.2% (95% confidence interval 59.8% – 100.0%), similar to the 2 years EFS which was 80.2% (95% confidence interval 59.8% – 100.0%) (Fig. 2).

Discussion

In the present study, all disease sites detected by ^{18}F-FDG-PET were concordant with CT and BMB. This was similar to adult studies on lymphoblastic lymphoma where all involved lymph nodes, bone marrow and extra-nodal lesions were FDG-avid [13].

In the current study ^{18}F-FDG-PET/CT did not contribute in up- or down-staging of any of included patients. Similar results had been detected in Nakatani et al study which included 3 patients with LL [14]. Our results also were concordant to Park et al. study on nine

Table 1. Patients' characteristics and ^{18}F-FDG-PET/CT findings at initial staging

Pt.	Gender	Age	Histology	LDH	Area with the highest SUV	SUVmax	Other areas involved	Stage
1	Male	13	T-LL	2942	Mediastinal adenopathy	6.9	Pleura	III
2	Male	16	B-LL	349	Mandibular lesion	4.5	Cervical adenopathy	II
3	Female	13	B-LL	556	Skull bone	8.6	Intracranial lesion	IV
4	Male	6	B-LL	1232	Both femur bones	6.2	Nasopharyngeal mass and BM	IV
5	Male	11	T-LL	442	Mediastinal adenopathy	8.7	Cervical, axillary, abdominal and inguinal adenopathy	III
6	Male	15	T-LL	6064	Mediastinal adenopathy	9.2	Cervical, axillary, abdominal, inguinal adenopathy and pleura	III
7	Male	15	T-LL	1269	Mediastinal adenopathy	5.2	Cervical and inguinal adenopathy, renal focal lesions and pleura	III
8	Male	11	T-LL	581	Mediastinal adenopathy	2.5	Cervical and axillary adenopathy	III
9	Male	15	T-LL	1162	Mediastinal adenopathy	7.3	Cervical adenopathy and pleura	III
10	Female	6	T-LL	663	Mediastinal adenopathy	2.7	Pleura	III
11	Male	12	B-LL	605	Cervical adenopathy	2.3	Cervical adenopathy	I
12	Male	18	T-LL	500	Cervical adenopathy	N/A	--	I
13	Male	3	B-LL	1512	Cervical adenopathy	7.8	Abdominal adenopathy	III
14	Female	13	T-LL	861	Mediastinal adenopathy	7.3	Cervical adenopathy	III
15	Male	11	T-LL	467	Inguinal adenopathy	3.7	Cervical, mediastinal and abdominal adenopathy	III
16	Male	16	T-LL	621	Mediastinal adenopathy	2.5	--	III
17	Female	8	B-LL	539	Abdominal adenopathy	3.8	--	III
18	Male	3	B-LL	1769	Cervical adenopathy	5.3	Mediastinal adenopathy and BM	IV

T-LL: T-cell Lymphoblastic Lymphomas B-LL: B-cell Lymphoblastic Lymphomas, BM: Bone Marrow, LDH: Lactate Dehydrogenase

Table 2. Response criteria using CT, 18F-FDG-PET/CT and IRC

Pt.	Response to Induction				Evaluation at Week 18		Relapse/Progression	Follow up duration (months)	Fate
	CT and BMB	FDG-PET	IRC	Deauville Score	FDG-PET	CT			
1	CR	Negative	CR	0	--	--	No	37	A
2	PR	Positive	PR	4	Negative	Positive	No	15	A
3	CR	Negative	CR	0	--	--	No	30	A
4	CR	Negative	CR	0	--	--	No	21	D
5	PR	Positive	PR	4	Negative	Negative	No	29	A
6	CR	Negative	CR	0	--	--	No	18	D
7	PR	Negative	CRu	0	--	Positive	No	25	D
8	CR	Negative	CR	0	--	--	No	24	A
9	PR	Negative	CRu	0	--	Negative	No	17	A
10	CR	Negative	CR	0	--	--	No	18	A
11	CR	Negative	CR	0	--	--	No	18	A
12	CR	Negative	CR	0	--	--	No	18	A
13	PR	Negative	CRu	2	--	Positive	No	24	A
14	PR	Negative	CRu	2	--	Negative	No	26	A
15	CR	Negative	CR	0	--	--	No	31	A
16	PR	Positive	PR	4	Negative	Positive	No	31	A
17	PR	Negative	CRu	0	--	Negative	No	17	A
18	CR	Negative	CR	0	--	--	No	24	A

CT: Computed Tomography FDG-PET: Fluorodeoxyglucose Positron Emission Tomography, BMB: Bone Marrow Biopsy, IRC: International Response Criteria, CR: Complete Remission, PR: Partial Response, CRu: Complete Remission Uncertain, A: Alive, D: Dead

adult Korean patients with T-LL, where no difference in staging occurred between FDG-PET and CT [13].

In the current study, 2 patients had bone marrow infiltration in both ^{18}F-FDG-PET/CT and BMB while the other 16 patients had negative bone marrow in both modalities. In Park et al. study, eight of the studied patients were found to have bone marrow involvement and all had abnormal bone FDG uptake, indicating that ^{18}F-FDG-PET may be useful for assessing the disease extent in T-LL [13].

In our study, all LL patients who did or didn't have residual after induction therapy, in both ^{18}F-FDG-PET and CT, didn't show signs of progression or relapse. This was different than results by Jain et al. who found that all T-cell LL adult patients who had residual masses on PET-CT (3/22) relapsed during later phase of therapy (all within 6 months) and the authors concluded that such patients should be considered for treatment intensification [15].

Another study that was done by the Swedish Lymphoma Registry included 39 adults with T-LL, of whom none had a PET scan at baseline but 13 had a PET scan at various times before consolidation. All 13 patients were negative, but seven relapsed (54%). Based on this, the authors concluded that PET was not predictive of survival, although there was limitations in their study as FDG-PET/CT was not performed in a uniform manner [16].

A recent retrospective study by Becker et al. on adult patients with T-cell LL concluded that the five-point Deauville score of residual lesions after induction chemotherapy was not predictive of the outcome — 7/20 of patients (35%) who had Deauville score ≤ 3 relapsed and in the same time 3/7 of patients (42.8%) had score 4–5 also relapsed [17].

In conclusion, in initial staging; ^{18}F-FDG-PET/CT is a useful tool for disease extent evaluation of pediatric LL. Moreover, it could provide a diagnostic hint for BM involvement. ^{18}F-FDG-PET/CT done after induction therapy has a good negative predictive value with higher specificity than CT alone, but is not an indication for treatment intensification due to false positive results. However, larger sample size is required for better conclusion.

References

1. Bollard CM, Lim MS, Gross TG, et al. COG Non-Hodgkin Lymphoma Committee. Children's Oncology Group's 2013 blueprint for research: non-Hodgkin lymphoma. Pediatr Blood Cancer. 2013; 60(6): 979–984, doi: 10.1002/pbc.24416, indexed in Pubmed: 23255391.
2. Burkhardt B, Zimmermann M, Oschlies I, et al. BFM Group. The impact of age and gender on biology, clinical features and treatment outcome of non-Hodgkin lymphoma in childhood and adolescence. Br J Haematol. 2005; 131(1): 39–49, doi: 10.1111/j.1365-2141.2005.05735.x, indexed in Pubmed: 16173961.
3. Uyttebroeck A, Suciu S, Laureys G, et al. Children's Leukaemia Group (CLG) of the European Organisation for Research and Treatment of Cancer (EORTC). Treatment of childhood T-cell lymphoblastic lymphoma according to the strategy for acute lymphoblastic leukaemia, without radiotherapy: long term results of the EORTC CLG 58881 trial. Eur J Cancer. 2008; 44(6): 840–846, doi: 10.1016/j.ejca.2008.02.011, indexed in Pubmed: 18342502.
4. Muljono A, Graf NS, Arbuckle S. Primary cutaneous lymphoblastic lymphoma in children: series of eight cases with review of the literature. Pathology. 2009; 41(3): 223–228, doi: 10.1080/00313020902756246, indexed in Pubmed: 19291533.
5. Murphy JJ, Tawfeeq M, Chang B, et al. Early experience with PET/CT scan in the evaluation of pediatric abdominal neoplasms. J Pediatr Surg. 2008; 43(12): 2186–2192, doi: 10.1016/j.jpedsurg.2008.08.064, indexed in Pubmed: 19040932.
6. Cistaro A, Saglio F, Asaftei S, et al. The role of 18F-FDG PET/CT in pediatric lymph-node acute lymphoblastic leukemia involvement. Radiol Case Rep. 2011; 6(4): 503, doi: 10.2484/rcr.v6i4.503, indexed in Pubmed: 27307925.
7. Pui CH, Relling MV, Sandlund JT, et al. Rationale and design of Total Therapy Study XV for newly diagnosed childhood acute lymphoblastic leukemia. Ann Hematol. 2004; 83 Suppl 1: S124–S126, doi: 10.1007/s00277-004-0850-2, indexed in Pubmed: 15124703.
8. Murphy SB. Classification, staging and end results of treatment of childhood non-Hodgkin's lymphomas: dissimilarities from lymphomas in adults. Semin Oncol. 1980; 7(3): 332–339, indexed in Pubmed: 7414342.
9. Sandlund JT, Guillerman RP, Perkins SL, et al. International Pediatric Non-Hodgkin Lymphoma Response Criteria. J Clin Oncol. 2015; 33(18): 2106–2111, doi: 10.1200/JCO.2014.59.0745, indexed in Pubmed: 25940725.
10. Boellaard R, Delgado-Bolton R, Oyen WJG, et al. European Association of Nuclear Medicine (EANM). FDG PET/CT: EANM procedure guidelines for tumour imaging: version 2.0. Eur J Nucl Med Mol Imaging. 2015; 42(2): 328–354, doi: 10.1007/s00259-014-2961-x, indexed in Pubmed: 25452219.
11. Cheson BD, Fisher RI, Barrington SF, et al. Alliance, Australasian Leukaemia and Lymphoma Group, Eastern Cooperative Oncology Group, European Mantle Cell Lymphoma Consortium, Italian Lymphoma Foundation, European Organisation for Research, Treatment of Cancer/Dutch Hemato-Oncology Group, Grupo Español de Médula Ósea, German High-Grade Lymphoma Study Group, German Hodgkin's Study Group, Japanese Lymphorra Study Group, Lymphoma Study Association, NCIC Clinical Trials Group, Nordic Lymphoma Study Group, Southwest Oncology Group, United Kingdom National Cancer Research Institute. Recommendations for initial evaluation, staging, and response assessment of Hodgkin and non-Hodgkin lymphoma: the Lugano classification. J Clin Oncol. 2014; 32(27): 3059–3068, doi: 10.1200/JCO.2013.54.8800, indexed in Pubmed: 25113753.
12. Hasenclever D, Kurch L, Mauz-Körholz C, et al. qPET - a quantitative extension of the Deauville scale to assess response in interim FDG-PET scans in lymphoma. Eur J Nucl Med Mol Imaging. 2014; 41(7): 1301–1308, doi: 10.1007/s00259-014-2715-9, indexed in Pubmed: 24604592.
13. Park JH, Pahk K, Kim S, et al. Fluorine-18 fluorodeoxyglucose positron emission tomography imaging of T-lymphoblastic lymphoma patients. Oncol Lett. 2016; 12(2): 1620–1622, doi: 10.3892/ol.2016.4806, indexed in Pubmed: 27446482.
14. Nakatani K, Nakamoto Y, Watanabe K, et al. Roles and limitations of FDG PET in pediatric non-Hodgkin lymphoma. Clin Nucl Med. 2012; 37(7): 656–662, doi: 10.1097/RLU.0b013e318238f72b, indexed in Pubmed: 22691506.
15. Jain H, Menon H, Epari S, et al. Whole Body PET-CT In Management Of Lymphoblastic Lymphomas In Adults: Does It Have a Prognostic Impact? Blood. 2013; 122(21): 4314.
16. Ellin F, Jerkeman M, Hagberg H, et al. Treatment outcome in T-cell lymphoblastic lymphoma in adults - a population-based study from the Swedish Lymphoma Registry. Acta Oncol. 2014; 53(7): 927–934, doi: 10.3109/0284186X.2014.889850, indexed in Pubmed: 24913153.
17. Becker S, Vermeulin T, Cottereau AS, et al. Predictive value of F-FDG PET/CT in adults with T-cell lymphoblastic lymphoma: post hoc analysis of results from the GRAALL-LYSA LLO3 trial. Eur J Nucl Med Mol Imaging. 2017; 44(12): 2034–2041, doi: 10.1007/s00259-017-3776-3, indexed in Pubmed: 28733763.

VIA MEDICA

Nuclear Medicine Review 2019, 22, 1: 29–33
DOI: 10.5603/NMR.2019.0005

ISSN 1506–9680

Original

Relationship between parathyroid gland scintigraphy and its histopathology, oxyphil cell content and volume: a retrospective study

Małgorzata Kobylecka[1], Łukasz Koperski[2], Witold Chudziński[3], Paweł Pihowicz[2], Joanna Mączewska[1], Maria Teresa Płazińska[1], Magdalena Bogdańska[2], Leszek Królicki[1]

[1] Nuclear Medicine Department, Medical University of Warsaw, Warsaw, Poland
[2] Department of Pathology, Medical University of Warsaw, Warsaw, Poland
[3] Department of General, Endocrine and Vascular Surgery, Medical University of Warsaw

[Received 5 XI 2018; Accepted 11 XII 2018]

Abstract

BACKGROUND: Mechanisms that are responsible for positive ^{99m}Tc-MIBI uptake in parathyroid glands are not clearly understood, some authors suggest there is a correlation between ^{99m}Tc MIBI accumulation and oxyphil cell content or parathyroid gland volume. The aim of our work was to assess the relationship between the pathological structure of parathyroids, their volume, oxyphil cell content and parathyroid ^{99m}Tc-MIBI retention.

MATERIAL AND METHODS: A total of 62 hyperfunctioning parathyroid glands in 46 patients were retrospectively analyzed. Preoperative ^{99m}Tc-MIBI scintigraphy was performed according to the double-phase and subtraction protocol. After surgery all glands were evaluated histologically, oxyphil cell content was assessed and volume of each excised gland was calculated.

RESULTS: Scintigraphy was positive in 41 of 62 parathyroid glands (66%). The median volume of positive glands was larger than that of negative glands (1.33 ml vs 0.7 ml, $p = 0.015$). Of the parathyroid lesions, there were 14 (22.6%) cases of nodular hyperplasia, 23 (37.1%) cases of diffuse hyperplasia, and 25 (40.3%) cases of adenomas. A high (≥ 25%) oxyphil cell content was found in 16 glands (25.8%) and a low (< 25%) oxyphil cell content in 46 (74.2%) glands. Histopathology of parathyroid glands was related to the scintigraphy result ($p = 0.002$), but not to the 99mTc-MIBI uptake pattern ($p = 0.868$). The overall result of scintigraphy was not related to the oxyphil cell content ($p = 0.797$). ^{99m}Tc-MIBI uptake pattern wasn't related to the oxyphil cell content ($p = 0.833$). In general, parathyroid lesions with low oxyphil cell content were larger than parathyroid glands with high oxyphil cell content (1.33 ml vs 0.5 ml, respectively; $p = 0.01$). The median volume of parathyroids containing a high number of oxyphil cells and having a prolonged ^{99m}Tc-MIBI retention was larger than those without prolonged ^{99m}Tc-MIBI retention (1.62 ml vs 0.3 ml, respectively; $p = 0.008$). The median volume of parathyroids with low oxyphil cells content and showing prolonged ^{99m}Tc-MIBI retention was larger than those without prolonged ^{99m}Tc-MIBI retention (1.95 ml vs 1.07 ml, respectively; $p = 0.014$).

CONCLUSIONS: Our findings suggest that a positive scintigraphy result depends on parathyroid histopathology and gland volume and does not depend on the presence of oxyphil cells. Prolonged ^{99m}Tc-retention is not related to the parathyroid gland histopathology and the presence of oxyphil cells but to the gland volume.

KEY words: parathyroid scintigraphy, ^{99m}Tc-MIBI, oxyphil cells, parathyroid adenoma, parathyroid hyperplasia, parathyroid volume

Nucl Med Rev 2019; 22, 1: 29–33

Introduction

One of the primary methods of localizing diseased parathyroid glands is scintigraphy. There is no controversy that the sensitivity of scintigraphy (mean 83%) is superior to other imaging techniques: ultrasonography (36–76%), CT (46–55%) and MRI (50–78%) [1, 2, 3, 4]. However, there are significant differences in the sensitivity of scintigraphic studies, depending on the clinical form of hyperparathyroidism. The majority of positive results are obtained in patients with primary hyperparathyroidism 93% [5] and with a single parathyroid adenoma 82–100% [6, 7, 8]. Lower sensitivities were noted for primary hyperplasia (62%), secondary and tertiary hyperthyroidism (41%–50%) [5, 9, 10]. The reasons for such

Correspondence to: Łukasz Koperski, Department of Pathology, Medical University of Warsaw, Warsaw, Poland, e-mail: lkoperski@wum.edu.pl

differences are not fully explained. The complex mechanisms responsible for the degree of radiopharmaceutical accumulation in parathyroid glands are not fully understood [11]. ^{99m}Tc-MIBI accumulates in tissues with high cellular metabolism, including enlarged parathyroid glands. Accumulation of ^{99m}Tc-MIBI may be influenced by many factors, including gland size, microscopic structure, tissue blood flow, functional status of the parathyroid, PTH and calcium levels, drugs and many others. [12]. The aim of our work was to assess the relationship between the histopathology of parathyroid glands, oxyphil cell content, gland volume and parathyroid ^{99m}Tc-MIBI retention.

Material and methods

Patients

A retrospective analysis of 62 parathyroid glands in 46 patients (34 females and 12 males with an average age of 58.4 years) was performed. The study group consisted of 35 subjects with primary hyperparathyroidism (including 6 patients with MEN1), 5 subjects with secondary hyperparathyroidism and 6 patients with tertiary hyperparathyroidism. All patients were operated, 13 patients were re-operated. The surgical procedure involved double-sided exploration of the neck with the assessment of all parathyroid glands. The size and the exact position of parathyroid glands were assessed.

Imaging techniques

In all patients prior to surgery, a double phase and subtraction scintigraphy after administration of 555–740 MBq (15-20 mCi) ^{99m}Tc-MIBI and a ^{99m}Tc thyroid scintigraphy after injection of 60 MBq ^{99m}Tc was performed. A low energy high resolution collimator was used. Images were recorded in a 128 x 128 pixel matrix. Parathyroid evaluation was started with thyroid scintigraphy, performed 10 minutes after iv administration of 60MBq ^{99m}Tc, for the purpose of subtraction of thyroid images. Subsequently, 20 min after administration of ^{99m}Tc-MIBI, an "early" image was recorded followed after 120 min by "late" image acquisition. The acquisition time was 10 minutes; approximately 1.200 kcts/picture were obtained. The parathyroid image was obtained after subtraction of ^{99m}Tc thyroid image, from an "early" image of standard two-phase ^{99m}Tc-MIBI scintigraphy. An abnormal focus of radiopharmaceutical accumulation with or without prolonged ^{99m}Tc-MIBI retention, which was positively verified surgically was assumed to be a pathologic parathyroid gland. The radiopharmaceutical retention was assessed visually. The result of ^{99m}Tc-MIBI scintigraphy was considered to be non-diagnostic in the presence of large goiter.

Histopathological examination

Surgically removed parathyroid specimens were immediately fixed in 10% neutral buffered formalin, then processed into paraffin embedded sections and stained with hematoxylin and eosin (H&E). Parathyroid lesions were classified according to histological criteria suggested by Ghandur-Mnaymneh et al. [13]. Cell types were identified as follows: chief cells, clear cells and oxyphil cells. The oxyphil cell content of each lesion was determined based on semi-quantitative assessment of the percentage of oxyphil cells on each section as proposed by Carpentier et al.: group 1: 0%, group 2: 1–25%, group 3: 26–50%, group 4: 51–75%, group 5: > 75% [14]. For statistical purposes, results were grouped into: high (> 25%) oxyphil cell content (groups 3–5) and low (≤ 25%) oxyphil cell content (groups 1–2). The parathyroid volume was calculated on the basis of histopathological measurements obtained using the formula $V = (a + b + c) \times 0.52$

Statistical analysis

Statistical analyses were performed using STATISTICA (data analysis software system), version 12, StatSoft, Poland. The association between parameters was assessed by chi-square test (contingency tables) for categorical variables and by the Mann-Whitney test for comparison of continuous variables. For all tests, the significance threshold was set at $p \leq 0.05$.

Results

All analyzed parathyroid glands were removed surgically and verified by histopathological examination. In 5 patients (8%) ectopic glands were found intraoperatively: among them 2 parathyroid glands were located in the tracheoesophageal groove, in 2 cases the gland was found below the level of the jugular notch (Fig. 1); in one case parathyroid tissue was located inside the left lobe of the thyroid gland.

Parathyroid scintigraphy revealed 41 (66%) out of the 62 excised glands verified histopathologically. In 25 (61%) out of 41 of positive results of scintigraphy, prolonged ^{99m}Tc-MIBI retention was observed.

Histopathologically, nodular hyperplasia was found in 14 (22.6%) glands, diffuse hyperplasia in 23 (37.1%), and adenoma in 25 (40.3%) glands. 16 (25.8%) of the parathyroid lesions (including 8 cases of adenoma, 2 cases of diffuse hyperplasia and in 6 cases of nodular hyperplasia) were characterized by a high (> 25%) oxyphil cells content (Fig. 2). In this group the oxyphil cell content in 7 lesions was 26–50%, in 4 lesions 51–75% and in 5 lesions > 75%. In 46 (74.2%) parathyroid lesions (including 17 cases of adenoma, 21 cases of diffuse hyperplasia and 8 cases of nodular hyperplasia) the percentage of oxyphil cells was low (≤ 25%), of which 27 lesions had no oxyphil cells, and 19 lesions had an oxyphil content of 1–25% cells.

The histopathology of the parathyroid glands was related to the scintigraphy result ($p = 0.002$), but not to the 99mTc-MIBI uptake pattern ($p = 0.868$). 11 cases of parathyroid lesions with high oxyphil cell content had positive scintigraphy results, of which 4 cases did not demonstrate prolonged ^{99m}Tc-MIBI retention. In 5 cases, despite the presence of oxyphil cells, scintigraphy was considered to be negative. The overall result of scintigraphy was not related to the oxyphil cell content ($p = 0.797$). The ^{99m}Tc-MIBI uptake pattern was not related to the oxyphil cell content ($p = 0.833$). The median volume of scintigraphy positive glands was larger than that of scintigraphy negative glands (1.33 ml vs 0.7 ml, $p = 0.015$). The median volume of parathyroid glands with prolonged ^{99m}Tc-MIBI retention was larger than those without prolonged ^{99m}Tc-MIBI retention (1.89 ml vs 0.95 ml, respectively; ($p = 0.037$) (Tab. 1). In general, parathyroid lesions with low oxyphil cell content were larger than

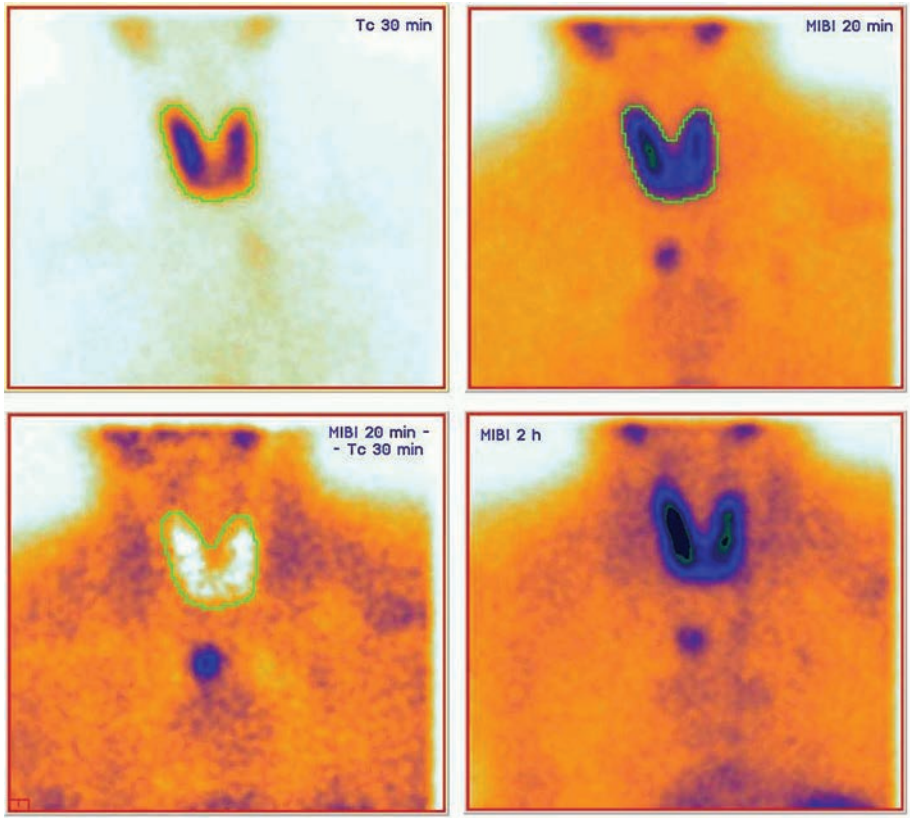

Figure 1. ^{99m}Tc-MIBI scintigraphy: ectopic parathyroid is visible below the thyroid gland; it was found below the level of the jugular notch

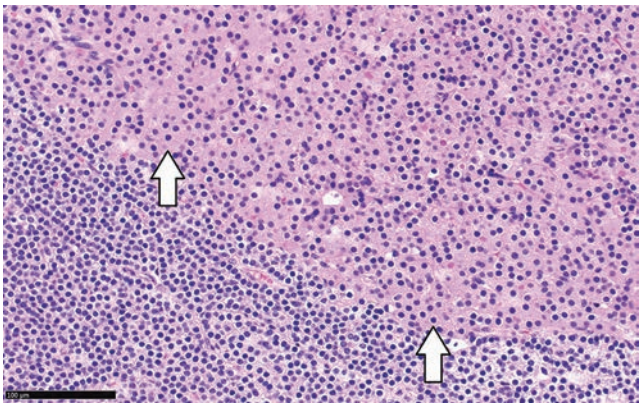

Figure 2. Parathyroid nodular hyperplasia with high (> 25%) oxyphil cell content (arrows — oxyphil cells). Scale bar: 100 μm

parathyroid glands with high oxyphil cell content (1.33 ml vs 0.5ml, respectively; p = 0.01). The median volume of parathyroids containing a high number of oxyphil cells and having a prolonged ^{99m}Tc-MIBI retention was larger than those without prolonged ^{99m}Tc-MIBI retention (1.62 ml vs 0.3 ml, respectively; p = 0.008). The median volume of parathyroids with a low oxyphil cell content and showing prolonged ^{99m}Tc-MIBI retention was larger than those without prolonged ^{99m}Tc-MIBI retention (1.95 ml vs 1.07 ml, respectively; p = 0.014) (Tab. 2).

Discussion

In the available literature, discussions on the nature of marker retention in the parathyroid glands include the impact of a variety of factors, including the impact of histological structure and location. A factor that unquestionably influences the sensitivity of scintigraphic studies is the parathyroid gland size. Lesions smaller than 1 cm are generally not visible in scintigraphy; however, there are cases of positive scintigraphy in smaller glands. Our current results confirmed that a positive result of scintigraphy depends mainly on the parathyroid volume. Most authors agree that there is a relationship between mass (size) and degree of marker accumulation in parathyroid glands [15, 16, 17]. Wada et al. obtained a sensitivity of 40.7% for parathyroid volume less than 0.5 cm^3. In patients with parathyroids larger than 0.5 cm^3, sensitivity was 95% [18]. Fujimoto et al. found difficulty in visualizing parathyroid glands below 300 mg [19]. Other results were obtained by Pons et al. analyzing the weight and size of glands in a group of 20 patients, there was no statistically significant difference in mean parathyroid weight in patients with positive and negative scintigraphy, but this may be due to the small sample size and patient selection [20]. Blocklet et al. on the other hand, found that the weight of the gland was related to the extent of ^{99m}Tc-MIBI accumulation in the case of adenomas, but did not find correlation in patients with parathyroid hyperplasia [21].

The second important factor influencing the visualization of the gland in scintigraphy is its location. In this study, an ectopic gland was found in 8% of excised parathyroids. This result is in

Table 1. Comparison of variables according to result of scintigraphy and ^{99m}Tc-MIBI retention pattern

	All (n=62)	Negative scintigraphy (n = 21)	Positive scintigraphy (n = 41)	P value	Positive scintigraphy (n = 41)		P value
					Prolonged retention (n = 25)	No prolonged retention (n = 16)	
Histology, n (%)							
adenoma	25 (40.3%)	5 (23.8%)	20 (48.8%)	0.002*	13 (52%)	7 (43.8%)	0.868
diffuse hyperplasia	23 (37.1%)	14 (66.7%)	9 (22%)		5 (20%)	4 (25%)	
nodular hyperplasia	14 (22.6%)	2 (9.5%)	12 (29.2%)		7 (28%)	5 (31.2%)	
Oxyphil cells, n (%)							
≤ 25% (low content)	46 (74.2%)	16 (76.2%)	30 (73.2%)	0.797	18 (72%)	12 (75%)	0.833
> 25% (high content)	16 (25.8%)	5 (23.8%)	11 (26.8%)		7 (28%)	4 (25%)	
Volume [ml]							
mean ± SD	1.75 ± 2.04	0.98 ± 0.9	2.14 ± 2.34	0.015*	2.5 ± 2.48	1.59 ± 2.07	0.037*
median (range)	1.13 (0.06-12)	0.7 (0.06-3.1)	1.33 (0.08-12)		1.89 (0.1-12)	0.95 (0.08-8.25)	

*p < 0.05

Table 2. Comparison of parathyroid volume according to the oxyphil cell content and ^{99m}Tc-MIBI retention pattern

	Low OCC (<25%)	High OCC (≥ 25%)	P value	Low OCC and PR	Low OCC and no PR	P value	High OCC and PR	High OCC and no PR	P value
n (%)	46 (74.2%)	16 (25.8%)		18 (39%)	28 (61%)		7 (43.8%)	9 (56.2)	
volume [ml]									
mean ± SD	2.02 ± 2.22	0.96 ± 1.16		2.81 ± 2.75	1.52 ± 1.67		1.7 ± 1.45	0.39 ± 0.30	
median (range)	1.33 (0.06-12)	0.5 (0.08-4.5)	0.01*	1.95 (0.1-12)	1.07 (0.06-8.25)	0.014*	1.62 (0.5-4.5)	0.3 (0.08-1.0)	0.008*

OCC, oxyphil cell content; PR, prolonged retention; *p < 0.05

agreement with the published literature. Parathyroid glands are present in the ectopic positions in about 10% of cases, occurring in various neck and mediastinal locations: from the level of the salivary glands to the level of the heart. Since the basic scintigraphic examination is performed only in the AP projection, the greater the distance from the head and the greater the thickness of the gamma radiation suppressing tissue, the smaller the number of gamma rays that are recorded. The SPECT study is helpful, but this study was of a retrospective nature and SPECT data were not available. Moreover SPECT significantly prolongs the study acquisition time and rules out subtraction. In the studied material, an ectopic position of the parathyroid gland did not noticeably affect the scintigraphy outcome: in one case, retention was not present in a parathyroid located retrosternally, while the remaining ectopic cases showed a positive scintigraphy result.

Another factor that influences the visibility and retention of the ^{99m}Tc-MIBI is parathyroid histopathology. It is well known that scintigraphy demonstrates the highest sensitivity for cases of adenomas, high sensitivity for primary hyperparathyroidism, and a lower sensitivity in secondary and tertiary hyperparathyroidism. Similarly, in the analyzed material, there was a statistically significant relationship between the scintigraphy result and the histopathologic type of parathyroid lesion. Most patients with a negative scintigraphy result had diffuse hyperplasia, whereas the most common lesion in patients with a positive scintigraphy result was parathyroid adenoma.

Due to the complex mechanism of ^{99m}Tc-MIBI accumulation in cells, it is not known which elements of the parathyroid structure are responsible for the accumulation and retention of the marker. Cinti et al. analyzed the microscopic structure of 271 parathyroid glands and described the normal structure of parathyroid glands, which consists of the chief, clear, oxyphil and transitional oxyphil cells [22]. As it is known, ^{99m}Tc-MIBI is mainly concentrated in the mitochondria, present in abundance in oxyphil cells [23]. Carpentier et al. found a correlation between ^{99m}Tc-MIBI accumulation and the oxyphil cell content [14]. Prolonged retention was found in 78% of cases with high oxyphil cell content, and in 33% of cases with a low oxyphil cell content. Glands that did not have any of the oxyphil cells showed no prolonged retention of the marker. In the analyzed material ^{99m}Tc-MIBI retention in parathyroid glands was compared in two groups: parathyroid glands containing more than 25% oxyphil cells (high oxyphil cell content) and parathyroid glands with no or less than 25% oxyphil cells (low oxyphil cell content). There was no statistically significant relationship between the presence of oxyphil cells and a positive scintigraphy result. The presence of prolonged ^{99m}Tc-MIBI retention was not associated with the presence of oxyphil cells but with the parathyroid volume. The results of Allen et al. were surprising: in the group of 114 patients with hyperparathyroidism, oxyphil cells were present in 91% secondary hyperthyroidism cases, in 69% of adenoma cases and in 55% of primary hyperplasia cases [24]. Assuming a strict dependence on ^{99m}Tc-MIBI cellular accumulation on oxyphil cell content, in the light of the data provided, the sensitivity of scintigraphy in secondary and tertiary hyperparathyroidism should be comparable or even superior to that of primary hyperthyroidism. In fact, the ^{99m}Tc-MIBI retention does not depend solely on the presence of oxyphil cells, but rather is a more complex process. This observation is confirmed

by our study's results. In spite of the presence of oxyphil cells, no ^{99m}Tc-MIBI retention was observed in 4 parathyroids, and in 5 cases parathyroid glands containing oxyphil cells were not visible in scintigraphy. According to Koizumi et al there is no strict correlation between ^{99m}Tc-MIBI uptake and cellular composition [25]. They noted a positive correlation between the accumulation of ^{99m}Tc-MIBI and the presence of oxyphil cells, which is related to the high mitochondrial density compared to other cell types. However, regardless of the histological structure in the cited work, all visualized glands in 10 investigated patients were greater than 220 mg. This result confirms our observation that the ^{99m}Tc-MIBI accumulation would not depend on cellular composition but on the size and functional status of the cells.

Conclusions

Our findings suggest that a positive scintigraphy result depends on the histopathology and the volume of the parathyroid gland and does not depend on the presence of oxyphil cells. Additionally, prolonged ^{99m}Tc-retention is not related to the histopathology of the parathyroid gland and the presence of oxyphil cells, but to the gland volume.

References

1. Ishibashi M, Nishida H, Hiromatsu Y, et al. Comparison of technetium-99m-MIBI, technetium-99m-tetrofosmin, ultrasound and MRI for localization of abnormal parathyroid glands. J Nucl Med. 1998; 39(2): 320–324, indexed in Pubmed: 9476944.
2. Mitchell BK, Merrell RC, Kinder BK. Localization studies in patients with hyperparathyroidism. Surg Clin North Am. 1995; 75(3): 483–498, indexed in Pubmed: 7747254.
3. Touska P, Elstob A, Rao ND, et al. SPECT-CT-guided ultrasound for parathyroid adenoma localisation — a one stop approach. J Nucl Med Technol. 2018 [Epub ahead of print], doi: 10.2967/jnmt.118.209767, indexed in Pubmed: 30139883.
4. Botushanova AD, Botushanov NP, Yaneva MP. Nuclear Medicine Methods for Evaluation of Abnormal Parathyroid Glands in Patients with Primary and Secondary Hyperparathyroidism. Folia Med (Plovdiv). 2017; 59(4): 396–404, doi: 10.1515/folmed-2017-0054, indexed in Pubmed: 29341944.
5. Torregrosa JV, Palomar MR, Pons F, et al. Has double-phase MIBI scintigraphy usefulness in the diagnosis of hyperparathyroidism? Nephrol Dial Transplant. 1998; 13 Suppl 3: 37–40, indexed in Pubmed: 9568818.
6. Biaco I, Carril J, Banzo I, et al. Double-Phase Tc-99m Sestamibi Scintigraphy in the Preoperative Location of Lesions Causing Hyperparathyroidism. Clinical Nuclear Medicine. 1998; 23(5): 291–297, doi: 10.1097/00003072-199805000-00005.
7. Norman J, Chheda H, Farrell C. Minimally invasive parathyroidectomy for primary hyperparathyroidism: decreasing operative time and potential complications while improving cosmetic results. Am Surg. 1998; 64(5): 391–5; discussion 395, indexed in Pubmed: 9585770.
8. Martin D, Rosen IB, Ichise M. Evaluation of single isotope technetium 99M-sestamibi in localization efficiency for hyperparathyroidism. Am J Surg. 1996; 172(6): 633–636, indexed in Pubmed: 8988665.
9. Olaizola C, Zingraff J, Fajardo L, et al. (99m)Tc-sestamibi parathyroid scintigraphy in chronic haemodialysis patients: static and dynamic explorations Nephrology, Dialysis, Transplantation. 2000; 15(8): 1201–1206.
10. Pham TH, Sterioff S, Mullan BP, et al. Sensitivity and utility of parathyroid scintigraphy in patients with primary versus secondary and tertiary hyperparathyroidism. World J Surg. 2006; 30(3): 327–332, doi: 10.1007/s00268-005-0279-3, indexed in Pubmed: 16470331.
11. Hindié E, Ugur O, Fuster D, et al. Parathyroid Task Group of the EANM. 2009 EANM parathyroid guidelines. Eur J Nucl Med Mol Imaging. 2009; 36(7): 1201–1216, doi: 10.1007/s00259-009-1131-z, indexed in Pubmed: 19471928.
12. Hoang TD, Jani AG, Mai VQ, et al. Associations of serum ionized calcium, phosphate, and pth levels with technetium-99 sestamibi parathyroid spect/ct scan in primary hyperparathyroidism. Endocr Pract. 2018 [Epub ahead of print], doi: 10.4158/EP-2018-0414, indexed in Pubmed: 30289305.
13. Ghandur-Mnaymneh L, Kimura N. The parathyroid adenoma. A histological definition with a study of 172 cases of primary hyperparathyroidism. Am J Pathol. 1984; 115: 70–83.
14. Carpentier A, Jeannotte S, Verreault J, et al. Preopereative localization of parathyroid lesions in hyperparathyroidism: relationship between Technetium 99mTc-MIBI uptake and Oxyphil Cell Content. J Nucl Med. 1998; 39: 1441–1444.
15. Fujimoto N, Itoh K, Kishikawa H, et al. [Preoperative localization of enlarged parathyroid glands by 99mTc-MIBI scintigraphy]. Nihon Hinyokika Gakkai Zasshi. 1997; 88(9): 795–800, indexed in Pubmed: 9364845.
16. Jeanguillaume C, Ureña P, Hindié E, et al. Secondary hyperparathyroidism: detection with I-123-Tc-99m-Sestamibi subtraction scintigraphy versus US. Radiology. 1998; 207(1): 207–213, doi: 10.1148/radiology.207.1.9580138, indexed in Pubmed: 9580138.
17. Neumann DR, Esselstyn CB, Madera A, et al. Parathyroid detection in secondary hyperparathyroidism with 123I/99mTc-sestamibi subtraction single photon emission computed tomography. J Clin Endocrinol Metab. 1998; 83(11): 3867–3871, doi: 10.1210/jcem.83.11.5241, indexed in Pubmed: 9814460.
18. Wada A, Sugihara M, Sugimura K, et al. Magnetic resonance imaging (MRI) and technetium-99m-methoxyisonitrile (MIBI) scintigraphy to evaluate the abnormal parathyroid gland and PEIT efficacy for secondary hyperparathyroidism. Radiat Med. 1999; 17(4): 275–282, indexed in Pubmed: 10510900.
19. Fujimoto N, Itoh K, Kishikawa H, et al. Preoperative localization of enlarged parathyroid glands by 99mTc-MIBI scintigraphy. Nihon Hinyokika Gakkai Zasshi. 1997; 88(9): 795–800, indexed in Pubmed: 9364845.
20. Pons F, Torregrosa JV, Vidal-Sicart S, et al. Preoperative parathyroid gland localization with technetium-99m sestamibi in secondary hyperparathyroidism. European Journal of Nuclear Medicine and Molecular Imaging. 1997; 24(12): 1494–1498, doi: 10.1007/s002590050179.
21. Blocklet D, Martin P, Schoutens A, et al. Presurgical localization of abnormal parathyroid glands using a single injection of technetium-99m methoxyisobutylisonitrile: Comparison of different techniques including factor analysis of dynamic structures. European Journal of Nuclear Medicine. 1997; 24(1): 46–51, doi: 10.1007/bf01728308.
22. Cinti S, Sbarbati A. Ultrastructure of human parathyroid cells in health and disease. Microsc Res Tech. 1995; 32(2): 164–179, doi: 10.1002/jemt.1070320210, indexed in Pubmed: 8580510.
23. Joujoux JM, Marty-Double C, Godlewski G, et al. [Morphological aspects of parathyroid hyperplasia in patients with chronic renal insufficiency on dialysis]. Ann Pathol. 1986; 6(3): 164–169, indexed in Pubmed: 3778582.
24. Allen TB, Thorburn KM. The oxyphil cell in abnormal parathyroid glands. A study of 114 cases. Arch Pathol Lab Med. 1981; 105(8): 421–427, indexed in Pubmed: 6894851.
25. Arbab AS, Koizumi K, Hemmi A, et al. Tc-99m-MIBI scintigraphy for detecting parathyroid adenoma and hyperplasia. Ann Nucl Med. 1997; 11(1): 45–49, indexed in Pubmed: 9095323.

Clinical vignette

Nuclear Medicine Review 2019, 22, 1: 34–36
DOI: 10.5603/NMR.2019.0006

ISSN 1506–9680

VIA MEDICA

Chronic Total Occlusion of Coronary Artery Without Previous History of Myocardial Infarction: A Role Of Spect

Katarzyna Jóźwik-Plebanek, Artur Dębski, Marek Cacko, Jacek Wnuk, Anna Teresińska
Instytut Kardiologii im. Prymasa Tysiąclecia Stefana Kardynała Wyszyńskiego w Warszawie

[Received 1 X 2018; Accepted 11 XII 2018]

A 69-year-old man with arterial hypertension was admitted because of 30-minute episode of chest pain. His past medical history includes two similar episodes — myocardial infarction (MI) was excluded both times. One month before the admission an angio-computed tomography (angio-CT) of coronary arteries had revealed a total occlusion of the left anterior descending artery (LAD) (Fig. 1). Upon admission, BP was 195/100; the ECG showed a small R-wave progression in the V1–V3 leads. Laboratory test excluded MI. Patient was qualified for invasive coronary angiography which showed occlusion in the mid segment of LAD and insignificant atherosclerotic changes in other coronary arteries. A technetium-99m-methoxy-isobutyl-isonitrile (MIBI) myocardial perfusion SPECT study was performed. The exercise test carried out during SPECT was completed after reaching the target HR with no signs of ischemia. In the exercise SPECT images, a significant perfusion defect was found in the area of the apex, anterior and antero-septal LV wall, which significantly diminished in the rest SPECT (Fig. 2). Stress-induced perfusion defect (ISCH) involved 13% of the LV muscle. Based on these results, an elective LAD recanalization was performed (Fig. 3). In one year observation, there was no recurrence of chest pain, and in MIBI SPECT study; only a mild persistent reduction of perfusion in the previously described LAD territory was observed (Fig. 4).

Chronic total occlusion (CTO) of coronary artery is defined as a complete vessel occlusion and estimated occlusion duration of ≥ 3 months. There are no clear guidelines regarding the treatment of non-acute occlusions and, in spite of a few clinical trials, there is no evidence of the benefit of recanalization of CTO. Because of technical difficulties and higher risk of complications, patients with CTO are qualified for revascularization (REV) less frequently than other groups of patients. Accordingly, SPECT is also less frequently used.

SPECT studies of CTO with no MI history often show a significant degree of ischemia, which indicates that there is preserved tissue viability in the CTO territory. In our material, from the group of patients who had both SPECT and angiography of coronary arteries performed between 2010 and 2017, we selected patients with isolated CTO (without > 50% narrowing of any other coronary vessel) and no history of MI. In each patient (4M, 2F) we found

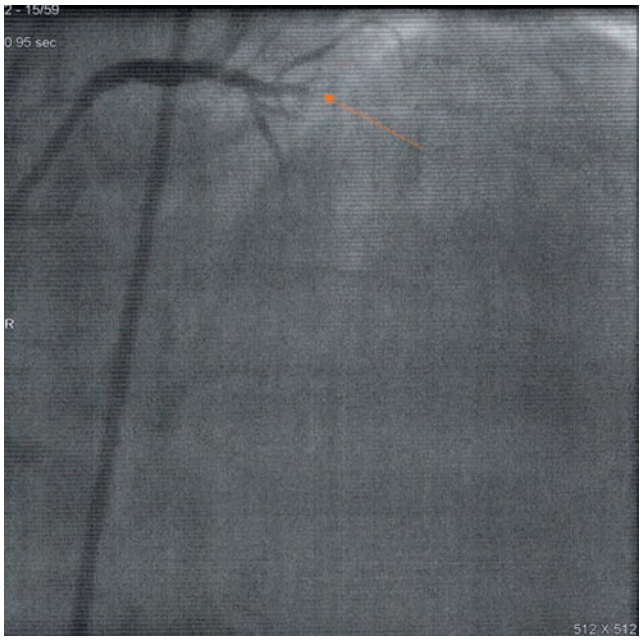

Figure 1. Occluded LAD

Correspondence to: Katarzyna Jóźwik-Plebanek, Institute of Cardiology, Alpejska 42, 04-628 Warsaw, Poland, e-mail: kjozwik@ikard.com

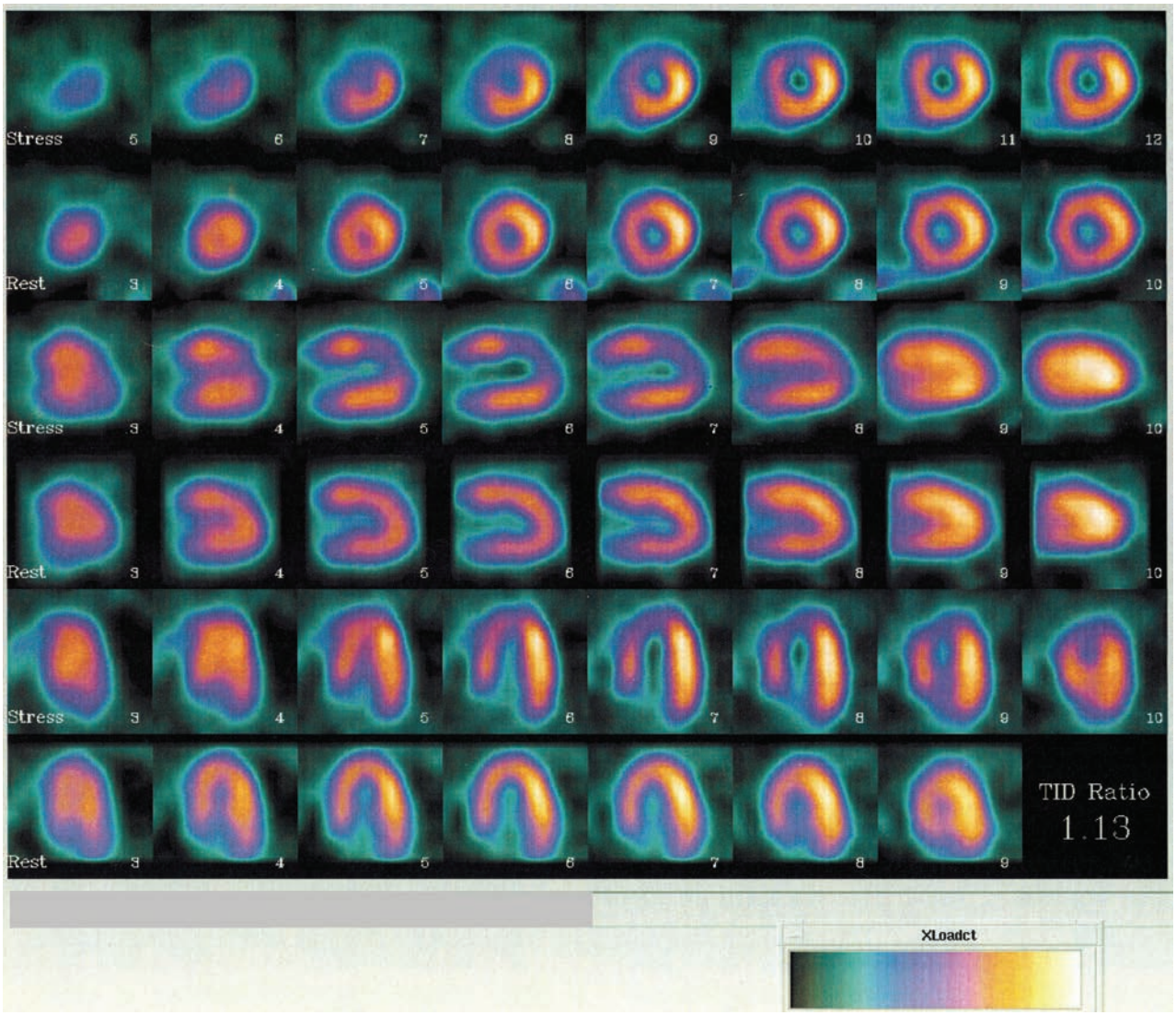

Figure 2. MIBG SPECT: perfusion defect in typical LAD territory

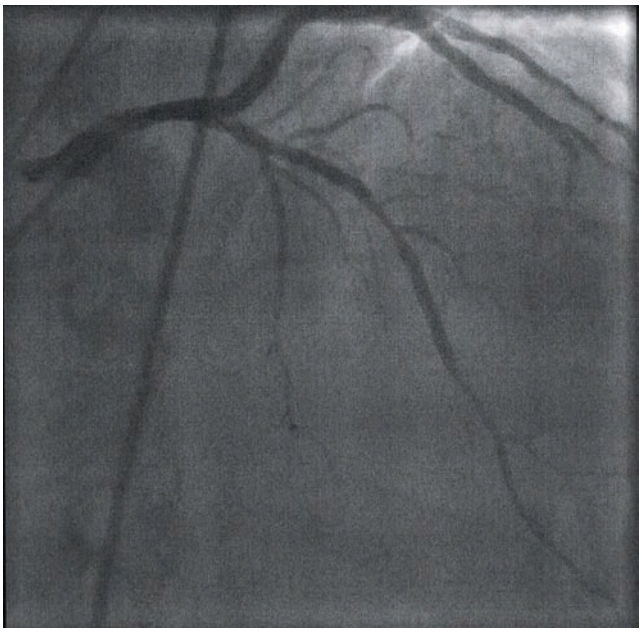

Figure 3. Recanalizated LAD

a transient perfusion defect in the SPECT study in the area corresponding to a typical blood supply of the occluded vessel (av. 11% of LV muscle). In 4 patients (67%), transient perfusion defect was > 10% of the LV muscle.

It seems that the presence of ISCH (not necrosis) is associated with the development of collateral circulation, owing to the chronic nature of the disease. SPECT studies help to select patients who will potentially benefit the most from REV: in our observation, 2/3 of patients had significant ischemia in the territory of CTO, which might require REV.

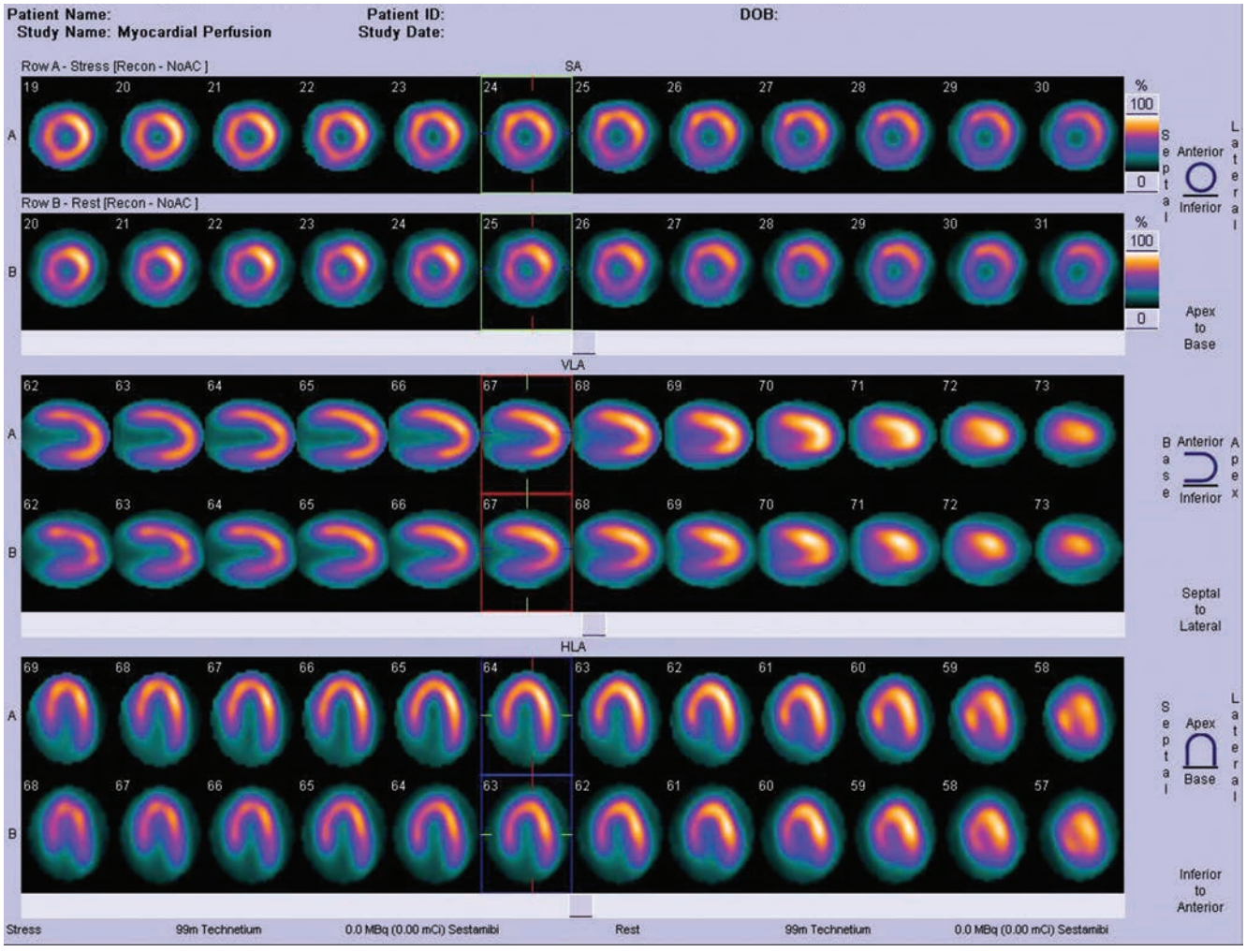

Figure 4. MIBI SPECT after 1 year

VIA MEDICA

Nuclear Medicine Review 2019, 22, 1: 37–39
DOI: 10.5603/NMR.2019.0007

ISSN 1506–9680

Clinical vignette

In-transit sentinel lymph nodes predicted by F-18 Fluorodeoxyglucose Positron Emission Tomography/Computed Tomography

Zehra Pinar Koc[1], Pelin Özcan Kara[1], Ahmet Dag[2], Ferah Tuncel Daloglu[3]

[1] Department of Nuclear Medicine, Mersin University, Turkey
[2] Department of General Surgery, Mersin University, Turkey
[3] Department of Pathology, Mersin University, Turkey

[Received 16 X 2018; Accepted 29 XI 2018]

Abstract

Although the in-transit lymph node is a well-known issue in malignant melanoma, it is not documented sufficiently in breast cancer. In this case report an in-transit lymph node demonstrated by both PET/CT and sentinel lymph node mapping and diagnosed by pathology is reported.

KEY words: in transit, sentinel, breast, pet, scintigraphy

Nucl Med Rev 2019; 22, 1: 37–39

Introduction

Sentinel lymph node is theoretically the first lymph node to drain the tumor. The pathologic examination of the sentinel lymph node presents the further lymph nodes, thus the lymph nodal status of the primary tumor [1]. Previous studies have provided sufficient evidence that the sentinel lymph node analysis predicts the local lymphatic status of the tumor and there is a low risk of skip secondary lymph node invasion [2], thus recurrence, in the case of negative sentinel lymph node [3]. In case of a positive sentinel lymph node, axillary dissection has to be performed [4]. There are several sentinel node identification methods, such as blue dye and radionuclide sentinel lymph node imaging. These methods may be performed together and have low false-negative rate; however, there is a learning curve and experience is required [5]. Another new and not well-documented issue in sentinel lymph node imaging is the in-transit lymph node. In-transit or intramammary lymph node is the lymph node that is surrounded by the breast tissue [5, 6]. The in-transit lymph node as a sentinel lymph node is an unknown part of the procedure. This is the first case report, as far as we know, with intramammary in-transit lymph node scintigraphy imaging in combination with PET/CT imaging.

Correspondence to: Zehra Pinar Koc, Department of Nuclear Medicine Mersin University, Turkey, e-mail: zehrapinarkoc@gmail.com

Case Report

Case 1. A 69-year-old female patient with identified right-breast carcinoma was referred for F-18 FDG PET/CT for staging. The F-18 FDG PET/CT images of the patient showed retroareolar lesion with significantly increased FDG uptake (2 x 1.5 cm; SUVmax = 12.6) and additional intramammary lymph nodes (the largest was 9 mm in diameter) without significant FDG uptake (Fig. 1). At the day of operation the sentinel lymph node imaging showed intramammary sentinel lymph node and during the operation the intramammary lymph node was excised at the border of axilla. The lymph node was positive for tumor and axillary dissection showed multiple (n = 6) positive nodes (Fig. 1).

Case 2. The patient was 58 years old and left-breast tumor showed invasive carcinoma; therefore, F-18 FDG PET/CT imaging was performed for staging. The imaging showed left upper inner quadrant hypermetabolic lesion (18 x 18 mm, SUVmax = 25.6) and millimetric lymph node in the parenchyma with FDG uptake and axillary lymph node with FDG uptake (SUVmax = 3.5 and SUVmax = 4.2, respectively) (Fig. 2). Sentinel lymph node imaging showed in-transit intramammary lymph node in early phase (dynamic) of the study, and in the late phase also additional multiple sentinel lymph nodes in axilla were observed (Fig. 2). All sentinel (n = 3) and axillary lymph nodes (n = 3) were positive in the histopathology (Fig. 2).

Discussion

There is very limited data about the in-transit lymph nodes in breast cancer. There are few cases reported in the literature and

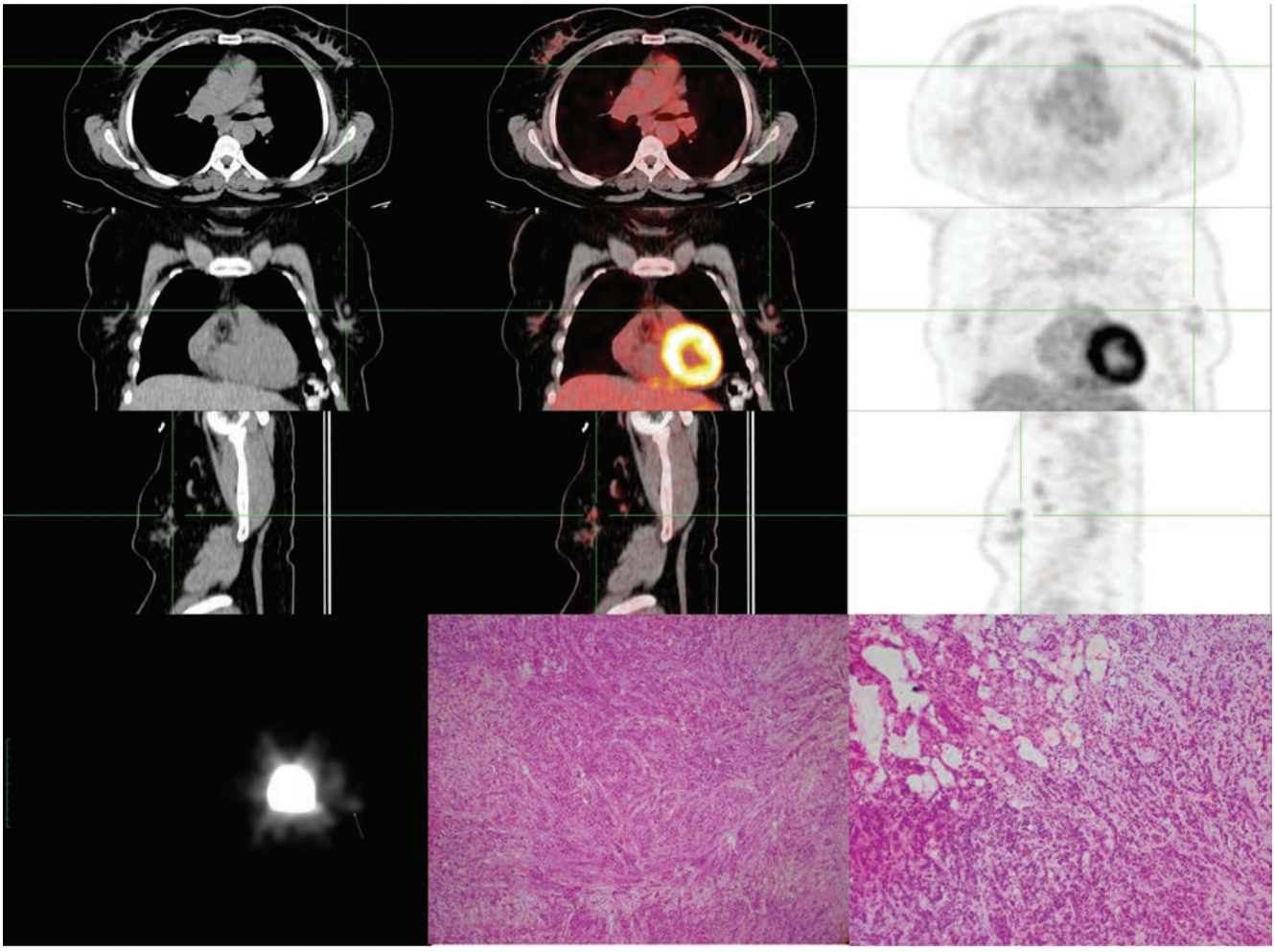

Figure 1. The F-18 FDG PET/CT images of the first patient with lesion suspicious of in-transit lymph node, adjacent to the primary tumor in outer upper quadrant of the left breast in the transaxial, coronal and sagittal projection. B. Tc-99m nanocolloid sentinel lymph node dynamic images that show the in-transit sentinel lymph node activity adjacent to the injection site. C. Pathology images of the lymph node sections stained with hematoxylin and eosin in x40 and x100 magnification

some review articles [5]. The in-transit lymph nodes are smaller diameter and closer to the lymphatic channels and the primary tumors. Although they are surrounded by the breast tissue and not exactly axillary lymph nodes, they are considered axillary lymph nodes in staging. They may be not recognized by the gamma camera imaging or the surgeon due to close proximity (shine-through effect) and small volume and underestimated; however, previous reviews have demonstrated that they might be a source of local recurrence [5]. As in the case described by van Deurzen et al., in this case report we presented a patient with in-transit lymph node that was observed in first few second and disappeared immediately after identification. Also axillary lymph nodes of the patient were positive as well. In the other patient, the intramammary lymph node was the single sentinel lymph node and the axillary lymph nodes were also positive. However it is problematic to determine the in-transit or intramammary lymph node during the scintigraphy, because it requires significant consideration by the physician.

In previous studies about the in-transit lymph node in malignant melanoma the incidence was reported to be between 3–10% [6]. In 14–20% of these cases, the in-transit lymph nodes were found to be positive and considered one of the local recurrence causes in malignant melanoma [7]. Van Deurzen et al. suggested that these lymph nodes in breast cancer might also have major clinical impact [5].

Previous case reports have pointed out that in-transit lymph nodes in intramammary region might develop from the lymphatic emboli and be directly connected to the primary tumor [8] and might be one of the causes of false negative sentinel lymph node examinations, which can be as high as > 10% [9]. Obviously, it is difficult to localize the intramammary lymph nodes because of surrounding normal breast tissue and they usually are not radioactive and blue. In the case of breast conserving surgery, the node may be missing. Scintigraphy also has disadvantage of shine-through effect originating from the primary tumor injection site. However, in our experience the intramammary lymph nodes were determined by the first diagnostic procedure F-18 FDG PET/CT. This is the first study that demonstrates the intramammary lymph nodes by both PET/CT and scintigraphy.

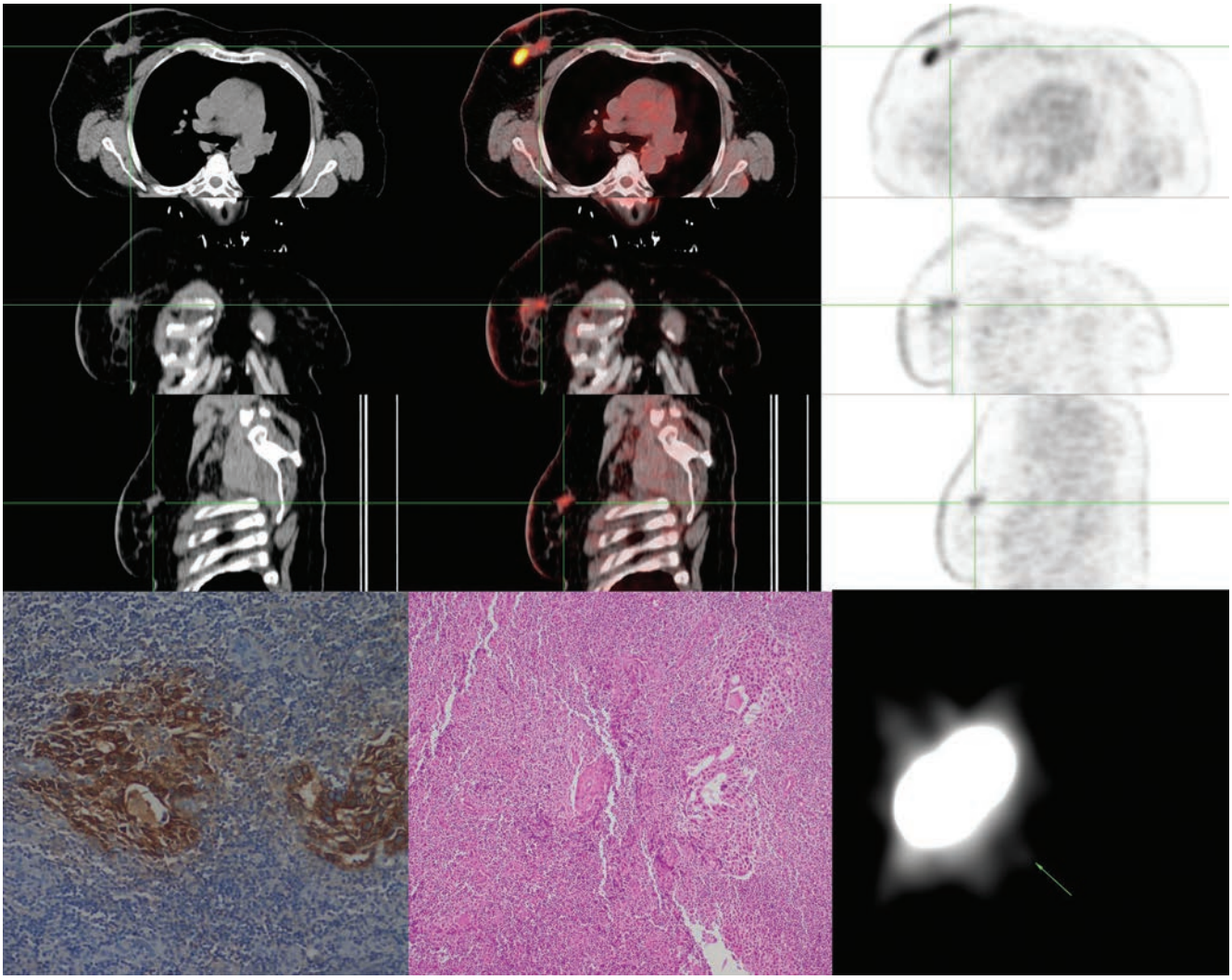

Figure 2. A. The transaxial, sagittal and coronal projection PET, CT and fusion images of F-18 FDG PET/CT of the second patient demonstrating the suspicious hypermetabolic lesion medial to the primary tumor in upper outer quadrant of the right breast B. Pathology section of the lymph node with immunostaining in x100 and hematoxylin eosin in x40 magnification C. Sentinel lymph node dynamic images showing the in transit lymph node activity (arrow)

References

1. Giuliano AE, Kirgan DM, Guenther JM, et al. Lymphatic mapping and sentinel lymphadenectomy for breast cancer. Ann Surg. 1994; 220(3): 391–8; discussion 398, indexed in Pubmed: 8092905.
2. Keskek M, Balas S, Gokoz A, et al. Re-evaluation of axillary skip metastases in the era of sentinel lymph node biopsy in breast cancer. Surg Today. 2006; 36(12): 1047–1052, doi: 10.1007/s00595-006-3322-6, indexed in Pubmed: 17123131.
3. Lyman GH, Temin S, Edge SB, et al. American Society of Clinical Oncology Clinical Practice. Sentinel lymph node biopsy for patients with early-stage breast cancer: American Society of Clinical Oncology clinical practice guideline update. J Clin Oncol. 2014; 32(13): 1365–1383, doi: 10.1200/JCO.2013.54.1177, indexed in Pubmed: 24663048.
4. Galimberti V, Cole BF, Zurrida S, et al. International Breast Cancer Study Group Trial 23-01 investigators. Axillary dissection versus no axillary dissection in patients with sentinel-node micrometastases (IBCSG 23-01): a phase 3 randomised controlled trial. Lancet Oncol. 2013; 14(4): 297–305, doi: 10.1016/S1470-2045(13)70035-4, indexed in Pubmed: 23491275.
5. van Deurzen CHM, Borgstein PJ, van Diest PJ. In-transit lymph node metastases in breast cancer: a possible source of local recurrence after Sentinel Node procedure. J Clin Pathol. 2008; 61(12): 1314–1316, doi: 10.1136/jcp.2008.059600, indexed in Pubmed: 18794198.
6. Vidal-Sicart S, Pons F, Fuertes S, et al. Is the identification of in-transit sentinel lymph nodes in malignant melanoma patients really necessary? Eur J Nucl Med Mol Imaging. 2004; 31(7): 945–949, doi: 10.1007/s00259-004-1485-1, indexed in Pubmed: 14997348.
7. Statius Muller MG, van Leeuwen PAM, van Diest PJ, et al. Pattern and incidence of first site recurrences following sentinel node procedure in melanoma patients. World J Surg. 2002; 26(12): 1405–1411, doi: 10.1007/s00268-002-6197-8, indexed in Pubmed: 12297910.
8. Cserni G, Cserni G, Cserni G, et al. European Working Group for Breast Screening Pathology. Estimating the overlap between sentinel lymph nodes and axillary node samples in breast cancer. Pathol Oncol Res. 1999; 5(2): 129–133, indexed in Pubmed: 10393365.
9. Kim T, Giuliano AE, Lyman GH. Lymphatic mapping and sentinel lymph node biopsy in early-stage breast carcinoma: a metaanalysis. Cancer. 2006; 106(1): 4–16, doi: 10.1002/cncr.21568, indexed in Pubmed: 16329134.
10. Cserni G. Commentary on in-transit lymph node metastases in breast cancer: a possible source of local recurrence after Sentinel Node procedure. J Clin Pathol. 2008; 61(12): 1233–1235, doi: 10.1136/jcp.2008.060848, indexed in Pubmed: 18829625.

Clinical vignette

Nuclear Medicine Review 2019, 22, 1: 40–42
DOI: 10.5603/NMR.2019.0008

ISSN 1506–9680

VIA MEDICA

Multiple photopenic vertebrae in the bone scintigraphy of a young man with Gorham disease: CT and MRI correlation

Ramin Sadeghi, Sara Shakeri, Toktam Massoudi, Fatemeh Farahmandfar, Farnaz Nesari Javan
Nuclear Medicine Research Center, School of Medicine, Mashhad University of Medical Sciences, Mashhad, Iran, Islamic Republic Of

[Received 3 XI 2018; Accepted 29 XI 2018]

Abstract

We report a rare pattern of extensive bone abnormalities on the Tc-99m MDP bone scintigraphy in a patient with Gorham disease. This rare condition is the result of vascular and lymphatic channel proliferation in bony structures which induce bone resorption. Our case is a 28-year-old man with a history of biopsy-proven soft tissue hemangioma in the left thigh, encountered with a recent diagnosis of multiple vertebral hemangiomata in the axial skeleton and progressive bony destructions in the pelvis on CT and MRI images, referred for bone scintigraphy. Multiple photopenic hemangiomata were noted on bone scan.

KEY words: Gorham disease, bone resorption, vascular proliferation, hemangioma

Nucl Med Rev 2019; 22, 1: 40–42

Introduction

Gorham disease is known as a rare disappearing-bone disease [1] most commonly in the shoulders and the pelvic girdles; however, various bone structures can be involved such as skull, mandible, humerus, scapula, clavicle, sternum, axial skeleton, hands and feet [2, 3]. Primary involvement of the spine is infrequent [4]. We present a rare form of extensive bony involvement in multiple areas including the spine and pelvis, with photopenic appearance in the whole-body bone scan.

Case report

A 28-year-old man with a history of biopsy-proven soft tissue hemangioma in the left thigh since 3 years ago, admitted with a chief complaint of recently progressive disability of walking. The plain radiography of the pelvis showed subtle osteolysis in the sacrum, left sacroiliac joint, left iliac bone and left femoral head. For precise evaluation, Thoraco-abdomino-pelvic multislice computed tomography [CT] scan and transaxial magnetic resonance images [MRI] were performed (Fig. 1, 2 and 3).

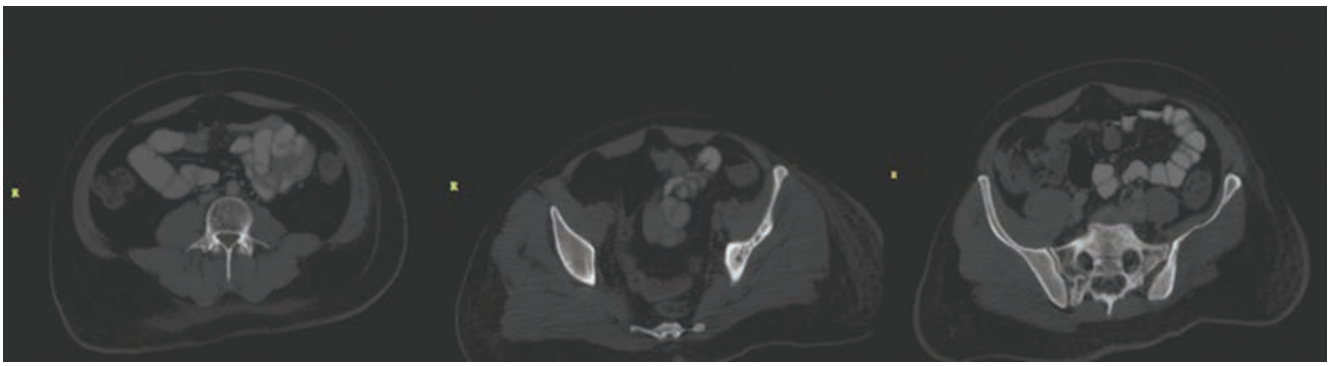

Figure 1. CT images showed Polka-dot sign or salt and paper appearance in T12, L1 and L3–L5 vertebrae, as well as lytic lesions in the sacrum and destructed left iliac bone

Correspondence to: Ramin Sadeghi, Nuclear Medicine Research Center, School of Medicine, Mashhad University of Medical Sciences, Mashhad, Iran, Islamic Republic Of, e-mail: sadeghir@mums.ac.ir

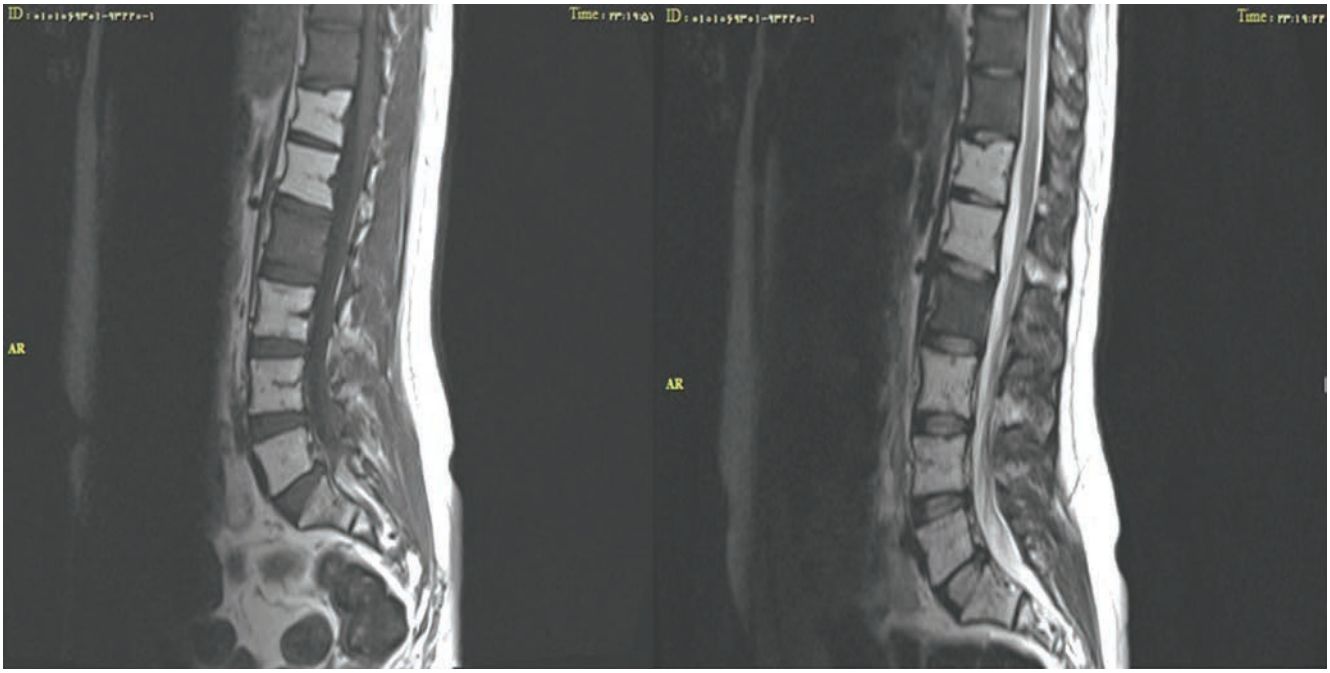

Figure 2. Spine MRI revealed multiple hypersignal vertebrae on T1 (left) and T2-weighted (right) sections in T12, L1, and L3–L5 vertebrae

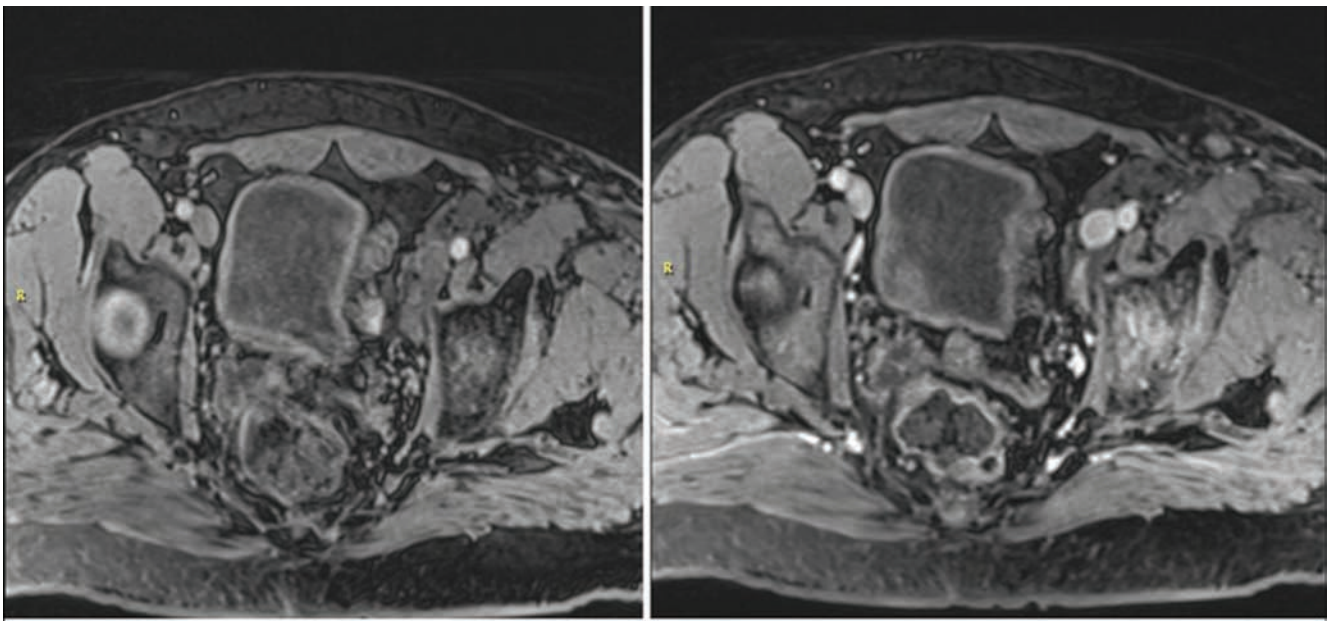

Figure 3. Pelvic MRI with IV contrast showed soft tissue enhancement in the left thigh and confirmed the extensive soft tissue hemangioma in this region

Whole-body bone scan and following SPECT acquisition were performed four hours after IV injection of 740 MBq (20 mCi) Tc-99m-methylene diphosphonate [Tc-99m MDP], using a dual-head variable angle gamma camera with a low-energy high-resolution parallel-hole collimator (Fig. 4).

Discussion

As we report in our case, vascular proliferation and replacement of bone matrix with fibrous tissue lead to bone destruction and osteolysis [5–7]. The etiology of the disease is still unknown. Notably,

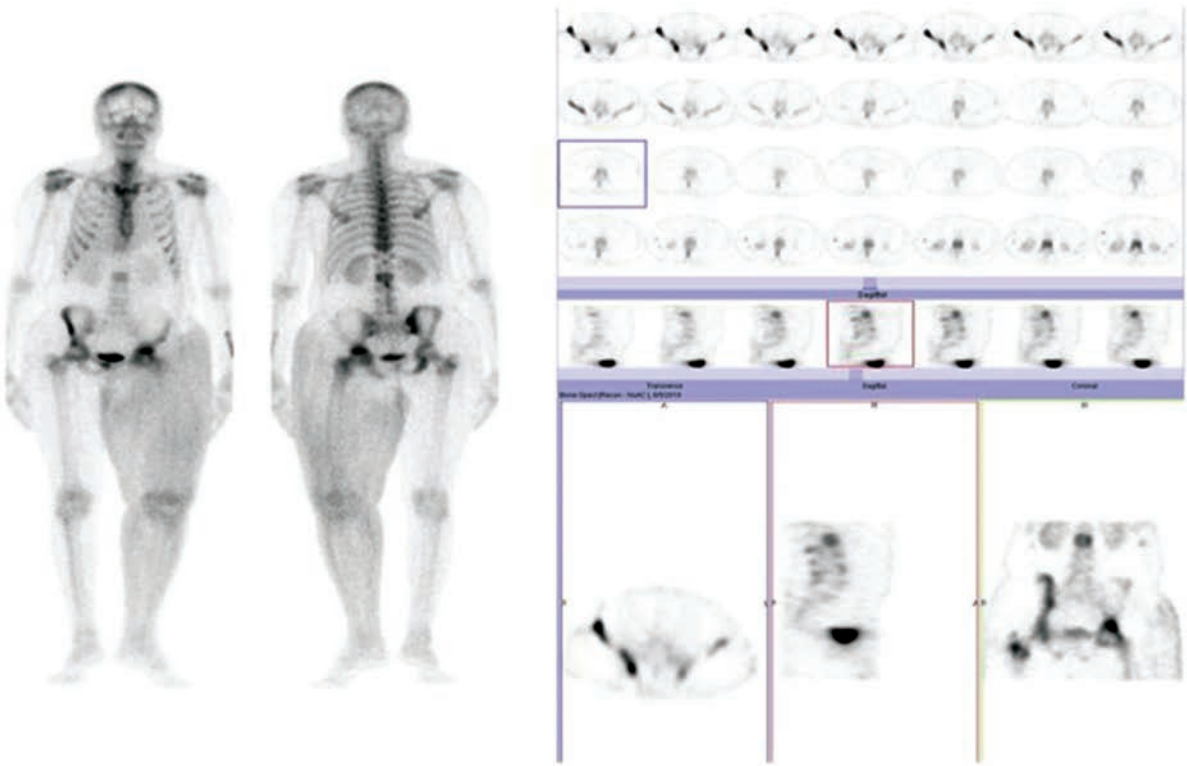

Figure 4. Tc-99m MDP whole-body bone scan showed multiple zones of absent tracer uptake in the T12, L1and L3–L5 vertebrae, sacrum, left sacroiliac joint, left iliac bone and right femoral head, as well as increased tracer activity in the left femoral head and left thigh swelling. SPECT images on the right side, also confirmed the whole-body scan findings

suspicion of the vanishing-bone disease should be considered only after excluding the other significant differential diagnosis such as infection, malignancy, inflammatory and endocrine pathologies. Despite the benign pathology of the disease, the prognosis is unpredictable with possibly serious consequences like pathologic fractures [3].

It was mentioned that increased Tc-99m MDP uptake in the affected bony regions may indicate the active phase of bone disease [8]; however, limited photopenic involved sites in the whole-body bone scan were reported in the sacroiliac joint [9], mandible [10], lumbar spine [11] and left lower rib cage [8].

Conflict of interest

None declared.

References

1. Ruggieri P, Montalti M, Angelini A, et al. Gorham-Stout disease: the experience of the Rizzoli Institute and review of the literature. Skeletal Radiol. 2011; 40(11): 1391–1397, doi: 10.1007/s00256-010-1051-9, indexed in Pubmed: 20972870.
2. Patel DV. Gorham's disease or massive osteolysis. Clin Med Res. 2005; 3(2): 65–74, indexed in Pubmed: 16012123.
3. Nikolaou VS, Chytas D, Korres D, et al. Vanishing bone disease (Gorham-Stout syndrome): A review of a rare entity. World J Orthop. 2014; 5(5): 694–698, doi: 10.5312/wjo.v5.i5.694, indexed in Pubmed: 25405099.
4. Flörchinger A, Böttger E, Claass-Böttger F, et al. [Gorham-Stout syndrome of the spine. Case report and review of the literature]. Rofo. 1998; 168(1): 68–76, doi: 10.1055/s-2007-1015184, indexed in Pubmed: 9501937.
5. Papadakis GZ, Millo C, Bagci U, et al. 18F-NaF and 18F-FDG PET/CT in Gorham-Stout Disease. Clin Nucl Med. 2016; 41(11): 884–885, doi: 10.1097/RLU.0000000000001369, indexed in Pubmed: 27648707.
6. Gorham LW, Stout AP. Massive osteolysis (acute spontaneous absorption of bone, phantom bone, disappearing bone); its relation to hemangiomatosis. J Bone Joint Surg Am. 1955; 37-A(5): 985–1004, indexed in Pubmed: 13263344.
7. Posadas MD, Viejo Stuart S, Romano O, et al. Gorham-Stout syndrome: a case report. Eur Rev Med Pharmacol Sci. 2014; 18(1 Suppl): 81–83, indexed in Pubmed: 24825048.
8. Yang RH, Chen PCH, Chang CP, et al. Gorham's disease: the disappearing bone. Clin Nucl Med. 2013; 38(5): 361–364, doi: 10.1097/RLU.0b013e318286bf93, indexed in Pubmed: 23486335.
9. Brown RD, Studentsova Y, Margouleff D. Vanishing bone disease of the pelvis. Clin Nucl Med. 2004; 29(11): 709–711, indexed in Pubmed: 15483484.
10. Park SB, Choi JY, Kim SJ. Gorham-Stout Disease Affecting the Mandible: Bone Scintigraphy and Computed Tomography Findings. Clin Nucl Med. 2017; 42(10): 779–781, doi: 10.1097/RLU.0000000000001800, indexed in Pubmed: 28806245.
11. Mabille L, Berenger N, Laredo JD, et al. Vanishing vertebra. Clin Nucl Med. 1997; 22(1): 49–51, indexed in Pubmed: 8993876.

VIA MEDICA

Nuclear Medicine Review 2019, 22, 1: 43–44
DOI: 10.5603/NMR.a2019.0009

ISSN 1506–9680

Clinical vignette

Incidental detection of os acromiale mimicking a fracture on 18F-Fluoride PET-CT

Vincenzo Militano, Mark Hughes, Sobhan Vinjamuri, Nagabhushan Seshadri
Royal Liverpool and Broadgreen University Hospital — NHS Trust, Liverpool, United Kingdom

[Received 30 VII 2018; Accepted 29 XI 2018]

Abstract

Os acromiale represents an unfused accessory center of ossification of the acromion of scapula. It may cause shoulder impingement, rotator cuff tear or degenerative acromio-clavicular joint disease. A 38-year-old male with a history of degenerative disc disease presented with persistent backache. MRI of the lumbar spine had earlier showed left paracentral disc protrusion of L5/S1 vertebrae impinging the left S1 nerve root for which the patient underwent fluoroscopic guided nerve root block. Due to persistent bilateral sciatica and worsening leg pain a decompression surgery was planned. A bone scan was requested to exclude other causes of pain prior to surgery for which the patient underwent 18F-Fluoride PET-CT examination. We report a case of incidental detection of os acromiale mimicking fracture. As the management strategy for both is quite different this case highlights the importance of correct recognition of this identity for appropriate management.

KEYWORDS: 18F-Fluoride, PET/CT, os acromiale

Nucl Med Rev 2019; 22, 1: 43–44

Os acromiale is relatively rare, seen in about 8% (range 1–15%) of the population [1, 2] but may be bilateral in 60% of individuals[5].They are usually asymptomatic [3]. The acromion normally has a secondary center of ossification which usually fuses to the rest of the acromion by the age of 25 years. Os acromiale represents persistence of this center without fusion. It may cause shoulder impingement, rotator cuff tear or degenerative AC joint disease [4]. The subtypes develop due to the variation in fusion pattern of the three acromial ossification centers (preacromion, mesoacromion and metacromion) [5] and are classified on their pattern of articulation with the acromion (from proximal to distal) as basi-acromial, meta-acromial, meso-acromial and pre-acromial. Meta and meso-acromial are the most common variants [4].

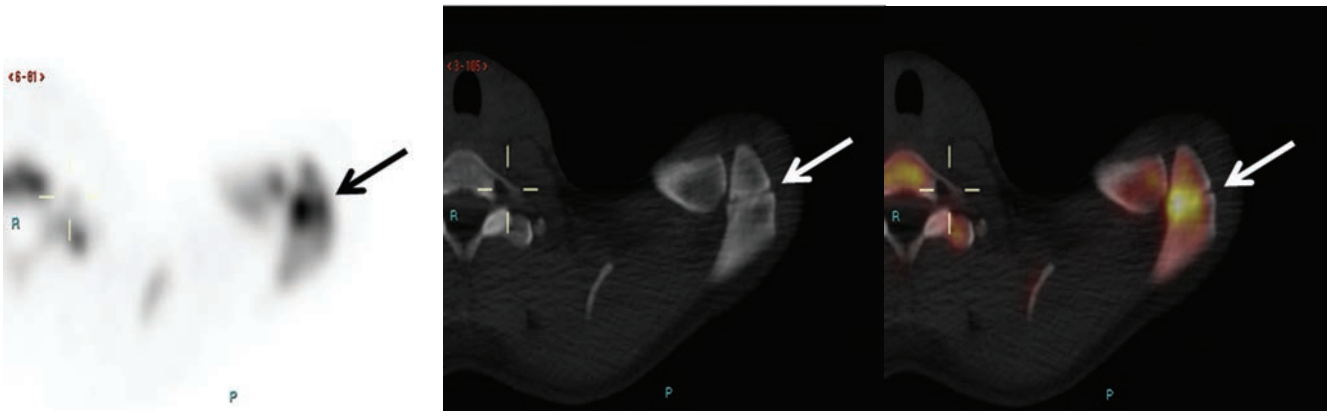

Figure 1. The 18F-Fluoride PET-CT showed a focus of moderate grade activity on the left shoulder which on axial images localized to the lateral end of the left acromion (black arrow) corresponding on CT to a linear defect with subtle sclerotic margins (white arrow) in keeping with os acromiale

Correspondence to: Vincenzo Militano, Department of Nuclear Medicine, Royal Liverpool University Hospital, Prescot Street, Liverpool L7 8XP, United Kingdom, e-mail: vinmilitano@gmail.com, tel: +44 7871266523

It is well known that the treatment of non-displaced fracture of the acromion is immobilization and analgesics, while the treatment of symptomatic os acromiale is initially non-operative activity modification, corticosteroid injection and use of nonsteroidal anti-inflammatory medication and, if there is no remission of symptoms, following by surgical intervention in the form of internal fixation or excision and acromioplasty [6, 7]. Although os acromiale occurs rarely, recognition of this identity is important, as it can mimic a fracture [8]. This knowledge is important as identification of os acromiale in symptomatic patients frequently alters the kind of treatment instituted.

References

1. Park JG, Lee JK, Phelps CT. Os acromiale associated with rotator cuff impingement: MR imaging of the shoulder. Radiology. 1994; 193(1): 255–257, doi: 10.1148/radiology.193.1.8090902, indexed in Pubmed: 8090902.
2. Papatheodorou A, Ellinas P, Takis F, et al. US of the shoulder: rotator cuff and non-rotator cuff disorders. Radiographics. 2006; 26(1): e23, doi: 10.1148/rg.e23, indexed in Pubmed: 16352733.
3. Edelson JG, Zuckerman J, Hershkovitz I. Os acromiale: anatomy and surgical implications. J Bone Joint Surg Br. 1993; 75(4): 551–555, indexed in Pubmed: 8331108.
4. Uri DS, Kneeland JB, Herzog R. Os acromiale: evaluation of markers for identification on sagittal and coronal oblique MR images. Skeletal Radiol. 1997; 26(1): 31–34, indexed in Pubmed: 9040140.
5. Neer CS. Rotator cuff tears associated with os acromiale. J Bone Joint Surg Am. 1984; 66(8): 1320–1321, indexed in Pubmed: 6490713.
6. Harris JD, Griesser MJ, Jones GL. Systematic review of the surgical treatment for symptomatic os acromiale. Int J Shoulder Surg. 2011; 5(1): 9–16, doi: 10.4103/0973-6042.80461, indexed in Pubmed: 21660192.
7. Youm T, Hommen JP, Ong BC, et al. Osacromiale: evaluation and treatment. Am J Orthop. 2005 Aug; 34(8): 382.
8. Swain RA, Wilson FD, Harsha DM. The os acromiale: another cause of impingement. Med Sci Sports Exerc. 1996; 28(12): 1459–1462, indexed in Pubmed: 8970138.